5-2017

A Study of Lignin and Lignin Models in Chemical and Electrochemical Systems

Luke Thomas Servedio
University of Tennessee, Knoxville, lservedi@vols.utk.edu

To the Graduate Council:

I am submitting herewith a dissertation written by Luke Thomas Servedio entitled "A Study of Lignin and Lignin Models in Chemical and Electrochemical Systems." I have examined the final electronic copy of this dissertation for form and content and recommend that it be accepted in partial fulfillment of the requirements for the degree of Doctor of Philosophy, with a major in Chemical Engineering.

Thomas A Zawodzinski, Major Professor

We have read this dissertation and recommend its acceptance:

Joseph Bozell, Robert Counce, Arthur Ragaskas

Accepted for the Council:

Dixie L. Thompson

Vice Provost and Dean of the Graduate School

(Original signatures are on file with official student records.)

A Study of Lignin and Lignin Models in Chemical and Electrochemical Systems

A Thesis Presented for the
Doctor of Philosophy
Degree
The University of Tennessee, Knoxville

Luke Thomas Servedio
May 2017

DEDICATION

To my role model – my father, who, through his tireless example, showed me the true worth of a curious heart.

ACKNOWLEDGEMENTS

I would first like to thank Dr. Thomas Zawodzinski for providing me with such an incredible opportunity to work in this research group. I would also like to thank Dr. Shane Foister for his daily guidance and expertise in the realms of synthetic and analytical chemistry and for helping me become a halfway decent chemist over the last few years. I'd also like to thank my committee members, Dr. Joseph Bozell, Dr. Art Ragauskas and Dr. Pete Counce for their suggestions on my research and the presentation of it.

There are specific people that I'd like to thank for some specific areas to which they contributed: I'd like to thank Dr. Jamie Lawton for her help with performing EPR spectroscopy in the early days and for keeping us on our toes in the office. Dr. Ramez Elgammal for helping me with the NMR work and for being a resource regarding anything chemistry related. Dr. Gabriel Goenaga for his assistance with the testing of the many sub-par materials that I synthesized over the years. To Nelly Cantillo for taking her time to run some of my samples on the high-resolution SEM/TEM. I also need to thank Brian Fane and Donovan Layton – I would likely not be here without both of you and the month of marathon study sessions, just to get up the next morning and start all over again. Whatever it takes to pass quals! And to everyone that has come and gone in the Z-Lab over the years. Your support and camaraderie has been an invaluable source of inspiration and levity – as both are needed in equal parts to get through the day – I cannot thank you enough.

I would be remiss if I did not mention the support of my parents, Mike and Loretta. For the example you've always set – that the hard road is somehow always worth taking. Your unwavering support for all the tough decisions I've made along the way – thank you doesn't seem to do it justice. To Jess, who has stuck with me through all the lost weekends and late nights in the lab and who's positivity and belief in me has kept me grounded – your love has meant the world to me.

A few odds and ends worth mentioning – I need to thank Old City Java for giving me sanctuary and coffee when I could no longer bare the drop ceiling and fluorescent oppression of our 1st floor SERF office. To the band TAUK, whose music became the unofficial soundtrack of this dissertation, the absence of lyrics and deep grooves made the pages fly by. To the chemistry department for unwittingly allowing me to use a number of instruments in the 3rd floor analytical lab and to the Buehler and SERF janitorial staff, who broke the rules countless times to let me in to locked labs afterhours after getting to know my face. Thanks for everything!

ABSTRACT

The use of biomass as a viable, renewable feedstock for the production of energy and as a surrogate for the petrochemical industry has generated a tremendous amount of research over the last 40 years. With lignin comprising 25-35% by weight of the dry mass of much of that material, much time and energy has been devoted to investigating a viable, scalable value-added proposition for the use of lignin and lignin pre-cursor materials. The bulk of lignin produced today comes as a by-product of the de-pulping process in the production of paper – most of which is used as a combustion fuel by these paper plants to offset their carbon footprint. Considering that lignin has a heating value generally considered to be about half that of most industrial combustion fuels and that the heterogeneous nature of lignin lends itself well to chemical production, the burning of lignin is an inelegant use of its potential.

With this premise in mind, we have functionalized unmodified organosolv lignins to attempt to utilize them as a structural scaffold to increase the chemical and mechanical durability of various polymer materials for usage as anion exchange membranes (AEMs). The modifications, which can be selective based on the native reactivity of the modification sites, not only impart structural support to the polymer matrix, but also ionic character to increase the ion exchange capacity (IEC) of the polymer. By altering the concentration of the modified lignin, as well as other ionic and cross-linking constituents, we can the improve the mechanical and chemical properties of the polymer to make a strong case for the premise that the addition of

lignin increases the polymer's ability to accept a higher loading of charge sites before precipitation. By measuring conductivity, water uptake, IEC and the number of water molecules per ion, we are able to make determinations regarding the link between synthetic modifications and performance properties of the membrane.

PREFACE

The topics of this dissertation cover a wide range of chemical disciplines from lignin chemistry to synthetic polymer chemistry. As a result, some of the terminology and nomenclature and paradigms found in this work may be native to one field and, simultaneously, seem foreign or erroneous to another. For example, the counting scheme of aromatic carbon substituents may be different in lignin/wood chemistry than in synthetic/polymer chemistry. This can be confusing when switching between model compounds (3,5-methoxy-4-hydroxy----) vs monolignols (2,6-methoxy---phenol) as both schemes are referring to the same structure. Generally, with lignin chemistry, the phenol is attached to the 1-C whereas in synthetic chemistry, precedent is given to standard IUPAC naming convention.

TABLE OF CONTENTS

LIST OF TABLES

LIST OF FIGURES

List of Acronyms

AcOH	acetic acid
ACN	acetonitrile
AEM	anion exchange membrane
AFC	alkaline fuel cell
AEMFC	anion exchange membrane fuel cell
ATR	attenuated total reflectance
ATRP	atom transfer reversible polymerization
CL	cross linking
CV	cyclic voltammetry
Da	daltons
DIEA	diisopropylethylamine
DMA	dimethylamine
DMF	dimethylformamide
DMIm	1,2-dimethylimidazole
Eq	equivalents (molar)
ESI	electrospray ionization
EtOH	ethanol
FTIR	Fourier transform infrared spectroscopy
GC/MS	gas chromatography mass spectrometry
GDL	gas diffusion layer
GPC	gel permeation chromatography

hf	hyperfine
HMIm	2-methylimidazole
HOMO	highest occupied molecular orbital
LMPPO	lignin-modified poly-phenylene oxide
LMOB	lignin-modified olefin-based
LUMO	lowest unoccupied molecular orbital
MBnIm	2-methylbenzimidazole
MeOH	methanol
MEA	membrane electrode assembly
mmol	millimole
NMP	N-methylpyrrolidinone
NMRP	nitroxide mediated reversible polymerization
ORR	oxygen reduction reaction
PEG	polyethylene glycol
PEM	polymer electrolyte membrane
PEMFC	polymer electrolyte membrane fuel cell
PGM	platinum group metal
PPO-Br	brominated polyphenylene oxide
pVBC	*p*-vinylbenzyl chloride
pyr	pyridine
RAFT	reversible addition-fragment chain-transfer polymerization
RCRA	Resource Conservation and Recovery Act
RRDE	rotating ring disk electrode

SEC	size exclusion chromatography
%T	percentage of transmission
TEA	triethylamine
TEG	tetraethylene glycol
TFA	trifluoroacetic acid
THF	tetrahydrofuran
TMA	trimethylamine
TLC	thin layer chromatography

Key Words:

Lignin modification, lignin polymerization, biomass, ionomer, Schiff base

CHAPTER 1 –

BACKGROUND MATERIAL

1.1 Alkaline System Fuel Cells

The history of the alkaline solvent system fuel cell is a convoluted one at best. With the earliest prototypes dating back to the 1930's, the chemistry and engineering of the alkaline electrochemical cell predates the modern-day polymer electrolyte membrane (PEM) fuel cell by almost 50 years.[1] Generally speaking, alkaline fuel cells utilize a liquid electrolyte solution of aqueous potassium hydroxide to facilitate the transfer of ions, as shown in **FIGURE 1**. This is in contrast, to some degree, to PEM fuel cells that use a conductive polymer electrolyte membrane that makes use of the humidity in the gaseous fuels along with polymeric charge-carrying groups to facilitate the transfer of charge.[2] Traditionally, AFCs utilized porous sintered metal electrodes but a lack of selectivity allowed for carbon dioxide poisoning of the electrolyte and eventual precipitation of the carbonate.[3] Among other variables, these electrodes were also extraordinarily thick, a characteristic that caused these early cells to have intrinsically high ohmic losses. In recent years, however, there has been a concerted effort to develop anionic electrolyte membranes (AEM) as the advent of the PEM fuel cell proved the successful concept of a conductive polymeric membrane with ionic selectivity.

Due to thermodynamic considerations, AFCs and especially alkaline exchange membrane fuel cells (AEMFC) are considered by many to be stronger candidates for energy production than traditional, acidic PEMFCs. Generally speaking, AEMFCs have these specific potential advantages over their acidic counterparts.[4, 5, 6]

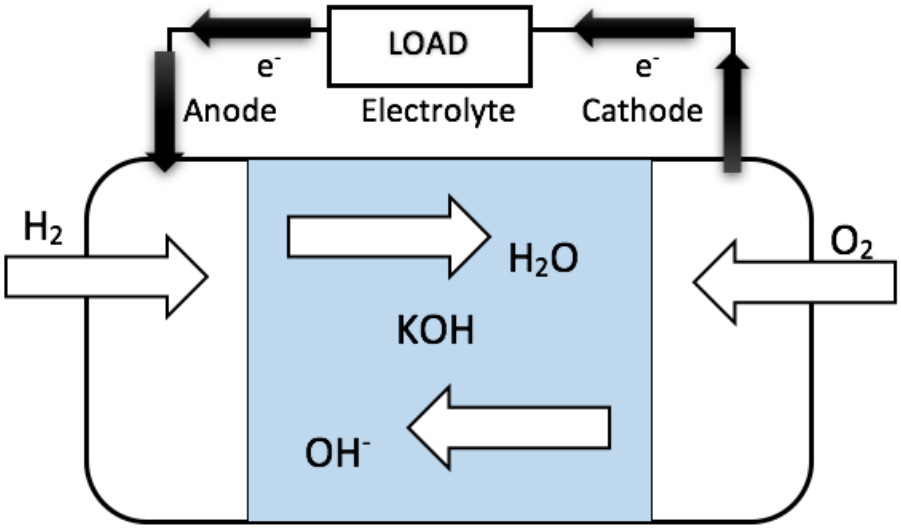

Cathode: $O_2 + H_2O + 4e^- \rightarrow 4OH^-$

Anode: $2H_2 + 4OH^- \rightarrow 2H_2O + 4e^-$

Overall Rxn: $H_2 + O_2 \rightarrow H_2O$

Figure 1 - Traditional alkaline fuel cell with liquid electrolyte and associated electrochemical reactions.

1. An alkaline medium allows for the potential use of non-platinum group metal-based (PGM) catalyst systems due to lower overpotentials for the oxygen reduction reaction (ORR).

2. Alkaline conditions significantly lower the oxidizing power of hydroperoxyl radicals (produced by a side reaction during ORR) and therefore the membrane should be less vulnerable to oxidative attack.

3. This could lead to lower material cost membranes by alleviating the need for heavily fluorinated polymers.

4. Lower potential liquid fuel (i.e. methanol) crossover than comparative acidic PEM fuel cells due to the opposite flow of hydroxide ions from cathode to anode.

Despite the numerous positive attributes of the traditional hydrogen-powered AFC and AEM fuel cell, the major drawback from this technology is the sensitivity of the liquid electrolyte and, subsequently, the electrodes to carbonate formation. [7]

$$CO_2 + 2OH^- \rightarrow CO_3^{2-} + H_2O$$

$$CO_2 + OH^- \rightarrow HCO_3^-$$

This issue can be somewhat mitigated, however, through the use of neat oxygen or through engineering controls such as inlet gas chemical scrubbers. Additionally, circulation and periodic refreshing of the liquid electrolyte can also reduce the effects of carbonate precipitation; however, all of these controls and limitations cause this technology to be restricted to specific applications where these requirements are not a barrier to implementation. For this reason, the most prevalent usage of these systems has been for the NASA space program where the use of pure oxygen is already a requirement due to volumetric considerations.[8]

1.2 Anionic Exchange Membrane Chemistry

Anion exchange membrane (AEM) chemistry has been a challenging and promising field of research over the last several decades with significant interest from the Department of Energy. Analogous in function to more traditional polymer electrolyte membrane (PEM) systems that allow for the selective permeability of protons across the space from the anode to cathode, AEMs are designed to facilitate the flow of hydroxide ($^{-}$OH) as part of the membrane-electrode assembly (MEA), as shown in FIGURE 2.[9] Currently, unlike with Nafion, which was developed for PEM

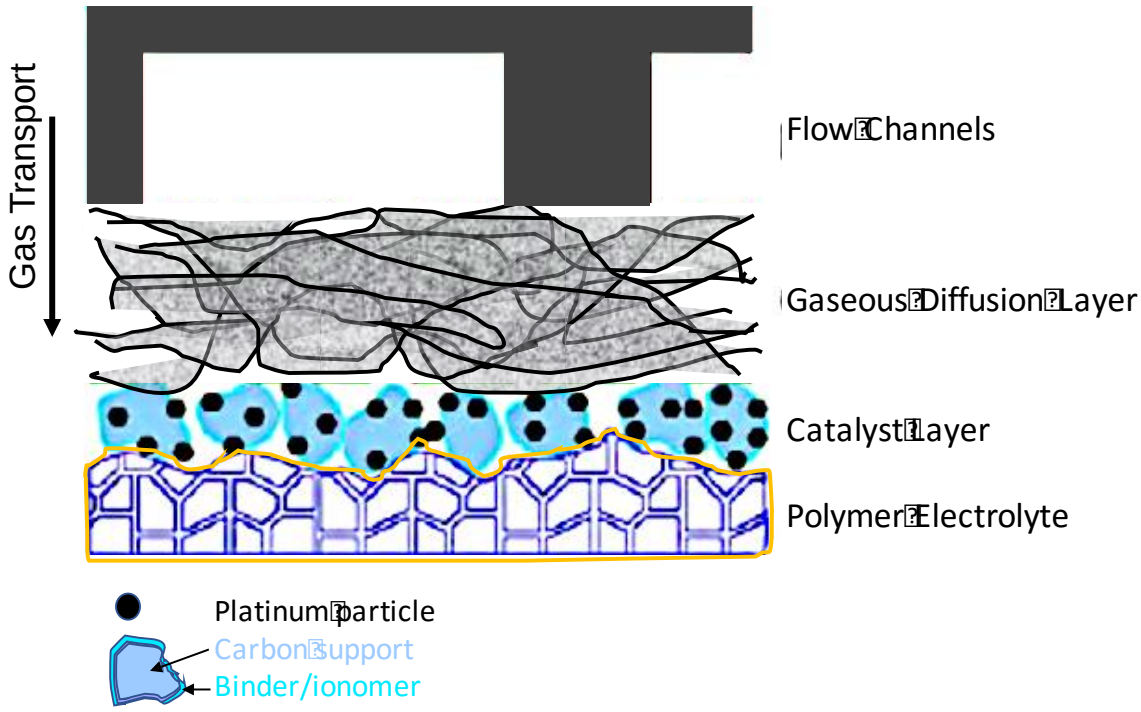

Figure 2 - Schematic of the membrane-electrode assembly showing the flow of gas through a diffusion layer to a carbon-supported catalyst layer.

fuel cells, there have been no landmark developments in the field of AEM synthesis that mitigate all the main issues of low ionic conductivity, poor chemical, thermal and mechanical stability, and geometric issues swelling.[10] AEMs generally suffer from a deficiency in at least one of these characteristics but almost all seem to have less-than acceptable mechanical stability during prolonged exposure to free-hydroxide anions. Most notably, AEMs, especially those with traditional backbone architecture/structure of styrene/vinyl polymers, tend to suffer from one of several free-hydroxide-induced elimination pathways that lead to degradation of either the cation sites or backbone chemistry. Hoffman elimination is a semi-reversible degradation pathway that attacks the cationic sites and results in either the demethylation/de-alkylation of the cation (causing a loss of ionic character) or what essentially amounts to β-elimination adjacent to the cation site which causes the complete dissociation of the charge-carrying moiety from the chain. Backbone degradation is most notably associated with traditional β-elimination resulting in brittle membranes as the polymer sheets begin to disassociate from one another.[11] Both of these elimination pathways are outlined in **FIGURE 3**, below.

Although vinyl-based polymer systems are less susceptible to β-elimination backbone degradation pathways, prolonged exposure and elevated temperatures will still result in significant loss of mechanical stability.[12] For this reason, much attention has been devoted to developing and synthesizing novel polymer systems that provide a robust chemical/mechanical scaffold upon which to build a polymer electrolyte capable of meeting similar demands set by the DOE for PEMFC systems.

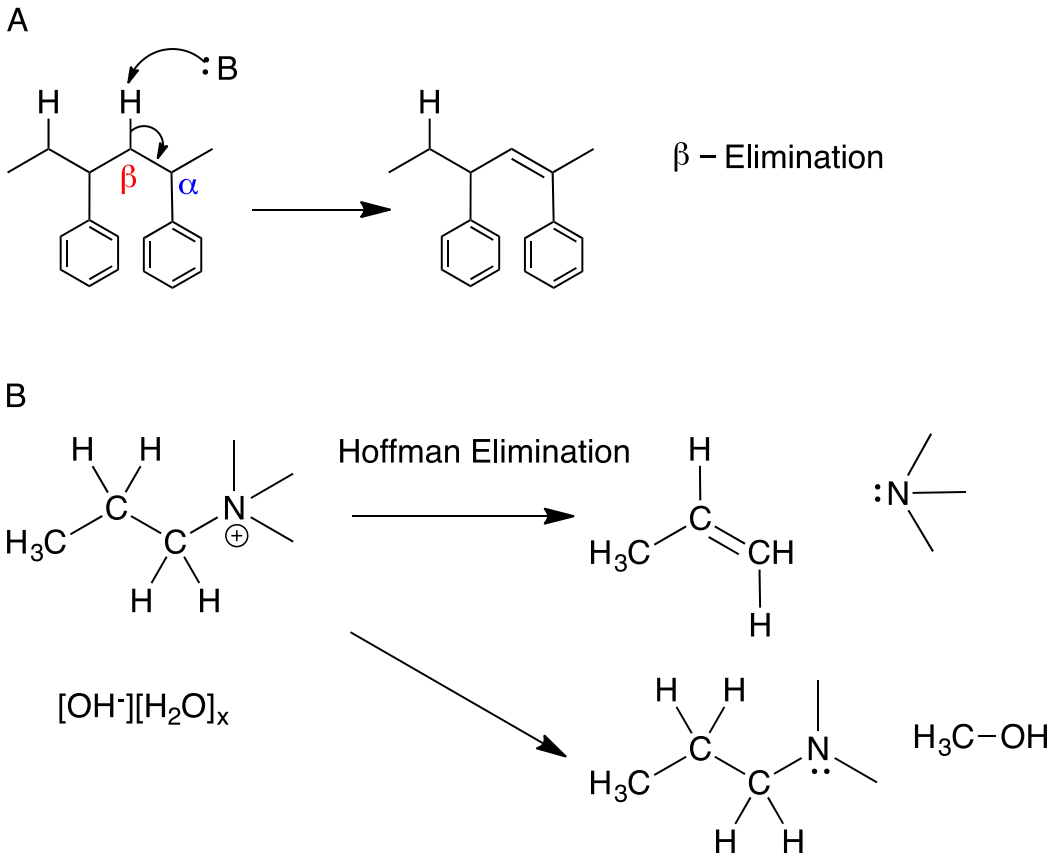

Figure 3 - Anion exchange membrane elimination pathways. a) Shows traditional β-elimination resulting in mechanical instability. b) Displays the more specific Hoffman Elimination scheme that results in the net loss of ionic conductivity.

Significant effort has also been put-forth in the direction of developing functional charge-carrying moieties and associated “chains” that are not readily susceptible to Hoffman-type degradation pathways.[13]

1.3 Lignin and Biomass

At the present time, more than three quarters of the world energy production relies upon the use of fossil-based fuels.[14] The other quarter is provided primarily by hydro-electric, nuclear and biomass with only about 1% of the current power production for the world coming from solar and wind. Depending on varying estimates, biomass actually accounts for as much as 10-14% of the total world’s energy production.[15] Exploration in the area of sustainable, renewable energy production is an important endeavor towards curbing carbon and other harmful emissions affecting climate and other environmental degradation or damage. To that end, biomass provides an extremely abundant and generally carbon neutral feedstock for the production of energy and many industrial chemicals and commodity materials.[16] In particular, lignin, one of the main components of woody or stalky biomass, is the second most abundant biological compound on the planet, making it an ideal source for the production of power or as a precursor material.[17,18]

The conversion of biomass for energy production has been an important and fruitful field of research for the last 40 years. Stalky and woody plants comprise several different types of diverse polymeric biomaterials. Lignin, itself, contains a significantamount of chemical potential energy as studies have shown that lignin

has a comparable energy density to wood coal or charcoal (bituminous) as well as containing thirty [30] percent more energy than cellulosic carbohydrates currently used to make biofuels, or, approximately 2.27 KJg^{-1}.[19,20] The higher heating values of woody biomass have also been calculated using a variety of methods, all of which indicate that the energetic value of biomass sources increase linearly with increasing lignin concentration.[21] The potential for biomass and, more specifically, lignin rests in the exploration of efficient processing techniques for catalysis or modification – as currently, it is exactly the difficulty in efficient processing that has relegated lignin to being used mostly as a low-energy combustible fuel. A process diagram, detailing the numerous industrial pathways for biomass conversion is shown in **FIGURE 4**. This translates into an immense amount of potential energy, provided that efficient methods of processing or catalyzing are implemented.[22]

Following the fractionation of lignin from cellulosic and hemi-cellulosic materials, it can then undergo several different processes from which to extract suitable fuel – namely high temperature cracking, pyrolysis and gasification.[23, 24]

1.3.1 Composition

Lignin is a long, heterogeneous polymer associated with both woody and stalky (i.e. grasses and shrubs) plants. It is the most abundant naturally occurring polymer on earth, second to lignocellulose.[25] Lignin is thought of as a sticky glue type material

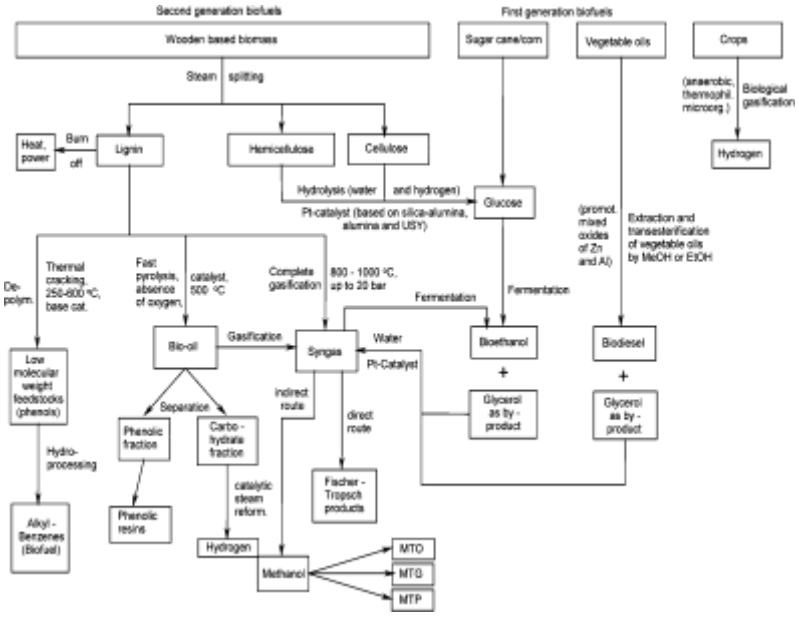

Figure 4 – Biomass Processing Schematic (Stöcker, 2008)

that serves the purpose of binding together the fibrous, cellulosic structural strands within plants. It is also believed to protect plant cells from pathogenic attack.

Although heterogeneous and highly irregular, there are generally considered to be three chemically distinct families of lignin: softwoods (gymnosperms), hardwoods (angiosperms) and grasses and annuals (graminaceous).[26] These three classifications are generally represented by a predominance of one or another phenylpropyl subunit called a monolignol. Guaiacyl (G) lignin, or that having a predominance of monosubstituted phenol units, is mainly found in softwoods. Guaiacyl/syringyl (G/S) lignin, similarly, is comprised predominantly mono- and di-substituted phenol units and is mainly found within hardwoods.[27] Coumaryl lignin is the least substituted of the three polymeric classifications and is mainly found in grassy annuals and perennials like switchgrass. A schematic of the phenylpropane

units which dominate each native lignin type is seen below in FIGURE 5 as a function of the R-groups that differentiate them.

Currently, certain varieties of willow, switchgrass (indigenous to the North American grasslands) and hybrid poplar trees are being grown for the purpose of harvesting potential bioenergy crops, however, none have been scaled to commodity-level harvestable resources for energy production.[28] A prime characteristic of lignin is its amorphous structure, which probably translates to its high biological stability and also for its intractability regarding industrial processing.[29,30] As a feedstock, this material has high potential as both a fuel source and a starting material for several commodity chemicals. Due to the numerous and varied energetic linkages associated with the lignin molecule, it would be highly advantageous to utilize a robust and specific catalyst to cleave these linkages in

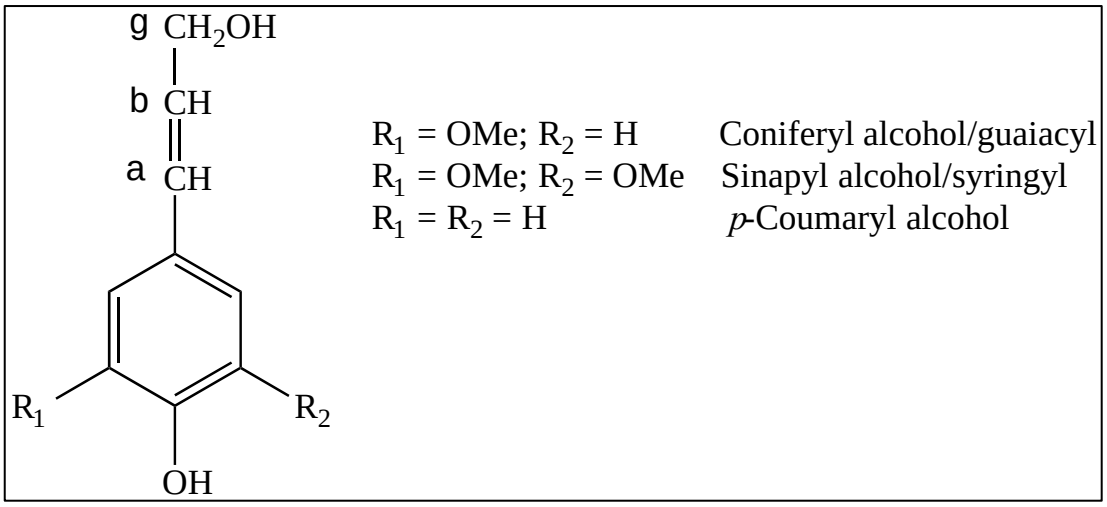

Figure 5 - Lignin phenylpropane subunits

order to degrade the polymer into a more pliable and useful set of molecules. FIGURE 6 shows a generic schematic of the lignin polymer and several of the important linkages associated with the molecule. Certainly, the frequency of particular linkages is dependent upon the particular source of the lignin. The β-O-4 linkage is generally the most prevalent in lignin and its cleavage, as well as that of other prevalent bonds, constitute some of the main, low molecular weight aromatic subunits used to characterize the lignin substructure.[31]

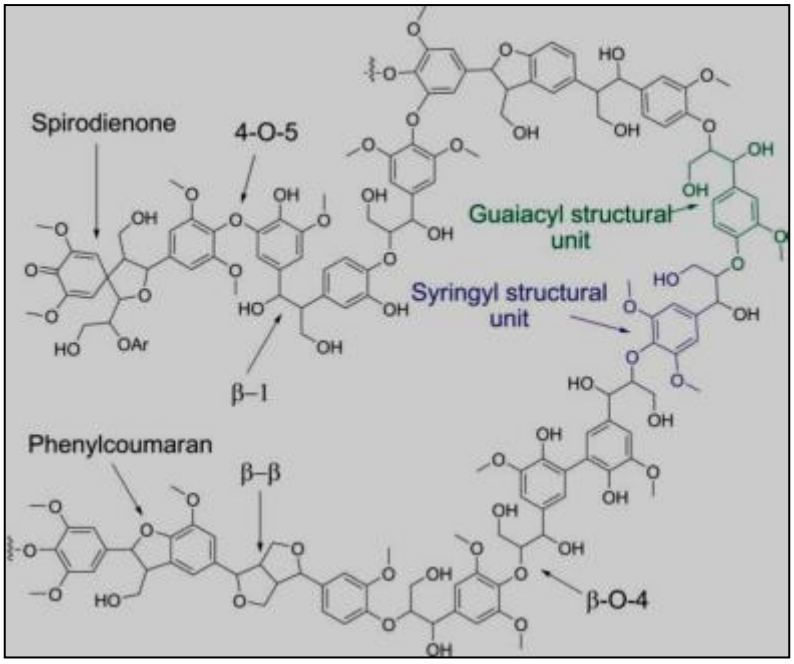

Figure 6 - Schematic Representation of Hardwood Lignin (Zakzeski, *Green Chem*., 2010)

CHAPTER 2 –

ELECTROCHEMICAL OXIDATION OF LIGNIN MODEL COMPOUNDS

2.1 Abstract

Heightened interest in sustainable energy sources have led to a multitude of forays into technologies dealing with biomass refining and energy conversion. In considering renewable biomass as a potential unmodified material for energy and chemical production: while it offers attractive possibilities as a virtually unlimited feedstock, the inherent complexities associated with the heterogeneous lignin polymer make the problem of efficient processing a difficult one.

In this chapter, we investigate the use of lignin as a sustainable fuel source for the electrochemical production of power or hydrogen. It is well known that certain organometallic Schiff bases have been shown to oxidize *para*-substituted phenolic monomers in batch reactions, and utilizing this approach, we show that it is possible to electrochemically recycle or re-activate these organometallics in order to allow the reaction to continue to proceed without the use of a strong Bronstead base. Using both electrochemical methods as well as spectroscopic techniques, an in-depth approach is taken to characterize the redox behavior of these molecules and show that electrochemical regeneration is possible, however, with certain limitations based around the salen ligand stability.

2.1 Introduction

Lignin is one of the three components of unmodified biomass and is regarded as one of the most robust and ubiquitous biopolymers in nature. Non-cellulosic biomass has been of interest to the scientific community as possible renewable energy feedstock for a large portion of the last century. To date, however, inadequate processing efficiency as well as the relative low cost of fossil fuels have led to its sole usage as a source of combustion fuel – mainly for paper mills. While lignin-containing biomass materials have been shown to be a relatively high quality fuel for combustion, the potential remains for this material to be utilized as a surrogate for petroleum in the petrochemical industry or as a possible source of clean hydrogen in a flow-battery set up.

There are several options for the catalytic oxidative degradation of lignin and lignin precursor molecules. One particular class of materials, known as metal salens, have been shown to readily oxidize a number of *para*-substituted lignin model compounds with a high degree of selectivity.[32] Metal salen class molecules are organometallic compounds, which are often planar in geometry (quaternary coordination) unless ligated axially with one of a number of organic bases. They take advantage of the multiple potential oxidation states of transition metals as well as their binding affinity to molecular oxygen in order to carry out molecular oxidation.

Used as recyclable electrocatalysts, the research indicates that metal salen molecules can be used in the capacity to oxidize downstream lignin feeds without the use of additional strong oxidizers to rejuvenate the oxygenated adduct for

continued catalytic activity. Literature has shown that several of these molecules exhibited reversible or quasi-reversible cyclic voltammogram behavior – producing a regular and symmetrical triangle waveform for a large range of voltammetric scan rates.[33] This research endeavors to explore the possibility of electrochemically regenerating cobalt salen materials in non-aqueous environment. By employing various electrochemical and spectroscopic techniques, cobalt salen is characterized to determine its potential suitability as an electrochemical mediator in the oxidation of lignin model compounds.

2.2 Experimental Methods

Electrochemical measurements were performed using a BioLogic SP-200 single-channel potentiostat and a Pine Instruments MSR rotating disk electrode apparatus with speed controller. Electrochemical measurements were performed in dry, Burdick and Jackson HPLC grade acetonitrile. A 3-electrode cell was used for all measurements employing a separated working, counter and reference electrode. Ferrocene was used as an internal reference by making a quasi-reference electrode via the method provided by IUPAC.[34,35] Measurements were performed in 60 mL of solvent which were saturated with either nitrogen or oxygen as necessary by 15 minutes of continuous bubbling. Cobalt salen, pyridine, and other reagents were commercially sourced and employed without further purification or modification.

UV-Vis spectroscopy was performed using a ThermoScientific Evolution 600 dual cell Photospectrometer. All measurements were taken using a 2-cell, dual beam system. Cuvettes were identical, quartz, 1cm cells. The reference cell

contained pure acetonitrile while the sample cell contained the material(s) of interest in a concentration of 2 millimolar in acetonitrile. The reference (I_o) and sample (I) signals were measured simultaneously and the absorbance given as a ratio of the two measurements and related to the transmission. The reference cell was used as a relative value of 100% transmission (T).

$$A = -\log\frac{I}{I_o} \qquad [2.1]$$

FT-IR was performed on a Bruker Vertex Series 80 spectrometer. All samples were measured in a Pike Technologies liquid absorbance cell with KBr cell windows. Sample compartment was purged with dry N_2 for 5 minutes prior to sampling to remove atmospheric moisture. All spectra were baseline corrected using 2nd order Savitzky-Golay smoothing.

EPR spectroscopy was performed on a Magnettech Miniscope MS400 EPR spectrometer using a Magnettech H03 temperature controller. Spectra were taken between 200 and 220K. Aliquots that were taken at time points were immediately frozen in liquid nitrogen to halt catalytic activity at the recorded time.

2.3 Results and Discussion

2.3.1 Electrochemical Characterization

Indeed, in our research, we were able to reproduce this reversible cyclic voltammogram waveform in acetonitrile and utilizing a standard glassy carbon disc

electrode as shown in FIGURE 7. By varying scan rates from 5 to 500 mV s^{-1}, various plots were generated that allow for an electrochemical description of the catalyst system in organic solvent. As shown in FIGURE 7B, based on the relationship represented by the Randles-Sevcik equation, for a reversible redox system, peak current response should vary linearly with the square root of scan according to equation 2.2 where i_p is peak current, n is the number of electrons transferred, A is the active area of the electrode, D is the diffusion coefficient, C_i is the concentration of the species of interest and υ is the scan rate.

$$i_p = (2.69\times10^5)n^{1.5}AD^{0.5}C_i v^{0.5} \qquad [2.2]$$

Part B of the figure clearly shows that the system is highly reversible through 500mV/s although some peak separation occurs as scan rate increases. This is expected as the rate of the oxidation outpaces the rate at which potential is applied. At scan rates of 5-10 mV/s, the peak separation (ΔE_p) was below 0.07V which, according to a simplification of the Nernst equation [2.3] concerning potential and electron transfer, proves to be quite representative of a reversible one-electron transfer - where n is the number of electrons transferred during the reaction.

$$\Delta E_p = \frac{0.058}{n} \qquad [2.3]$$

Following the figure to part C, the Laviron plot was used to describe the electrode-catalyst interaction considering the possibility that the catalyst interaction with the electrode was approximating the behavior of a thin film or adsorbed species.[36] Using the equation set [2.4] forth by Laviron in his series of papers covering such interactions, it is possible to use the relationship between the peak potential (E_p) and the natural log of scan rate (υ) to determine experimental values for the formal standard redox potential, $E^{o'}$, the electron transfer coefficient, α, and the electron transfer rate, k_s. By estimating the slope of the linear region of the Laviron plot, the value of αn was estimated to be 1.26 and k_s was estimated to be ~300 s^{-1}.[37,38,39,40]

$$E_p = E^{o\prime} + \frac{RT}{\alpha nF}\left[ln\left(\frac{RTk_s}{\alpha nF}\right) - ln(\upsilon)\right] \qquad [2.4]$$

Using equation 2.4, where *R* is the gas constant 8.314 J $K^{-1}mol^{-1}$, *T* is 293K and *F* is the Faraday's constant, it is possible to determine the value of k_s. The standard redox potential was graphically derived from part D of **FIGURE 7** which shows the relationship between potential (V) and scan rate (υ) as scan rate is extrapolated to zero. That value was determined to be approximately -0.384 V. vs the internal standard ferrocene/ferrocenium.[41]

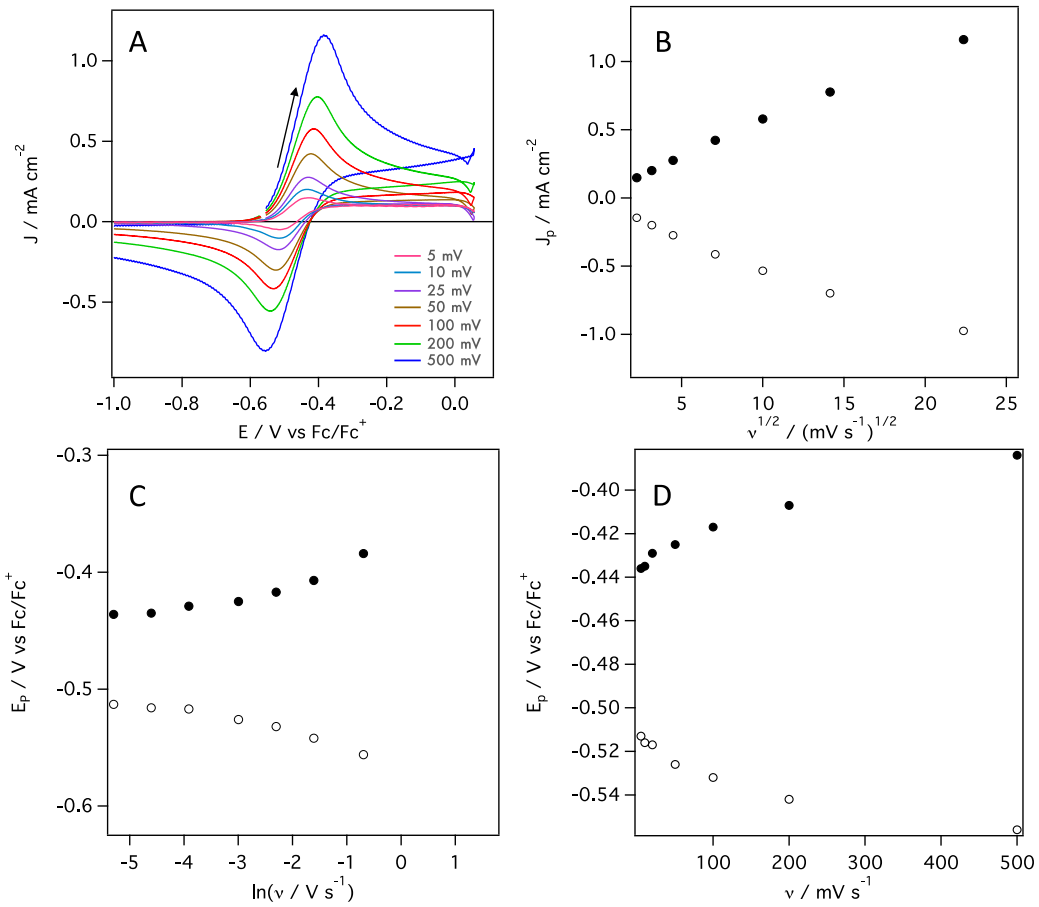

Figure 7 – a) Cyclic voltammetry of Co(II)salen relative to ferrocene/ferrocenium (Fc/Fc^+) in acetonitrile under nitrogen with varying scan rate; b) Randles-Sevcik plot illustrating the linear relationship between peak current density (J_p) and the square root of scan rate; c) Laviron Plot illustrating the relationship between peak potential and ln(scan rate); d) plots the relationship between peak potential and scan rate that shows the potential drift as scan rate is pushed higher.

Follow-on experiments were designed to probe the possibility of using these salen class molecules in a reversible redox couple to catalytically oxidize phenolic monomer model compounds and subsequently use the electrode potential to then oxidize the newly reduced catalyst thereby re-activating it and allowing for additional substrate oxidations. The chemical and electrochemical schematic of the experiments are conceptualized in **FIGURE 8**. In this type of cyclic voltammetry experiment, the wave shape takes on the visual characteristics of a more irreversible electrochemical system, however, what is being described chemically by this shape is a rapid two-step reaction occurring at the surface of the electrode which exhibits the type of current response shown below. As the potentiostat sweeps forward potentiometrically (forward sweeping is analogous to movement toward more positive potentials), the cobalt-salen catalyst is chemically oxidizing a substrate in the bulk solution. During much of this time, no current response is exhibited, as the redox potentials for the cobalt salen have not been reached. As the system is uniformly mixed, one can assume that this chemical reaction is occurring homogenously throughout the mixture and that the electrode behavior has little bearing on this step. However, as the potential sweep approaches the redox potential of the catalyst, a current response is exhibited. This measured current is a response to electrochemical oxidation of cobalt-salen(py)-O_2H occurring at the surface of the electrode. This sequence is indicative of a EC', or catalytic, mechanism. In this case, as shown in part A of **FIGURE 8**, the chemical step regenerates the initial reduced form of A. Part B of this figure shows the EC' reaction as it relates to the Co(salen)py-O_2 system in the oxidation of a phenolic substrate.

As illustrated, It is important to note that the chemical reaction that occurs everywhere in the bulk solution does so regardless of the behavior of the electrode. After the catalyst oxidation phenomena, the potential scan begins to reverse (potential moves more negatively). At the electrode surface, the newly oxidized catalyst system is chemically oxidizing the substrate while itself is being reduced. For this reason, in a reaction with facile kinetics, little to no reduction current is seen on the reverse scan because all of the catalyst material at the surface has already been reduced. As scan rate is increased, less catalyst is oxidized and eventually, the equilibrium in the bulk begins to shift toward the metal-salen-H catalyst. As this happens, the reduction current starts to appear. Likewise, if the concentration of the substrate is too low, the bulk concentration will not allow for the catalyst to re-oxidize another substrate molecule at the electrode surface such that, upon the reverse potential sweep, an increasing reduction current will be exhibited.

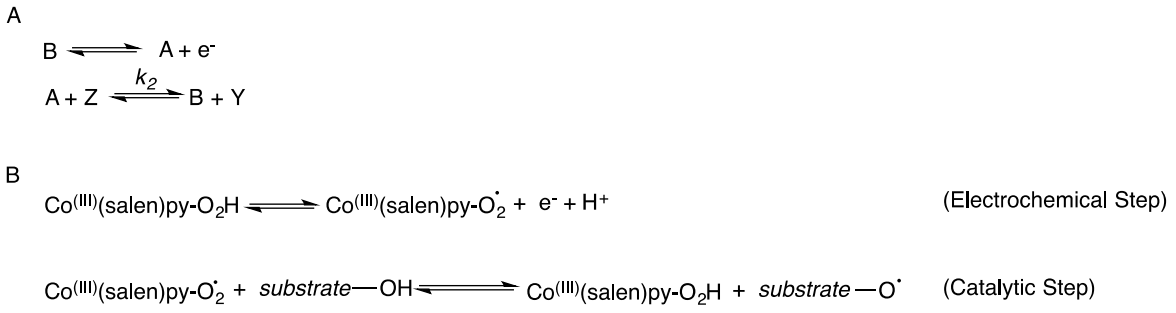

Figure 8 – A) The general kinetic reaction scheme of the catalytic electrochemical reaction (EC'). B) The general mechanistic schematic illustrating the EC' reaction as it relates to catalytic oxidation of a phenolic substrate by Co(salen)pyr-O_2.

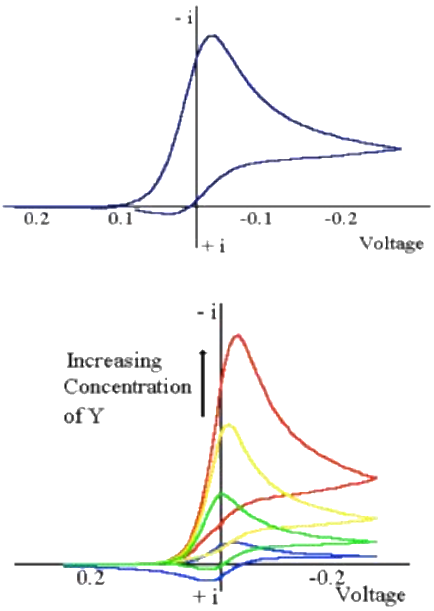

Figure 9 – Generic electrochemical behavior of a cyclic voltammogram illustrating an EC' mechanism. As the concentration of substrate (Y) is increased, the oxidative current increases while the reduction peak disappears. The colors are representative of different concentrations of substrate, resulting in increased peak current.

To probe the chemical-electrochemical catalytic properties of this system, a set of experiments was developed to determine if the EC' CV response would be exhibited. A general example of an EC' CV is displayed in **FIGURE 9.** In this case, the wave form of the EC' mechanism looks visibly like that of a quasi-reversible to irreversible redox reaction. For most of these experiments, syringyl alcohol was used as the substrate (labeled 'Y' in the figure) due to its simplicity as a phenolic monomer as well as its availability and relevance to the structure of lignin itself. A

solution of 5mM syringyl alcohol was bubbled under oxygen for 15 minutes and then kept under an oxygen atmosphere for the remainder of the experiments. 0.2 molar equivalents of the 4-coordinate salen catalyst was added to the solution and allowed to equilibrate for 15 minutes while stirring. In order to probe both the catalytic nature of the system as well as the importance of a variety of axially binding ligands to the reaction process, in this case pyridine, a titration experiment was performed while performing a traditional CV. As shown in **FIGURE 10**, as pyridine is titrated into solution and allowed to equilibrate, the reaction kinetics seem to improve. Due to the relatively constant concentration of substrate (small effective area of electrode results in inconsequential quantity of substrate oxidized during each cycle, relative to the bulk), the oxidative current response stays reasonably constant. The difference, however, may be seen in the reduction currents. With no pyridine added to the system, a reduction current is clearly shown -0.6 V relative to ferrocene/ferrocenium.[42] As pyridine is titrated into the system and allowed to equilibrate, the oxidation current response shifts and increases slightly as well as the reduction current begins to shift and decay altogether. The optimal molar ratio seems likely to lie between 1 and 2 molar equivalents of pyridine based on the fact that at 2 eq, the system begins to exhibit an additional oxidation feature, which is either the direct oxidation of free pyridine in the bulk solution or the competing oxidation current response of the bi-axially ligated salen adduct. This makes sense considering that it is reasonable to assume that all the pyridine does not make a complex with the metal in a 1:1 ratio and that, because of thermodynamics, it is likely necessary to use a slight molar excess of the ligand to ensure global ligation of the

metal centers. The true purpose of this titration was to confirm the hypothesis that large molar excess of the amine, while useful in some scenarios when using a small amount of metal is paramount, is in this case inhibiting the reaction due to the high affinity of pyridine for cobalt and the tendency to di-axially ligate the metal. This Co-salen- pyr_2 adduct is catalytically inactive in that the cobalt is no longer able to accept dissolved oxygen and therefore cannot form the cobalt-superoxo adduct responsible for substrate oxidation.

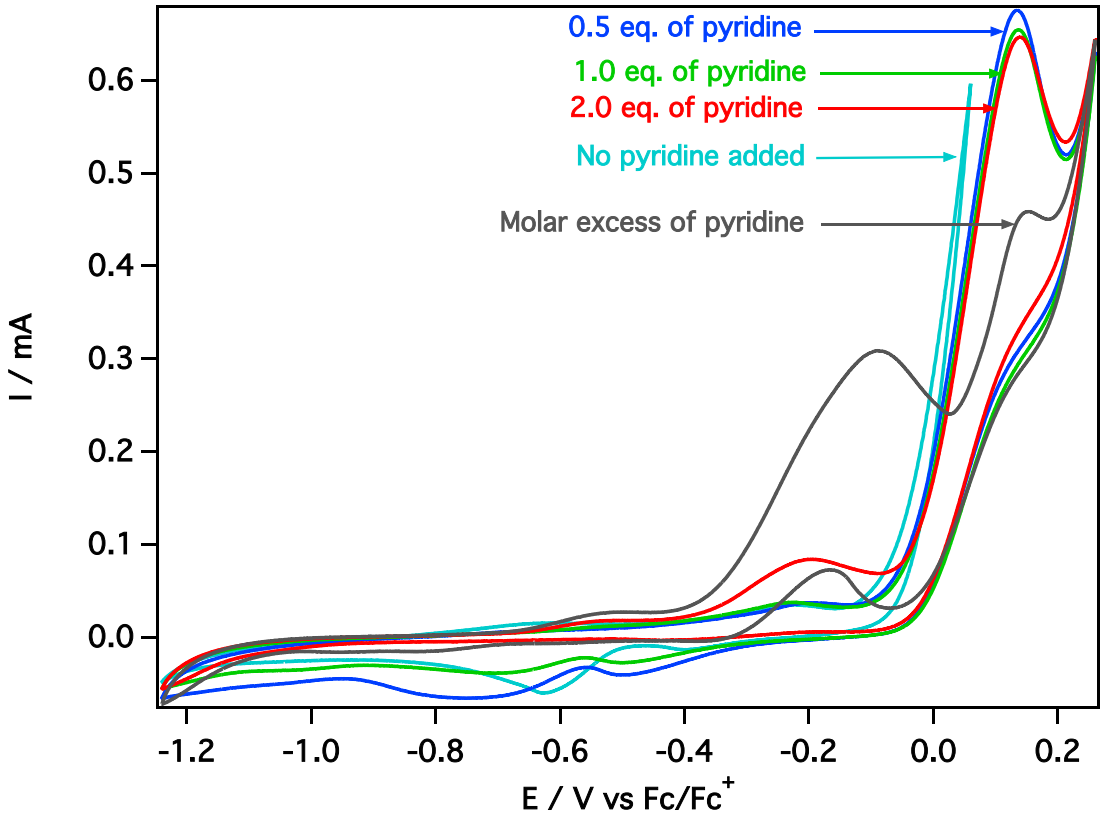

Figure 10 – CV of a titration of cobalt salen wtih pyridine in a 5 mM syringyl alcohol solution (oxygen-saturated acetonitrile).

In order to differentiate between the electrochemical current response of un-ligated cobalt salen as well as the axially ligated species, cyclic voltammograms were measured for both oxygen and nitrogen saturated solvents. Exhibited in **FIGURE 11**, one can see that there is almost no change in intensity or voltammetric shift of peak current in the un-ligated salen species in both oxygen and nitrogen. This is due to the fact that the 4-coordinate cobalt salen complex is known to poorly bind molecular oxygen in the absence of an axial ligand like pyridine.[43] The addition of a 1:1 ratio of free pyridine to cobalt to the solution causes the reduction peak potential to shift negatively. As proposed in the literature, cathodic peak potentials are strongly influenced by the basicity of the axial ligand. In this case, free pyridine in solution has likely complexed with cobalt in the axial position which, in the presence of oxygen, has caused this potential shift and quasi-reversible electrochemical waveform.[44]

In order to prove the theory that it is possible to use the cobalt-salen complex as an electrochemical mediator, a substrate was chosen as a model compound and analog to lignin. Syringyl alcohol was used in this case because it is a common lignin model because it contains both the phenolic and benzylic hydroxyl units that occur naturally in lignin.[45,46] Both of these functional units have significantly different pKa (phenol is approximately 10^5 times more reactive than benzylic –OH) values and therefore require significantly different oxidative potential.

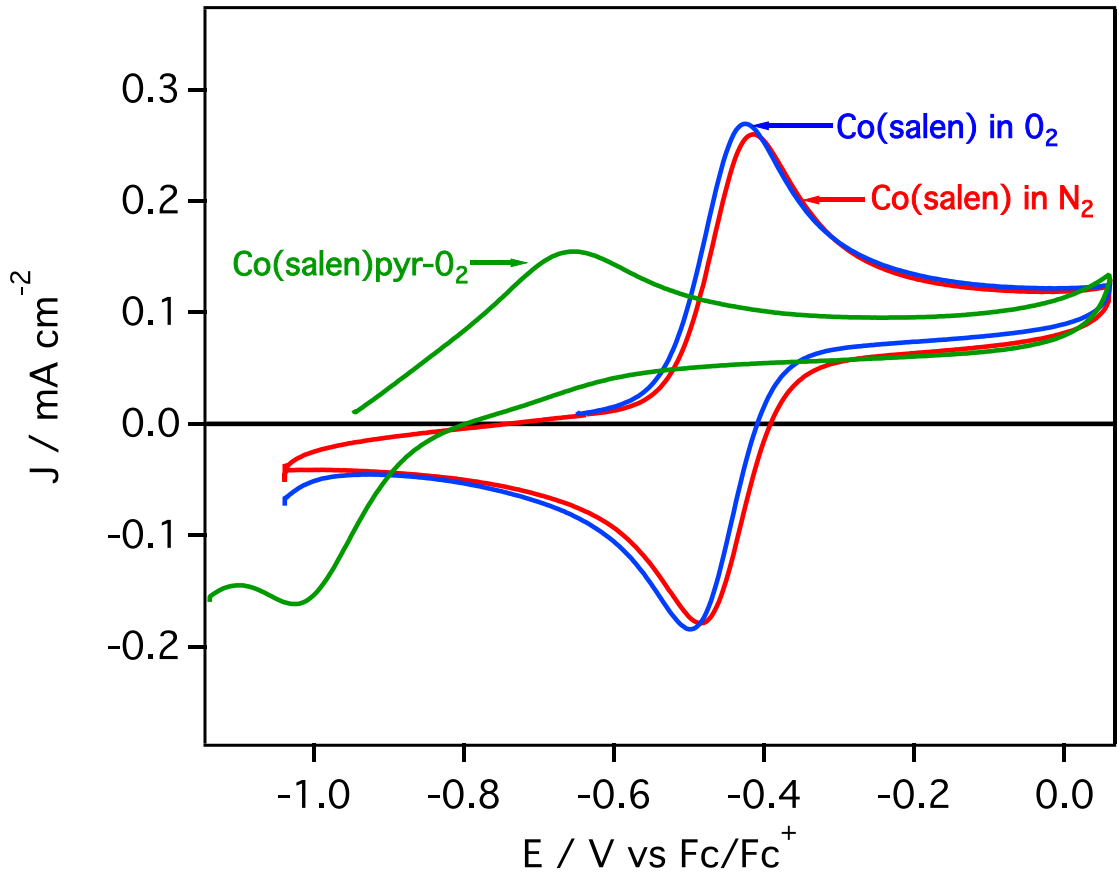

Figure 11 – Cyclic voltammetry of ligated and un-ligated Co(II)salen in acetonitrile

As shown above, a traditional EC' system is a two-step mechanism involving an electron-transfer step (E) and a chemical or catalytic step (C). The electron transfer step generates the active species of the catalyst (either by oxidation or reduction of the species) while the catalytic step, involving a substrate, returns the catalyst to the inactive form. If the catalytic step is sufficiently fast, the relationship between substrate concentration and peak current will remain linear. This is held by the relationship between concentration and peak current shown in the Randles-Sevcik equation [2.1].[47]

To probe the EC' behavior, both scan rate and the concentration of substrate were varied while the concentration of catalyst was held constant. As seen in **FIGURE 12**, the increase in substrate concentration resulted in a nearly linear increase in current density response – a factor of 2.5. Scan rates were increased to a maximum of 200 mV s^{-1} and the linear relationship was maintained. This indicates that the catalytic step of the system occurs rapidly enough to regenerate the inactive catalyst species at the electrode tip so that all (or nearly all) of the species in the diffusion layer is inactive. The absence of any reduction peak during the negative potential sweep also confirms the nature of this EC' reaction.

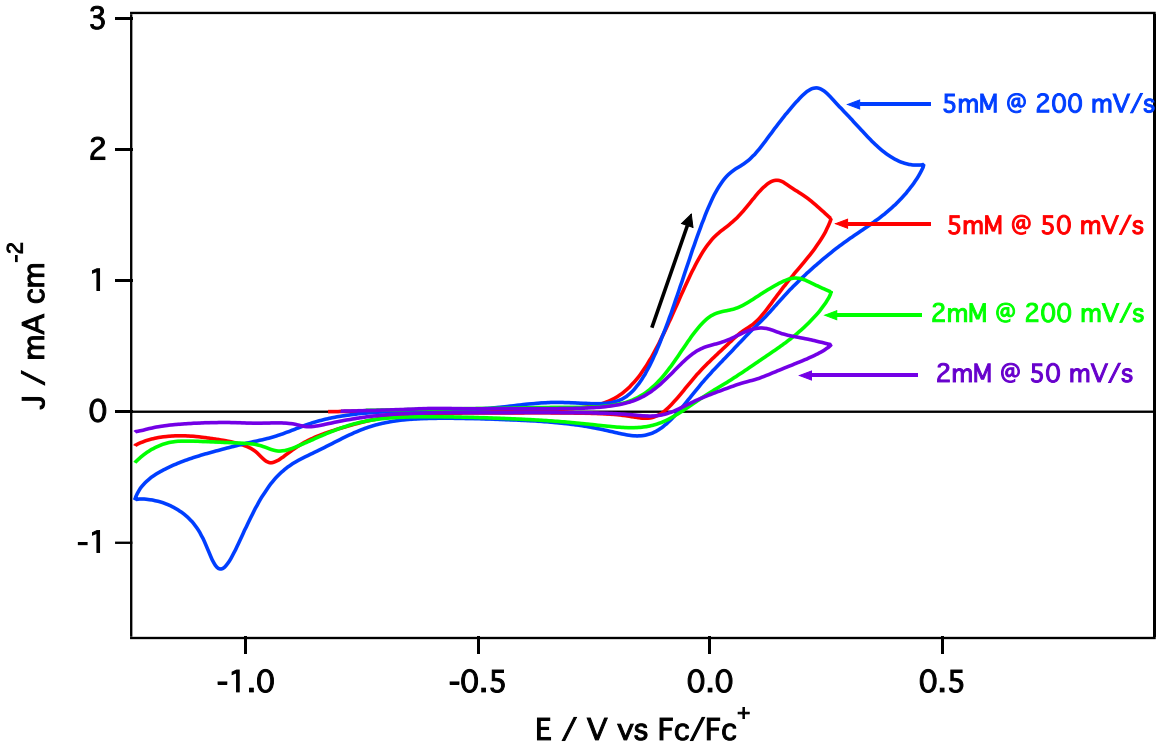

Figure 12 - Cyclic voltammogram of CoSalen-pyr adduct with varying concentrations of substrate in bulk. Arrows denoting concentration are in reference to syringic alcohol, used as a monomer model reaction to simulate the functional groups present in lignin.

Both the cyclic voltammetry titration experiment and the complexation experiment seem to electrochemically indicate the importance of the axially binding ligand to the overall catalytic activity of the dioxygen adduct as well as the metal's overall affinity to free oxygen in solution. In other words, the axial bound ligand seems to increase the activity of the catalyst system by stabilizing the metal center oxidation state and increasing the metal affinity toward di-oxygen in solution by lowering the overall bonding orbital energy.

A UV-Vis titration experiment was performed as an augment to the cyclic voltammetry experiment to continue to explore the nature of the axial ligand. Identical 1-cm quartz cuvettes were used simultaneously for light and dark measurements and samples were diluted with regard to the Beer-Lambert Law [2.5], which dictates the relationship between a solution's absorbance and the summation of the molar attenuation coefficient and concentration of each attenuating species.[48] Indicated molar equivalents of neat pyridine were titrated into 2mL aliquots of 2mM cobalt(II)salen, which was held at fixed concentration and then saturated with an appropriate gas. The laboratory did not have the capability to change gases (in order to start with a nitrogen-saturated solvent) so gases were bubbled in a separate laboratory prior to running successive experiments. Two exclusive experiments were performed in both nitrogen and oxygen. This factor may certainly have contributed to some aspect of the unexpected results for this experiment.

$$A = \varepsilon lc; \text{ where, } A = \Sigma A_i = l \Sigma \varepsilon_i c_i \qquad [2.5]$$

Based on the fact that 4-coordinate cobalt salen molecules are planar it is known that that *N*-donors like pyridine form adducts with the cobalt atom in the axial positions (±z). Shown in **FIGURE 13**, pyridine and oxygen can complex with the 4-coordinate cobalt salen complex to form an octahedral. The first titration was performed in an inert environment (N_2 blanket). As the concentration of ligand was increased, the expectation was that electronic transitions for n→π*, d→π* and d→d would all increase as a function of the N-donor ligand's ability to act as a weak π-acceptor in a metal-ligand back-bonding scenario. Additionally, due to the high-field ligand trait of increasing the metal d-orbital splitting energy, a low-spin cobalt complex is most likely.[49,50] A second titration was performed under an oxygen blanket. Due to the polarization effect of the oxygen on the metal, the d→d transition energy should theoretically increase as oxygen binds in increasing concentration and the d_z^2 orbital gains additional electron density. Essentially, the Co-O bond may act more like an ionic bond where the local electron density is significantly more focused on the oxygen atom than on the metal.[51] If this were true, one would expect the binding transitions to increase as oxygen binds to the metal center due to the localization of electron density on the more electronegative, out-of-plane di-oxygen. The additional binding of oxygen should also be indicated by a wavelength shift, as the metal center experiences an oxidation state change from Co(II) → Co(III). The electronic orbital arrangements of the different oxidation states of the complexed cobalt species and the geometric/spatial arrangement of the ligand field around the metal can be seen in **FIGURE 13**.

These hypotheses were not supported by the data as all aforementioned transition energies decreased as a function of increasing ligand concentration. The decrease in n→π* and d→π* transition energies is potentially caused by the Lewis base characteristic of the axially bound pyridine. The most likely cause for this, however, is the fact that the addition of an axial ligand alters the metal-ligand (M-L) geometry from square planar to square-pyramidal (disregarding potential solvent effects). This geometric change causes a substantial decrease in orbital splitting

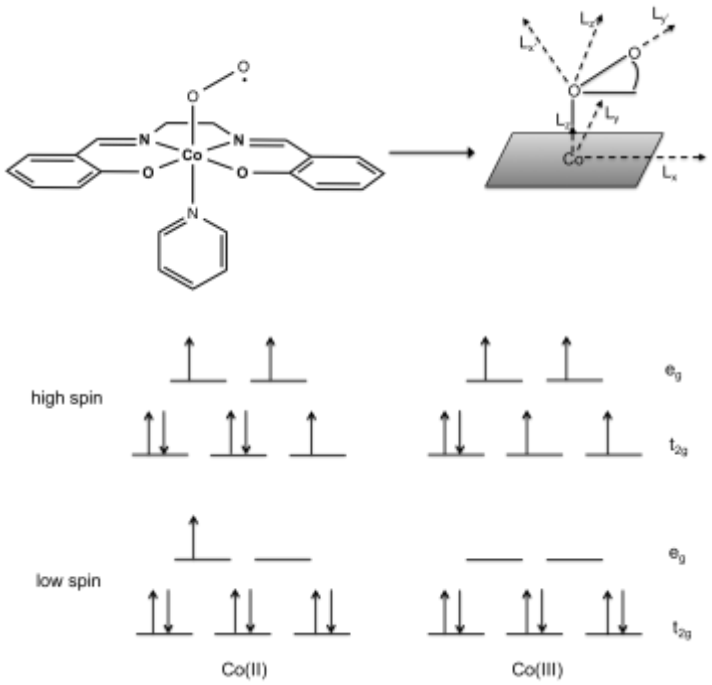

Figure 13 - Cobalt salen axial binding configuration and coordinate system

energy which is exhibited in the decreased absorptions shown in **FIGURE 15**. The π-accepting character of the N-donor ligand during 1:1 complexation, which was

anticipated to produce a positive correlation, is unseen during this UV-Vis analysis due to the greater difference in orbital splitting energy, Δ_o, caused by the geometric change. The absorption data for this experiment is tabulated in **TABLE 1**.

The effect of metal-ligand geometry on orbital splitting energy differences are illustrated in **FIGURE 14**. Co(II)salen is a highly conforming example of a square planar molecule, as seen on the right of the figure. In this case, the orbital energies of the HOMO (highest occupied molecular orbital) and LUMO (lowest unoccupied molecular orbital) are broadly spaced. This configuration results in a relatively large d-orbital transition energy.[52] For this reason, the Co(salen)-pyr-O_2 adduct shows a small relative d-orbital transition energy, relative to the non-pyridinium complex.

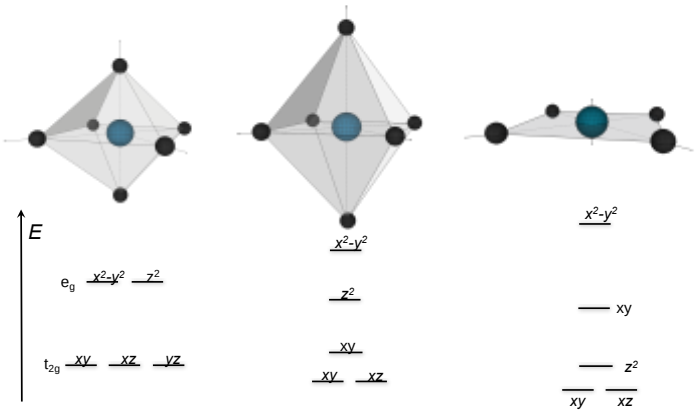

Figure 14 - Orbital energy diagram of the different ligand arrangements around a metal center. The diagram describes how bond length influences orbital energy.

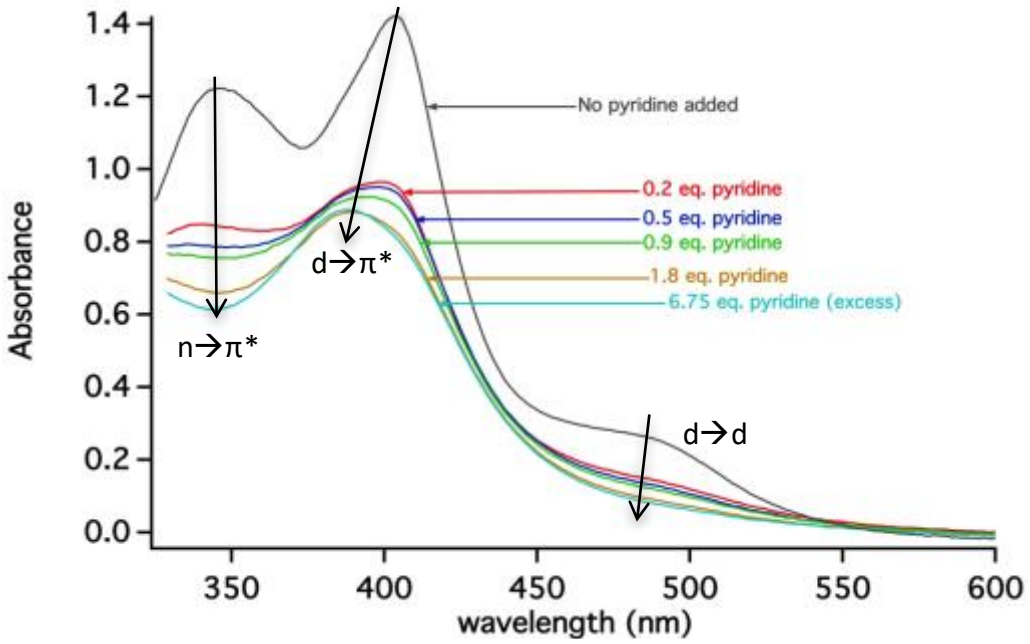

Figure 15 - UV-Vis spectroscopy of a cobalt salen axial ligand titration

Table 1 - Lambda(max) and absorbance values for the pyridine titration of Cobalt(II) salen in acetonitrile

Pure Cobalt Salen			Excess Pyridine		
λ_{max}	Absorbance	Transition	λ_{max}	Absorbance	Transition
347	1.223	n→π*	NA	---	n→π*
404	1.421	d→π*	386	0.886	d→π*
492	0.245	d→d	NA	---	d→d

An additional experiment was performed in which the ratio of pyridine to cobalt was varied while keeping the cumulative number of moles constant. This was performed in a nitrogen saturated environment. An isosbestic point was anticipated that would indicate the existence of two distinct species (Co-salen-pyr and Co-salen-pyr$_2$) in equilibrium with one another. As shown in **FIGURE 16**, a single isosbestic point appears near 560 nm. Physically, this point indicates the wavelength at which two different absorbing species share the identical molar absorption coefficient values. This result matches well with some previously published work on the subject.[53] The absorption data for this experiment is tabulated in **TABLE 2**.

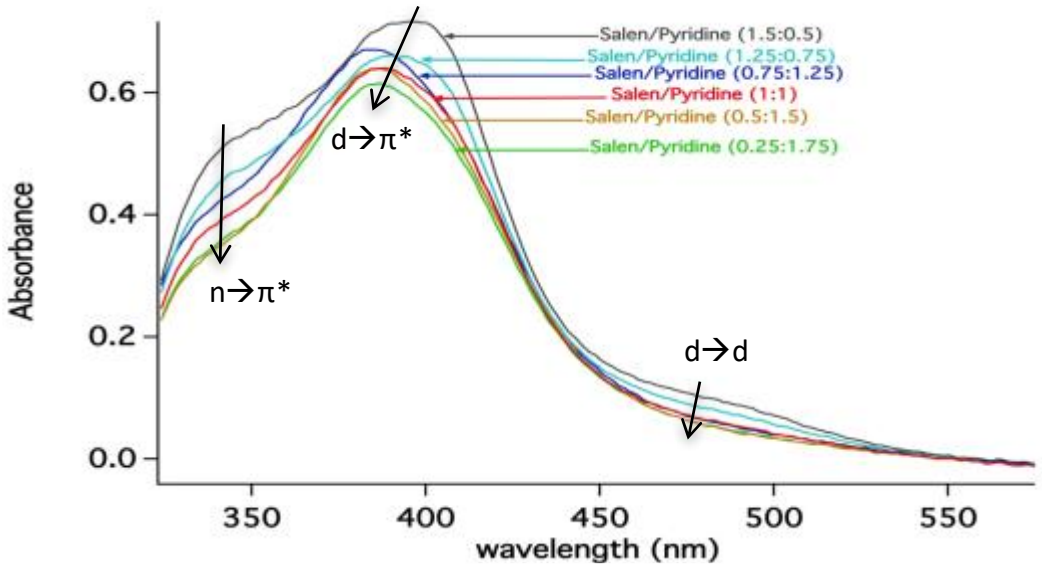

Figure 16 - UV-vis spectroscopy of Co(salen) in acetonitrile and varying ratio of pyridine ligand

Table 2 - Lambda(max) and absorbance values for the Co(salen) in the presence of increasing equivalents of pyridine. Increasing molar equivalents of pyridine resulted in the marked decline in absorbance measurements for all recorded transitions.

Salen/Pyridine (1.5:0.5)			Salen/Pyridine (0.25:1.75)		
λ_{max}	Absorbance	Transition	λ_{max}	Absorbance	Transition
342	0.512	n→π*	335	0.330	n→π*
395	0.716	d→π*	387	0.615	d→π*
489	0.088	d→d	NA	---	d→d

Using electron paramagnetic resonance (EPR) spectroscopy, it is possible to resolve the "out of plane" effect that the axial Lewis base ligand may have on the cobalt metal center of the complex. Cobalt(II) is a d^7 transition metal and can support several oxidation states, as is common amongst transition metals. To complicate the interpretation of the EPR spectra, both cobalt(II) and cobalt(III) can be paramagnetic and thus resolved via EPR depending on whether the system is high-spin or low-spin.[54] For this reason, the spectra were taken in an inert environment, having bubbled nitrogen into the solution for 30 minutes prior to the addition of the metal salen complex. FIGURE 17 illustrates the possibility that the Lewis base, pyridine, binds axially by means of electron pair donation and does not change the oxidation state of the metal, due to the absence of any significant Gauss shift. Also,

as shown above in **FIGURE 15**, there is no appreciable absorption spectra shift that would normally be associated with the color change that follows a change in oxidation state. Therefore, it is reasonable to conclude that the metal center remains cobalt(II). The crystalline 4-coordinate Co(II)salen is a square planar molecule and, in organic media, is most commonly a low-spin complex.[55,56] Because the orbital splitting energy, Δ, is higher than the pairing energy, P, (energy required to pair two electrons in the same orbital) the remaining electrons are energetically favored to form lower-energy pairs rather than occupy higher-energy orbitals as siglets.[57] Similar to DMF, acetonitrile can act as a weak Lewis base to ligate with transition metals. It is likely that the 4-coordinate cobalt(II) salen has only weak interactions with the organic solvent making the geometric conformation of the system a combination of planar and octahedron. If the solvent is thought of as a weak ligand, upon the addition of a stronger σ-donor ligand, like pyridine, it is easily displaced at the axial position. Pyridine, as an example used in this experiment, is a moderately high-field ligand in the spectrochemical series.[58,59] Since pyridine is a σ-donor and a moderate π-acceptor due to its end-on bonding, which causes unoccupied d-orbitals to act as lower energy π-orbitals, one would expect that ligation increases the overall Δ and tends to lead to low-spin complexes. With the addition of pyridine (1.1:1, pyridine to cobalt), the appearance of 8 hyperfine (hf) structures are resolved which indicate the complexation of 1 pyridine with 1 cobalt. This is in agreement with previous studies on cobalt complexation which also displayed 8 hf features after complexation with the d^7 cobalt (II) (I = 7/2).[60, 61]

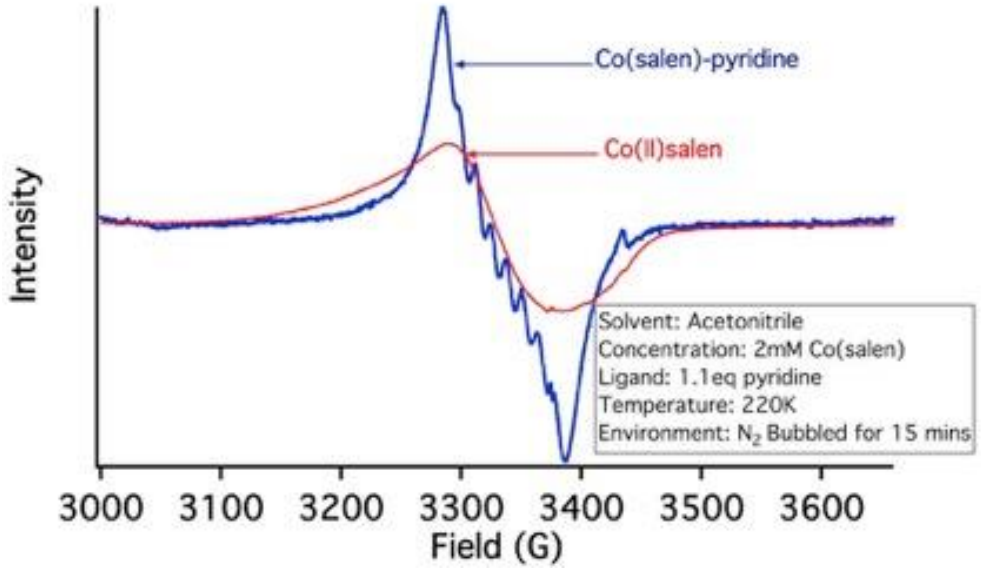

Figure 17 – Solution state electron paramagnetic resonance spectroscopy of cobalt(II)salen and cobalt(II)salen-pyr ligation in acetonitrile at 220k

An additional EPR experiment was performed in an oxygen saturated environment to determine how the Co(salen)-pyr-O_2 system would perform under electrolysis conditions. Using a platinum mesh electrode, a bulk solution of Co(salen)-pyr in O_2-saturated acetonitrile was added to an acetonitrile solution containing a molar excess of syringyl alcohol. The electrode was set to the oxidation potential of the Co(salen)-pyr-O_2H and aliquots were taken over an 18-hour period. An H-cell setup was used to separate the working and counter electrodes to that possible oxidation products could be characterized. In this experimental setup, catalyst in the bulk is free to react with available substrate (syringyl alcohol) while the reduced form of the catalyst is continuously oxidized at the electrode surface.

The results, shown in **FIGURE 18**, initially displayed the signature of a cobalt-superoxo adduct, as shown in prior publications.[62] The signal, however, began to decrease after 90 minutes. Prior publications have noted the instability of the cobalt-salen complex and a tendency for the ligand to decompose however, for less than 24 hours, elevated temperatures are required. Prior to taking the last sample at 18 hours, however, the solutions, which are normally a brownish-red color, had turned bright yellow and green on the counter electrode and working electrode side of the H-cell, respectively. This is almost certainly indicative of ligand decomposition.[44] The yellow color is likely cobalt(III) coordinated with 6 solvent molecules in an octahedral geometry. The greenish color, then, on the counter electrode side, is likely the reduced cobalt (II) species which, in tetrahedral geometry, have been reported green or blue.[63] Additional study is needed to identify the decomposition pathway.

FTIR was also employed in an attempt to characterize the system while holding a constant oxidation potential for cobalt-salen-pyr-O_2H adduct in the presence of syringyl alcohol. The results of this study are shown below in **FIGURE 19**. Four time-points were taken and aliquots were frozen immediately after sampling to halt the continuation of all chemical reactions.

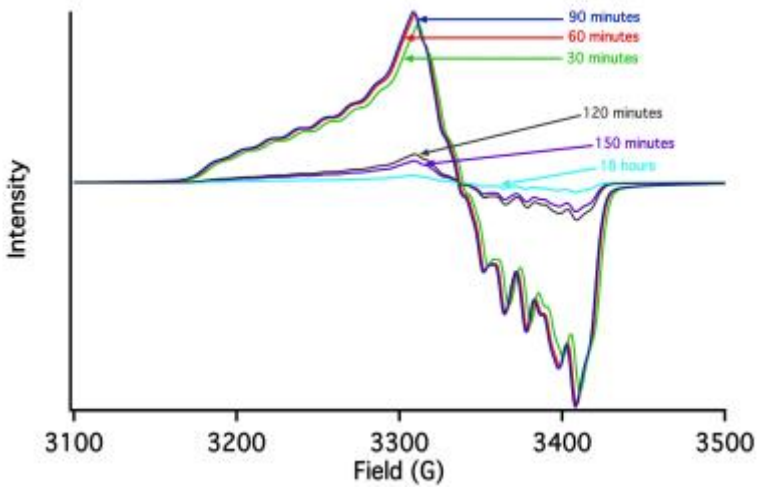

Figure 18 – Electron paramagnetic resonance of Co(salen) bulk solution reaction in molar excess of substrate while holding the electrode at the oxidation potential of Co(III). At timed intervals indicated in the graphic, aliquots of the mixture were taken and measured in the EPR. The reaction was performed in O_2 saturated acetonitrile at 200 K.

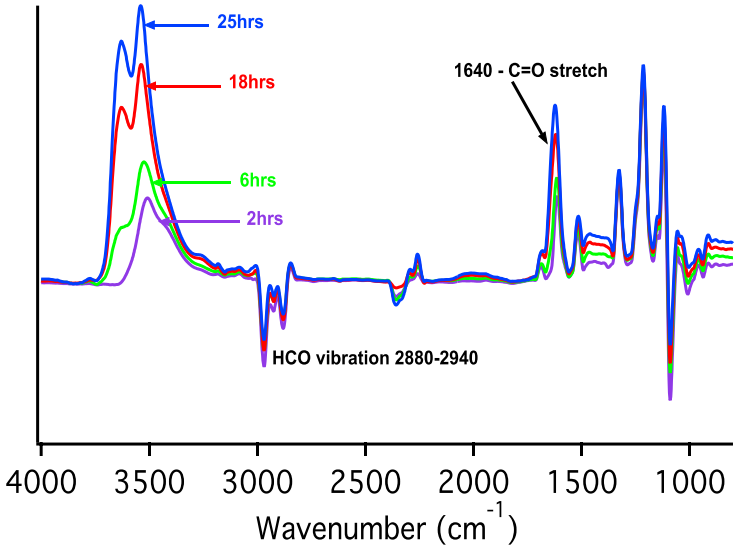

Figure 19 - FTIR spectrum of electrolytic oxidation of Co(salen)-pyr-O_2 in the presence of syringyl alcohol. Acetonitrile was oxygen saturated via bubbling for 15 minutes prior to addition of cobalt-salen.

As shown in prior studies, the FTIR spectra for the octahedral cobalt-salen-pyr-O_2 adduct does not change markedly from the square-pyramidal precursor.[64] As such, the background spectra was taken of the cobalt-salen-pyr-O_2 adduct in oxygen saturated acetonitrile to facilitate the characterization of the catalytic oxidation products. The most notable feature of the spectra is the increasing, bifurcated peak between 3500-3700 cm^{-1}. The nature of this increasing peak was wholly unexpected in that signatures associated –OH stretching (as is often the case with broad peaks ~3500 cm^{-1}) were expected to decrease. The literature reports that the initial step in the oxidation of syringyl alcohol relies upon the ability of the superoxo-cobalt adduct to oxidize the phenolic moiety, resulting in a resonance-stabilized phenoxy radical. It is this resonance form that is then trapped by an additional (or electrochemically oxidized) superoxo-cobalt adduct to form the benzoquinone with a molecule of formaldehyde.[65] This is supported by the increasing amplitude and shifting/broadening of the peak around 1640 cm^{-1}. This signature is likely caused by both the increase in concentration of the benzoquinone product as well as the increasing concentration of formaldehyde as a secondary product of the benzoquinone formation. As reported during the electrolytic EPR work, prior to sampling at the 18-hour mark, the working and counter electrode solutions had again turned yellow and green, respectively. This sample shows the distinct increase in the signature at 3700 cm^{-1} from shoulder to sharp peak as well as the continued increased amplitude of the peak at 3500 cm^{-1}. It is likely that one of these peaks increases as a function of the cobalt-hydroxy species formed during

the second step in the formation of the quinone. It has been reported that certain metal-bound salen ligands can be prone to decomposition via an imine reduction or alkylation route, however, it is unclear that this could be taking place in this system.[66] Additional study is needed to clarify the spectra associated with this system.

2.4 Conclusions

The goal of this research was to investigate the potential usage of cobalt salen molecules as an electrochemical mediator in the oxidation of lignin biomass in the production of fuel and/or hydrogen. Prior research had shown that certain metal-organics were redox active and that superoxo-cobalt-salen adducts were capable of catalyzing certain *para*-substituted phenolic compounds.

While the initial data seemed to indicate that Co(II) salen complexes were redox active and displayed reversible electrochemical behavior, additional characterization by FTIR and EPR seemed to indicate that the catalyst suffered from some type of deactivation pathway. This caused the rapid reduction of EPR signal for the superoxo-cobalt-salen adduct as well as significant bright yellow color change to the bulk solution around the working electrode. The mode of deactivation or degradation of the adduct is not clear. Further study would be needed to clarify the physical and chemical phenomena associated with these spectral results.

CHAPTER 3 –

LIGNIN MODIFICATION AND POLYMERIZATION FOR APPLICATION IN ELECTROCHEMICAL SYSTEMS

3.1 Abstract

Lignin is one of the most plentiful biological materials on the planet. Currently, the majority of lignin is produced as a byproduct of the paper industry pulping process and used as a combustion fuel by these plants. Lignin offers a cheap, readily available source of energy for these plants and it allows for the offsetting of the plant's carbon footprint.[67] Lignin, however, is not generally considered a high-energy fuel and therefore, burning it is at best, an inelegant solution to converting this aromatic, electron-rich heterogeneous biopolymer for energy or chemical production.[68,69] Due to the diversity in the structural and functional moieties present in lignin macromolecules, it has long been thought that the material could play a vital role in the production of commodity chemicals currently dominated by the petrol industry.[70] More recently, this work has extended into the realm of polymer synthesis, where lignin has been used as an inexpensive analog to petrol-based chemicals used to modify the morphology and physical properties relative to pure polymeric materials.[71]

Although the heterogeneity of the lignin polymer presents, likely, the largest hurdle to overcome in the efficient processing of the material, the sheer abundance of the material and the electron dense aromatic chains that dominate its structure make it an attractive surrogate for fossil fuel-based carbons. Using this premise as a starting hypothesis, the prior work and knowledge of the Zawodzinski group was used in the synthesis and testing of lignin-supported, non-carbonaceous, non-platinum group metal (PGM) oxygen reduction reaction (ORR) catalysts in acidic

media. Elongated lignin oligomers were also synthesized as ionic polymers to be used as an ionic conductive binder for use in the fabrication of fuel cell catalyst layers. These binders were also tested with some well-known, previously tested non-PGM catalysts for the ORR in alkaline media. Additionally, liberties were taken to explore a number of different synthetic routes for modifying lignin in a meaningful way so as to increases its utility as an anionic conducting polymer for application toward material modification in anionic exchange fuel cells and batteries.

3.2 Methods and Materials

Unmodified organosolv lignin was sourced in bulk from a local processing facility (TennEra). Rough numerical data were given for each batch concerning average molecular weight and polydispersity. For most of these experiments, lignin was used that measured an average molecular weight of 450 gram/mol with a dispersity factor of approximately 3.1 as measured by gel permeation chromatography (GPC) vs polystyrene (PS). Since larger molecular weight polymeric units of lignin are difficult to use in terms of approximating functional group numbers, 450 was assumed as the molecular weight for all molar equivalent (eq.) calculations. Based on an assumed structure from the literature, the 450g mol^{-1} would most likely account for a lignin trimer. Depending on the molecular configuration, polymeric lignin units of this size could have three to six possible hydroxyl groups to which specific functional groups could be attached. This is obviously important in terms of formulating appropriate synthetic methods for lignin

modification. Initially, selectively modifying lignin based on the different pKa values associated by the various structural moieties present on lignin to create bi/multifunctional materials was viewed as an attractive approach. This route was abandoned, however, in favor of global modification schemes to increase reaction conversion. A table showing the various pKa values of this moieties and common reagents used in this endeavor are shown in TABLE 3, below.

Table 3 - Table of pKa values of relevant functional groups and reagents relative to the modification of lignin.

	pKa
Benzoic acid	4.19
Phenol	9.8-10
Benzyl alcohol	~15
Carbonate (CO_3^{2-})	~10.5
Pyridine	~5.5
Et_3N	~10.75
Potassium *tert*-butoxide	~17.5
2-methylimidazole	7.8
DMSO/Dimsyl	~35

3.2.1 Chemical Methods and Procedures

Lignin was modified to function in numerous different single and multi-step reaction sequences. At least 0.5 mmol (1 eq.) of unmodified lignin was used for each synthesis step. Organosolv lignin was pulverized using a mortar and pestle to increase surface area and create a more uniform powder as opposed to the highly irregular “chip” that was generally received. Ground lignin was then dried in an oven at 80˚C in order to remove any remaining solvents from the grounds. Numerous solvent systems were used to solvate the lignin to include water, tetrahyrdofuran (THF), N-methylpyrrolidinone (NMP), 1,4-dioxane, N,N-dimethylformamide (DMF) and acetonitrile (ACN) with varying success and difficulty. Solvents were used in volumes between 1 and 2 ml to keep the substrate concentration between 0.25 and 0.5 molar and to both minimize materials used and ensure that the reaction has ample concentration to properly proceed (reaction concentrations below 0.2 molar often have difficulty initiating). Several inorganic and organic bases were also used in equivalents ranging from 3eq. ≤ $3x_{lignin}$ ≤ 6eq. to include potassium carbonate, cesium carbonate, diisopropylethylamine (DIEA), 2,2,6,6-tetramethylpiperidine, potassium hydroxide, sodium hydroxide, sodium hydride and several polymer-supported bases. Low-molecular weight, switchgrass-sourced organosolv lignin was found to be highly soluble in THF (approximately 100 mg ml^{-1}) and more so in NMP (>200 mg ml^{-1}) however, it was almost completely insoluble in neat methanol. Solubility tests for organic solvents showed that a number of solvents could dissolve lignin in suitable concentrations for chemical reactions although, the results did not

relate to relative solvent polarity, as anticipated. Regarding aqueous reactions, lignin was not at all soluble in pure water. Mixing lignin into equimolar alkaline water ($NaOH_{(aq)}$) results in the formation of the lignin sodium salt (and water) which is highly soluble. TABLE 4 shows experimentally measured solubility limits for the stock of unmodified organosolv lignin that was used during the bulk of these experiments.

Table 4 - Experimentally determined solubility limits of organosolv lignin stock 141440.

Solvent	mg/ml	Polarity
Acetone	<50	5.1
Acetonitrile	<50	5.8
Dioxane	100	4.8
DMF	>200	6.4
DMSO	>200	7.2
Isopropanol	insol	3.9
Methanol	<50	5.1
NMP	>200	6.7
THF	100	4.0
Toluene	insol	2.4
Water	insol	9.0

3.2.1.1 Lignin Functionalization

Unmodified, dried lignin was dissolved in 1-2 ml of solvent with a suitable base and allowed to stir at 60-80°C for 10 minutes. Following stirring on heat, a suitable electrophile (i.e. alkyl halide, glycol chain, etc) was added to the mixture link lignin subunits together and as a way to alter or amplify the physical properties of the native lignin material. This reaction required moderate heat and time and so, depending on the solvent system and associated boiling points, reaction times varied based on reaction monitoring with TLC. After the allotted reaction time, an additional nucleophile is added to introduce ionic character to the modified. Of these, 1,2-dimethylimidazole (DMIm), 2-methylimidazole (HMIm), and trimethylamine (TMA) were the most common. Steps involving the addition of a tertiary amine did not require the presence of additional base and were generally left to stir at 60°C in a sealed reaction vial for at least 24 hours, as shown in the literature.[72] A general reaction scheme for this modification method is shown in **FIGURE 20**. This reaction scheme would form the basis of lignin modification for much of the work in this project. This synthetic methods benefits from the fact that THF is incapable of solvating cationic lignin product, causing the desired product to precipitate. This allows for the use of excess reagent, which was removed by solvent washing of the resultant solid precipitate.

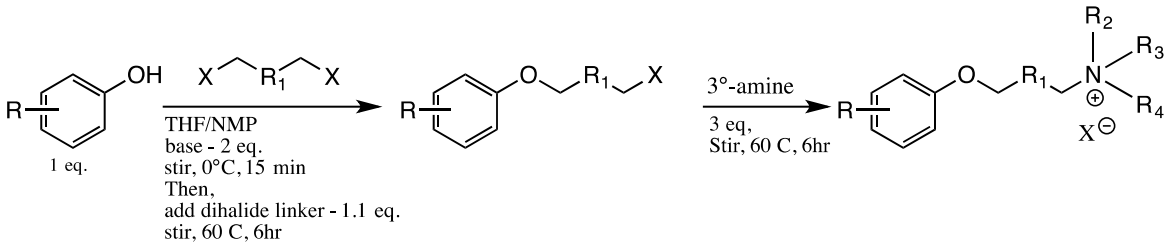

Figure 20 - General reaction scheme for the modification of lignin utilizing a two-step reaction sequence.

3.2.1.2 Reaction procedures and work-up

Lignin Acetylation – Organosolv lignin (25mg) was added to a 15mL screw-cap culture tube and dissolved in 500μL of pyridine. The mixture was allowed to stir for 15 minutes at room temperature (20°C) to ensure complete dissolution. The mixture was then moved into an ice bath and cooled to 0°C. An equivalent volumetric quantity (500μL) of acetic anhydride was then slowly added, dropwise, to the mixture and allowed to stir for 5 minutes in the ice bath until being moved to stir at room temperature for 24 hours (alternatively, this reaction can be accelerated by stirring at 60°C for 12 hours to the same effect). Following reaction completion, the mixture was diluted with an 8mL mixture of water/methanol and sonicated at room temperature for 20 minutes. The mixture was then centrifuged and the solvent decanted. The solid was then washed with pure, dry toluene under the same procedure stated above (sonication, centrifuging, solvent decanting) three times and the remaining solid was dried overnight at 60°C under vacuum. Remaining solid is weighed and stored for later use. It is worth noting that, depending on specific lignin

solubility properties in methanol, it may be necessary to alter the water/methanol mixture (or, to eliminate the methanol completely) in the first wash step to increase yields for further analysis.

Lignin Aminolysis (N-acetylpyrrolidine) – Acetylated lignin was dissolved in 1mL of 1,4-dioxane and sonicate at room temperature for 1 hour to completely dissolve. The solution was stirred at room temperature, treated slowly with 1 mL of a 1:1 (v/v) solution of dioxane/pyrrolidine and was stirred at 60°C for 8 hours until complete. Aliquots were taken periodically to monitor reaction and for the quantification of final product. Reaction was followed by TLC and GC/MS.

3-(4-bromobutyl)-1-butyl-2-methyl-1H-imidazol-3-ium ([BBBMIm][Br]). Sodium hydride (NaH) (60%) was added (440 mg, 11 mmol, 1.1 eq.) to dry THF (10mL) and stirred at room temperature until fully dissolved. (Appearance should be slightly cloudy, yellow-ish to clear). Following this, 2-methylimidazole (HMIm) was added (820 mg, 10mmol, 1 eq.) to the mixture and stirred at room temperature for 15 minutes or until gas evolution ceases. To this mixture, 1,4-dibromobutane (1300 μL, 11 mmol, 1.1 eq.) was added and the mixture was stirred for 6 hours at 60°C. Following stirring, solution appeared a light yellow color. Crude reaction mixture was centrifuged and the solvent filtered to remove solid salts and excess NaH. Following centrifuging/decanting, 1-iodobutane was added (1248 μL, 11 mmol, 0.95 eq.) to the mixture and stirred at 60°C for 12 hours. This yielded a chalky, white precipitate.

The mixure was centrifuged and the solvent discarded. The remaining solid was washed with ethyl acetate (2 x 20 mL) and diethyl ether (1 x 10 mL) and dried overnight under vacuum at 40°C. Purified product was verified by MS(ESI)(pos) – *m/z*: 139 (100%), 217 (80), 274 (48).

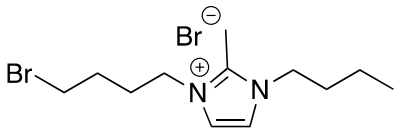

3-(4-bromobutyl)-1-butyl-2-methyl-1*H*-imidazol-3-ium bromide
Exact Mass: 352.01

1,3-bis(4-bromobutyl)-2-methyl-1H-imidazol-3-ium bromide ([bisBBMIm][Br]). [bisBBMIm][Br] was synthesized by refluxing 2-methylimidazole and excess 1,4-dibromobutane in acetonitrile in the presence of dry sodium hydroxide. Commercially available NaOH was pulverized using a mortar and pestle and dried overnight at 60°C under vacuum. Dry NaOH (720 mg, 18 mmol, 1.28 eq.) was added to 20 mL of acetonitrile. The mixture was stirred at room temperature in a round bottom flask. HMIm (99%) was then added (1148 mg, 14 mmol, 1 eq.) to the solution and stirred at 60°C for 15 minutes. Following this period, 1-4, dibromobutane (4.163 mL, 35 mmol, 2.5 eq) was slowly added and the mixture was stirred under reflux conditions for 24 hours. The mixture was then cooled and filtered after which the solvent was removed under vacuum. The resulting oil was washed with ethyl acetate (2 x 20 mL) and diethyl ether (1 x 20 mL) and dried overnight under vacuum at 60°C. MS(ESI)(pos) – *m/z*: 353 (100%), 351 (51), 355(48), 274, 446.

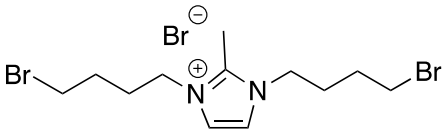

1,3-bis(4-bromobutyl)-2-methyl-1*H*-imidazol-3-ium bromide
Exact Mass: 429.93

N-(4-bromobutyl)-2-methylimidazole ([BBMIm]). [BBMIm] was synthesized by mixing 1,4-dibromobutane with 2-methylimidazole in a suitable solvent in the presence of a non-nucleophilic base. Commercially available NaH (60%) was added (44 mg, 1.1 mmol, 1.1 eq.) was dissolved in 2 mL of THF and stirred at 60°C until most of the solid is dissolved or suspended. The mixture was cooled to room temperature and HMIm (98%) was added (83 mg, 1.0 mmol, 1 eq.) and stirred at room temp until gas evolution ceases (about 10 minutes). Following this, 1,4-dibromobutane (99%) was added (121 μL, 1.0 mmol, 1 eq.) and the mixture was stirred at 60°C for 12 hours. Following reaction, mixture was centrifuged and the solvent recovered. Solids were discarded. The recovered solvent mixture is removed under vacuum using a rotary evaporator yielding a pale yellow waxy solid/oil. The solid was washed with diethyl ether (2x20 mL) and filtered to recover the desired product in the form of a clear, waxy solid. The resultant solid is dried overnight under vaccum 60°C. MS(ESI)(pos) – *m/z*: 216 (100%), 218 (98), 138 (51), 83 (57).

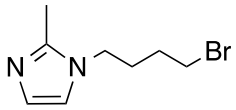

N-bromobutyl-2-methylimidazole
Molecular Weight: 217.11

1,4-bis(2-methylimidazol-1-yl)butane ([bisHMIB]) [bisHMIB] was synthesized by refluxing 1,4-dibromobutane and 2-methylimidazole in acetonitrile in the presence of a suitable, non-nucleophilic base. For this reaction, dry, crushed NaOH was added (720 mg, 18 mmol, 1.28 eq.) to 50 mL of acetonitrile and stirred at room temperature in a round bottom flask to solvate. NaOH is almost completely insoluble in acetonitrile, so rapid stirring is essential to facilitate the interfacial reaction between the base and nucleophile. Commercially available HMIm (98%) was added (1148 mg, 14 mmol, 1 eq.) to the mixture and stirred at 60°C until fully dissolved. Finally, 1,4-dibromobutane (99%) was slowly added (847 μL, 7 mmol, 0.5 eq) to the mixture and refluxed for 24 hours at approximately 80°C. The mixture was then cooled and the solid filtered and discarded. The solvent was removed and the product extracted with ethyl acetate (3x20 mL). Product mixture was transferred to a round bottom flask and the solvent was removed under vacuum. Resultant oil was dried overnight under vauum at 60°C. This method was adapted from Shun-Li Li, et. al., 2007 in the synthesis of 1,4-bis(2-ethyl-1*H*-imidazol-1-yl)butane.[73] MS(ESI)(pos) – *m/z*: 219 (100), 138 (51), 83.

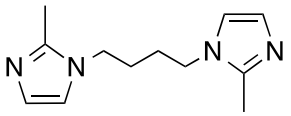

1,4-bis(2-methyl-1*H*-imidazol-1-yl)butane
Molecular Weight: 218.30

3-(4-bromopentyl)-1,2-dimethyl-1H-imidazol-3-ium ([BPDMIm][Br]). [BBDMIm][Br] was synthesized by reacting 1,2-dimethylimidazole and 1,4-dibromobutane in a suitable solvent at moderately high heat. For this reaction, DMIm (98%) (200 mg, 2.0 mmol, 1 eq.) and 1,4-dibromobutane (99%) (242 μL, 2.0 mmol, 1 eq.) were dissolved in 5 mL of THF and stirred for homogeneity at room temperature for 10 minutes. The temperature was then increased to 60°C and the mixture was stirred for 6 hours until reaction completion. Reaction was monitored via TLC. Following the reaction, solvent was removed under vacuum using a rotary evaporator. The remaining oil was diluted in 10 mL of acetone. The polar mixture was washed with 30 mL of toluene and sonicated for 10 minutes at room temperature. This creates a biphasic mixture that must be separated via a separatory funnel. The non-polar (toluene) fraction was discarded and the wash was performed 3 times. Following washing, solvent was removed under vacuum and the remaining waxy solid was dried overnight under vacuum at 60°C. MS(ESI)(pos) – *m/z*: 167 (100%), 246 (42), 138 (41).

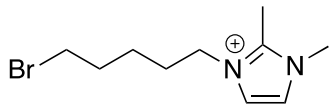

3-(5-bromopentyl)-1,2-dimethyl-1*H*-imidazol-3-ium
Molecular Weight: 246.17

Lignin Modifications

Alkylhalide-modified lignin. Dry organosolv lignin was added (1 g, 3.15 mmol – OH, 1 eq.) to a 20 mL solution of 0.25M $NaOH_{(aq)}$ and stirred until fully dissolved. Next, commercially available 1,4-dibromobutane (99%) was added (756 μL, 6.3 mmol, 4 eq – Br) to the mixture and stirred at 80°C for 12 hours. Following the reaction, a dark brown precipitate had formed. The mixture was centrifuged and the solvent removed by decanting. The solid was washed with water (2 x 50 mL) and ether (1 x 50 mL) and dried overnight under vacuum at 50°C. ν_{max}/cm^{-1} – 3456br (OH), 2933 (sp^3-hybridized CH), 1712 (non-conj. CO), 1594 (aromatic ring), 1244 (CO) – abs/KBr.

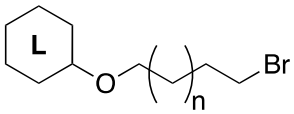

Bromoalkylated Lignin

Tetraethylene glycol-modified lignin. Dry organosolv lignin was added (1 g, 3.15 mmol – OH, 1 eq.) to a 20 mL solution of 0.25M $NaOH_{(aq)}$ and stirred until fully dissolved. After complete dissolution, commercially available tetraethylene glycol

ditosylate (98%) was added (3.23 g, 6.3 mmol, 2 eq.) to the mixture and stirred at 80°C for 12 hours. After cooling, the mixture was centrifuged and the solvent was discarded by decanting to yield a brown solid. The solid was washed with water (2 x 50 mL) and DCM (1 x 50 mL) and dried overnight under vacuum at 50°C. ν_{max}/cm^{-1} – 3417br (OH), 2931 (sp^3-hybridized CH), 1255 (aryl CO), 1124 (aliphatic CO) – abs/KBr.

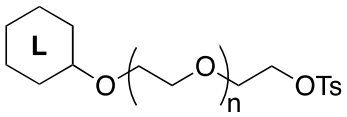

Ethylene Glycol-Modified Lignin

3.3 Lignin Phenolic Concentration Quantification

There are numerous methods employed to determine phenolic and total hydroxyl content in various streams of lignin – each with specific strengths and weaknesses regarding their methodology and ability to produce reproducible results. Of the various methods reported in literature, it seems that those utilizing various NMR methods as well as those utilizing GC/MS (or, just GC) are the most prevalent in modern publications. According to a statistical study of all major reporting on the spectroscopic quantification of phenolic and total hydroxyl content in lignin, aminolysis was determined to be the most statistically rigorous.[74] This is interesting considering that the efficiency of the aminolysis methodology is reliant on a 2-step process in which lignin is derivatized by acetylation and then that

derivatization is reversed in the second step whereby the N-acetylated structure is formed and the phenol is either reformed or precipitated as a salt.[75]

The lignin used for the majority of this project was initially quantified in terms of its specific phenolic and total hydroxyl content by means of ^{31}P NMR. This was performed outside of this lab by the Center for Renewable Carbon (CRC). SG_lig was a batch of organosolv switchgrass-based lignin and the primary sample used in this work. The results of this method for SG_lig and another sample of hybrid poplar are tabulated in **TABLE 5**. ^{31}P NMR quantification employs a 1-step derivatization using a phosphitylating agent, most notably, 2-chloro-4,4,5,5-tetramethyl-1,3,2-dioxaphospholane (CTMDP), as was reported early on in the quantification of coal pyrolysis condensates by A.E. Wroblewski, in the Verkade group and later on by Argyropoulos and Jiang in the quantification of lignin hydroxyl units.[76,77,78] In almost all cases, this reaction is performed in dry dichloromethane or chloroform with a catalytic quantity of pyridine.[79]

Table 5 - 31P measured hydroxyl-unit concentrations for CRC-45 and 141440 low molecular weight lignin stocks

Run ID	Carboxylic acid OH (COOH)	Phenolic OH			Total phenolic OH	Aliphatic OH
		p-hydroxyphenyl	C_5 substituted+Syringyl	Guaiacyl		
Hy_Pop	0.09	0.41	2.78	0.70	3.89	1.82
SG_lig	0.09	0.54	0.80	0.81	2.15	0.95

For this study, aminolysis was used as the predominant methodology for calculating total hydroxyl content. This decision was made for several reasons over that of NMR or UV-Vis quantification methods, the most notable being ease of sample preparation, low cost of reagents and unhindered access to the appropriate characterization equipment. Traditional aminolysis, as reported by Lai 1992, utilized lignin that had been previously acetylated in the most common method employing acetic anhydride (Ac_2O) as the acetylating agent and pyridine as both a solvent and non-nucleophilic base.[80] This method has been employed and discussed extensively in literature since the 1980s and in the endeavor of quantifying phenolic units, it has proven to be robust and reproducible. Several downfalls for this method exist, however, most notably the environmental issues associated with the toxicity of pyridine as well as the high boiling point of the solvent, which can complicate purification. The mechanism for this process is shown in **FIGURE 21 - Lignin acetylation reaction mechanism (base)**. Proposed as a replacement for pyridine and other tertiary amines in the acetylation process, Lugemwa, et. al. reported the use of bicarbonate bases in multiple solvents with conversion rates of 88-99% in the acetylation of numerous aliphatic and phenolic hydroxyl units.[81] Bicarbonate bases, aside from being significantly less toxic than pyridine, are also easily removed from the desired product during the aqueous wash. Once the lignin is acetylated and washed with a solvent gradient to remove excess acetic anhydride, the dried, acetylated lignin is then dissolved in an appropriate solvent and mixed with pyrrolidine to produce N-acetylpyrrolidine (NAP) (shown in **FIGURE 22**), which is the

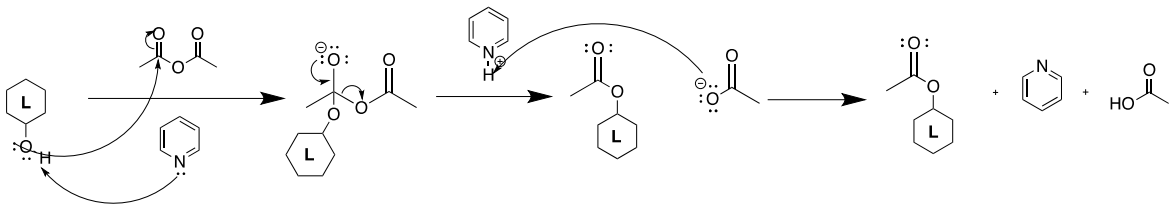

Figure 21 - Lignin acetylation reaction mechanism (base)

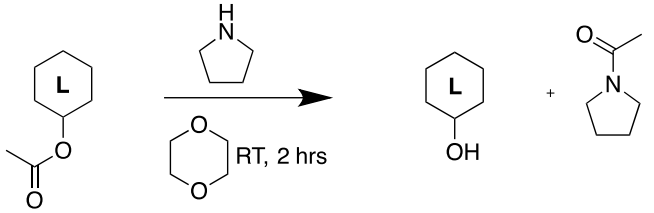

Figure 22 - lignin aminolysis general reaction conditions

quantified species that should exist in a 1:1 ratio with total lignin hydroxyl content. Special care must be taken to remove all excess acetic anhydride, as its presence during the aminolysis step will yield false results in the concentration of NAP.

In this study, a solution of acetic anhydride in dioxane of known concentration was mixed with pyrrolidine at 60°C for 4 hours in order to synthesize NAP. Once purified, serial dilutions were made and each diluted sample of NAP was measured on the GC/MS in order to create a calibration curve for this material. The dilutions were made in such a way that the upper and lower boundaries would be at least a half-decade change greater and lesser than the highest and lowest cencetrations of lignin hydroxyl units.

The stock solution of NAP was synthesized multiple times to ensure accuracy both at room temperature as well as at a reaction temperature of 60°C to determine if elevated temperatures would reduce any possible barrier to reaction. Diluted samples were then characterized on the GC/MS and the product peak was integrated to determine the area under the curve from which to create a calibration curve. The linear function generated was subsequently used to determine the total hydroxyl content of lignin samples based on the measured concentration of NAP. The measured values for the calibration curve for both the room temperature and heated cases are shown below (**FIGURE 23**) - both exhibit R^2 values of over 0.99 with the heated condition measuring a calculated R^2 value of over 0.9999 as an average of three parallel reactions. As the aminoloysis calibration performed at 60°C yielded a more accurate linear fit, subsequent aminolysis reactions were performed at 60°C in 1,4-dioxane on all lignin samples.

The concentration profiles for lignin hydroxyl content are shown in **FIGURE 24**. Both curves are the result of a numerical average in values from 3 parallel reactions. The lower values are those of switchgrass-sourced lignin (measured MW: 465 g mol^{-1}). The higher values are those measured from poplar-sourced lignin (measured MW: 950 g mol^{-1}). Both sources of lignin were acylated using sodium bicarbonate in place of pyridine. The poplar-sourced lignin was calculated to have a hydroxyl concentration of approximately 3.8 mmol g^{-1} while the switchgrass-sourced lignin that was the primary source of lignin in our studies was calculated to contain 2.9 mmol g^{-1}.

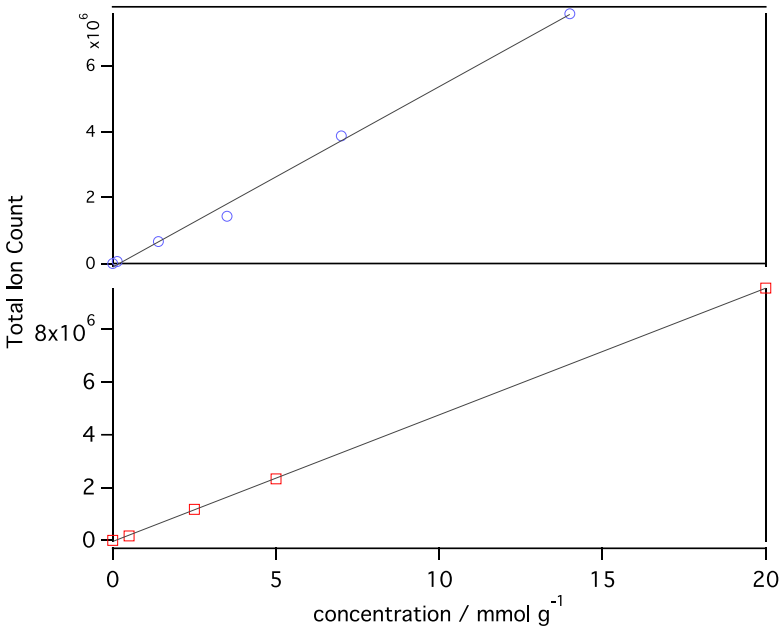

Figure 23 - Aminolysis concentration calibration curves (a) resultant curve of NAP synthesized at 25C; (b) resultant curve of NAP synthesized at 60C.

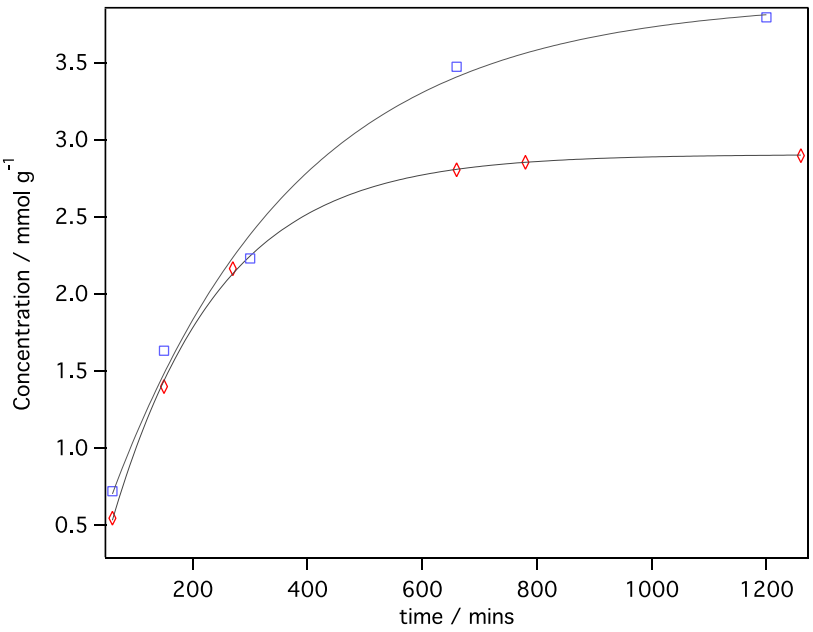

Figure 24 - concentration profile illustrating the formation of N-acetylpyrrolidine as a measure of the concentration of total hydroxyl content in the lignin sample.

These numbers differ somewhat from those obtained via 31P NMR, contained in TABLE 5. Results for different batches of lignin, both from a processing standpoint (pre-chemical modification) and from a source perspective (i.e. hardwood vs switchgrass, for example) vary greatly in the literature. Lignin processing is mainly a function of paper production where wood chips are treated with a solvent mixture and either an acid or base designed to extract pure cellulose from a lignocellulosic source material which involves the lignification of the unprocessed biomass. The result being the separation of lignin and cellulose and the secondary effect of the liberation of free-hydroxyl units within lignin as a result of chemical degradation of the phenylpropyl-ether linkages that hold the bulk of the lignin polymer together.[82] As indicated in nearly all literature, lignin is a heterogeneous material that necessitates that each batch must be characterized on its own as a novel material prior to secondary chemical modification.[83]

The main purpose of the chemical quantification of hydroxyl concentration in lignin was the numerical assessment of hydroxyl units to be used for stoichiometric calculations in the modification of lignin. As with any chemical reaction scheme, appropriate consideration must be given to molar quantities of the functional moieties of interest. Regarding lignin, quantity of hydroxyl units in millimoles was the method of stoichiometric quantification used in the building of reaction schemes used to modify lignin.

The majority of chemical and structural characterization work performed on modified lignin, Fourier transform infrared spectroscopy (FTIR) was the dominant method. FTIR has a number of characteristics that make it very well suited to this

type of characterization – excellent temporal resolution, ease of sample preparation, stability of samples post-preparation (samples can be queued for long periods of time) and high resolution for functional groups. ^{1}H NMR was also attempted in the characterization of modified lignin, however, the FTIR proved to be more valuable in resolving the chemical transformations undertaken during successive modifications. Initially, it was thought that NMR would provide an ideal method of resolving the changes in chemical shifts associated with lignin modification, especially regarding the substitution of various tertiary and quaternary amines. In practice, however, it was extremely difficult to interpret the NMR spectra of modified lignin due to the abundance of proton shifts inherent to the material. On the contrary, FTIR proved to be invaluable in this pursuit as most of the desired information about the functional groups of interest resided in the region of high resolution above 2000 cm^{-1}. Unlike NMR, it is difficult to quantify FTIR spectra and as such, the data are qualitative in nature.

Fourier transform infrared spectroscopy (FTIR) of both switchgrass and poplar indicates signatures for both that are in line with ^{31}P and GC/MS data for both stocks. Previous studies have shown that most hardwood lignins have a ratio of syringyl to guaiacyl units (S/G) of 4-6 while switchgrass generally exhibits an S/G ratio of about 0.5.[84] Looking at the spectrum between 2000 and 500 cm^{-1}, shown in **FIGURE 25**, and as previously demonstrated by Faix, Shultz and Glaser, Popescu and others, switchgrass lignin exhibits significantly higher signals for unconjugated carbonyls and C-O vibrations of guaiacyl units as well as the C-H deformation vibration of guaiacyl units shown at 1708, 1265 and 1130 cm^{-1}, respectively. The

poplar sample, meanwhile, indicates higher relative signals for structural moieties associated with synringyl units, most notably signals at 1325 and 1089 cm^{-1} which are indicative of the C-O stretch on C-5 substituted aromatics and the pronounced shoulder of aliphatic hydroxyl units, which tend to be more abundant in hardwood lignins than in that of switchgrass.[85,86,87,88,89] The various spectra generated via FTIR of different streams of processed lignin help to illustrate how both source and processing techniques can result in significant structural difference and specifically, in the "fingerprint" region of the spectra, one is able to extract important information about the possible reactivity of the material.

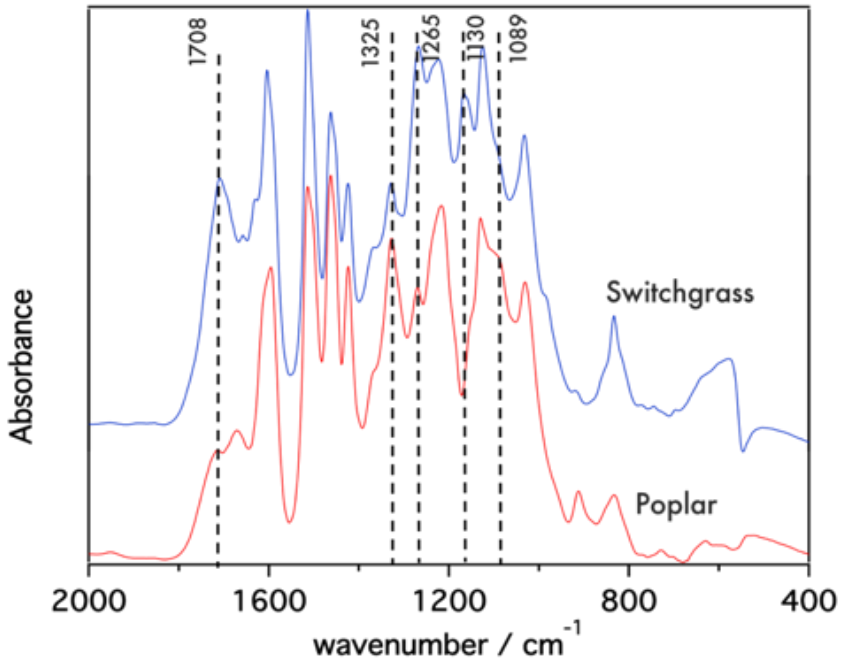

Figure 25 – A magnification of the absorbance FTIR spectrum of lignin from both switchgrass and poplar wood sources focused on the lower-energy skeletal vibration differences between lignins with varied phenylpropyl unit concentrations.

For researchers focused on the chemical modification and oligomerization of lignin, certainly, information regarding hydroxyl unit concentration, and more specifically, the distribution of hydroxyl units between phenolic and aliphatic hydroxyls, is the most pertinent. FTIR, however, has the capability to shed light on a number of other structural components of lignin that can aid the researcher in the design of more complex synthetic methods that can potentially make use of structures other than hydroxyl units. For example, information gained from the spectra of switchgrass-sourced organosolv lignin relative to that of poplar-sourced lignin shows increased guaiacyl vs syringyl signals. This information would support the conclusion that switchgrass-sourced lignin would serve as a more suitable material to support modification beyond substitution reactions involving hydroxyl units. The lower indicated concentration of 2,4,6-substituted mono-lignols (and subsequent higher relative concentration of 2,4-substitutued or 4-substitututed rings) allows for additional reactions involving benzylic carbons due to lower steric hindrance on the ring. In the opposite way, FTIR can be used to measure the effectiveness of a specific synthetic method by watching peaks associated with the unmodified material shift or disappear corresponding to specific modification techniques. Most importantly, however, these unmodified lignin spectra are able to serve as a baseline measurement in the qualitative characterization of post-modification and elongation lignin-based materials. These baseline spectra enable researchers to make relatively simple determinations on the effectiveness of a specific synthetic method by measuring the relative absorbance of a specific peak.

3.4 Lignin-based, Non-carbonaceous, Non-PGM Electrocatalysts

One of the most pressing issues facing the widespread introduction of PEMFCs as a viable energy technology is that of cost. Of particular concern to those technologies that are reliant upon oxygen reduction as part of the cell chemistry is the current dependence upon noble metal catalysts. Due to the strong dioxygen bond, the ORR is slow to occur at low temperature. This necessitates higher loadings of catalyst which causes the costs of cell and stack fabrication to increase beyond the point of commercial viability. For this reason, extensive research has been performed in the area of reducing or eliminating the use of platinum group metals in the synthesis of the catalyst layers of energy conversion devices. In fuel cell and electrochemical conversion research, one of the most prevalent areas of research is the synthesis and characterization of carbon supported catalyst systems utilizing non-platinum group metals as analogs to PGMs. Traditionally, PEMFCs have relied on platinum (or platinum/ruthenium alloys) to catalyze the ORR as well as for the anodic oxidation of hydrogen. In the realm of fuel cell and advanced battery architecture research, increasing the efficiency of the ORR is one of the most pressing and potentially lucrative issues of our time.

The Zawodzinski group has performed a large amount of work in the area of carbon supported diazonium coupled metal-triazole chemistries (shown in **FIGURE 26A**) and have seen some success in derivatizing these catalysts and approaching the activity of supported platinum catalysts in the area of acidic media ORR. Catalyst performance measurements, mainly onset potential, were taken by rotating disk

electrode (RDE) in a sulfuric acid solution saturated with pure oxygen. Onset potential is an experimental measure of the catalytic activity of a particular material. With regards to the ORR, it is ideal that the onset potential of a catalyst material measured by RDE in an oxygen saturated environment would be as close to the thermodynamic limit of the reaction as possible. The difference between the measured and theoretical values is known as the overpotential. Overpotential can be related to a particular cell's voltage efficiency – or, rather, the efficiency of a catalyst system in promoting a specific reaction. Specifically, the theoretical value for the ORR in acidic media is approximately 1.2V relative to a standard hydrogen electrode (SHE). As with all redox reactions, the potential at which a redox event takes place is pH dependent. For this reason, the reversible hydrogen electrode (RHE) potential is measured on platinum and is used to correct the measured reference potential.

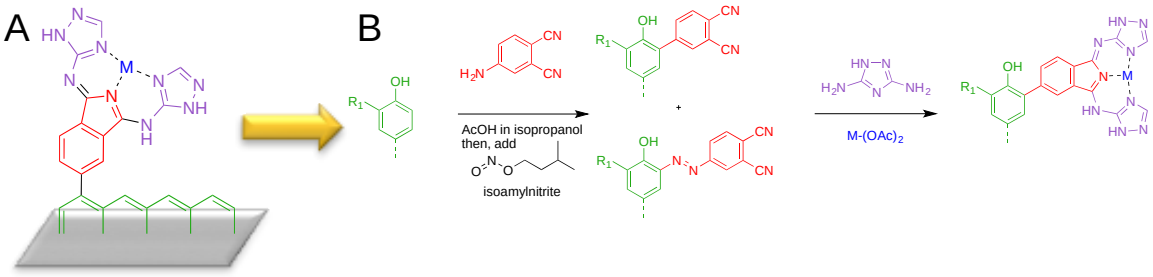

Figure 26 – A) Schematic illustrating a model of a carbon supported adsorbed copper catalyst utilzing a substituted 1,2,4-triazole ligand. B) Schematic of a diazonium coupling reaction performed on a 2,4-substituted mono-lignol resulting in a 1,2,4-triazole ligand capable of binding a variety of transition metals.

Like traditional high surface area carbon black media, lignin is an electron rich material with a high concentration of aromatic rings making C-C coupling reactions a potentially desirable reaction pathway. Utilizing a very similar method previously employed by the Zawodzinski group for modifying carbon for use as a supported catalyst for the ORR, it should be possible to functionalize the unmodified lignin with 1,2,4-triazole ligands capable of adsorbing various transition metals. As shown by FTIR spectroscopy, switchgrass-sourced lignin exhibits a high relative concentration of G-unit monolignols, making it a better carbon surrogate than poplar-derived lignin and more a more appropriate material to support diazonium chemistry. Numerous solvent choices and workup procedures were attempted to cope with the changing solubility properties of unmodified lignin after each reaction step. The initial reaction media solvent must reasonably dissolve lignin under acidic conditions and, ideally, allow the diazonium-coupled product to readily precipitate or be easily isolated using trituration. The initial reaction mechanism from lignin to functionalized catalyst is essentially a two-step process. As shown in **FIGURE 26B** below, the diazonium coupling mechanism is performed by the mixing of an aryl amine in the presence of an oxidizing agent to form the reactive aryl diazonium salt that, with or without the loss of N_2, is capable of forming the coupled product. The follow-on cyclocondensation reaction is performed in pure water utilizing a microwave reactor to achieve temperatures above the boiling point of the solvent.

3.4.1 Diazonium-coupled modified lignin for use as electrocatalysts

Several different methods were employed to functionalize unmodified lignin to be utilized as a potential candidate for the oxygen reduction reaction (ORR). Solvent choices and purification techniques were altered in order to determine a suitable recipe for synthesis. Solvents were chosen that sufficiently dissolved all starting materials but that allowed for the precipitation of the desired products to allow for easier separations and removal of undesired materials. Products were washed and sonicated in water and diethyl ether to remove excess isoamyl nitrite and phthalonitrile. After oven drying at 90°C overnight, metal acetates are added to an aqueous solution of triazole and reacted in a Biotage microwave reactor for 4 hours at 140°C and subsequently washed and dried.

Dried materials are then mixed in varying molar equivalents with a mixture of methanol, glycerin and 5% w/w Nafion solution (in methanol) for 48 hours at room temperature. Following mixing, between 250-300μg of these resultant “inks” are deposited on a glassy carbon rotating disk electrode (Pine Instruments model AFE2M050GC) and allowed to dry. A 3-electrode electrochemical cell was employed to investigate the ORR half reaction. This arrangement allows for current measurement as a function of applied voltage from the working electrode and independent of changes at the counter electrode. The employment of a dedicated reference electrode (rather than a coupled reference/counter electrode as employed in a 2-electrode cell) and close physical proximity to the working electrode allows for the direct measurement of current as a function of polarization of the working

electrode. This cell type is the preferred method employed to investigate an electrochemical half reaction such as the ORR.

FIGURE 27 shown below displays a general representation of an ancidic ORR polarization curve collected via RDE. There are several performance indicators labeled on the graph that are useful in assessing a particular catalytic system. In this example, the system is platinum on carbon (Pt/C) as noted by the particularly high onset potential, E_{onset}. Onset potential was the primary performance characteristic used to evaluate lignin-based catalysts. Also annotated in the graphic is the diffusion limited current, j_L which, along with other hydrodynamic and electro-

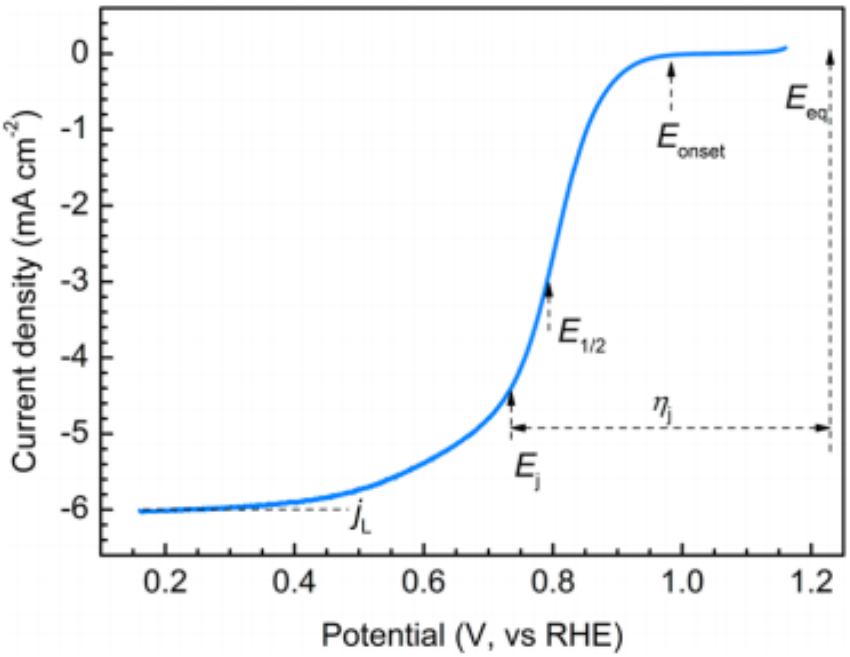

Figure 27 – General representation of an annotated ORR polarization curve using a Pt/C catalyst in acidic media as measured via RDE.

chemical properties of the RDE-generated graphic, is governed by the relationship outlined in the Levich equation [3.1] where *n* is the number of electrons transferred, *F* is the Faraday's constant, *C* is concentration of dissolved oxygen, *A* is the active area of the electrode, *D* is the diffusion coefficient (of O_2, in this case), *v* is the kinematic viscosity of the electrolyte solution and ω is the rate of rotation of the electrode, measured in rotations per minute.[90]

$$j_L = 0.201nFC_{O_2}AD_{O_2}^{\frac{2}{3}}v^{-\frac{1}{6}}\omega^{\frac{1}{2}} \qquad [3.1]$$

In its most basic form, the Levich equation describes the hydrodynamic relationship between the rotational velocity of the electrode and the experimentally observed limiting current. By varying rate of rotation and measuring the observed limiting current, it is possible to calculate diffusion coefficients via the slope of the linear fit of the plot of j_L v. $\omega^{\frac{1}{2}}$.[91] This plot also yields information about reaction kinetics in that deviations from an origin intercept indicate kinetic limitations are influencing the electron transfer reaction instead of solely diffusion effects at the limiting current.[92]

The capacitive background was taken in a nitrogen saturated solvent environment and then subtracted from the forward linear sweep voltammetry run taken after oxygen saturation. This is done to correct for uncompensated resistance in the cell that can occur as a result of solvent polarization – a phenomena known as the double layer effect.[93] As seen in **FIGURE 28**, unsupported lignin catalysts exhibit poor onset potential for the ORR and poor limiting currents when compared

to standard industry catalyst materials. These results indicate both poor catalyst activity, noted by the low onset potential, as well as likely low catalyst surface area, as indicated by the poor limiting current. As shown in the Levich equation, geometric area of the electrode is the main controllable variable that influences the diffusion-limited current. It is important to note that **FIGURE 28A** describes the onset activity for a catalyst using only unmodified lignin and no carbon support.

To address the issue of poor limiting current, DATz-$Fe_{0.5}Cu_{0.5}$-ML_{ipa}, the most active lignin catalyst tested, was mixted with Ketjen Black, a commonly-used, high surface area carbon. Several ratios were used ranging from 20 to 50% lignin catalyst and the mixture was pyrolyzed under flowing nitrogen at 1000°C for 4 hours. The rationale behind this experiment was that, if the post-pyrolysis lignin materials were no longer able to chemically support the metal-organic ligand complex, the addition of a high surface area carbon would act as an electron-rich sink upon which the catalytically active ligand-metal complex could covalently bond and help to increase the diffusion limited current. **FIGURE 28B** shows the post-pyrolysis results for these mixed materials. As is shown, onset potential decreases with the decreasing ratio of lignin catalyst indicating that the catalytically active sites were likely present in lower concentration as KJB was added. Diffusion limited current density, however, increases notably over the most active lignin catalyst tested. This result indicates that the modified lignin catalyst suffered from low geometric surface area which limited catalyst performance.

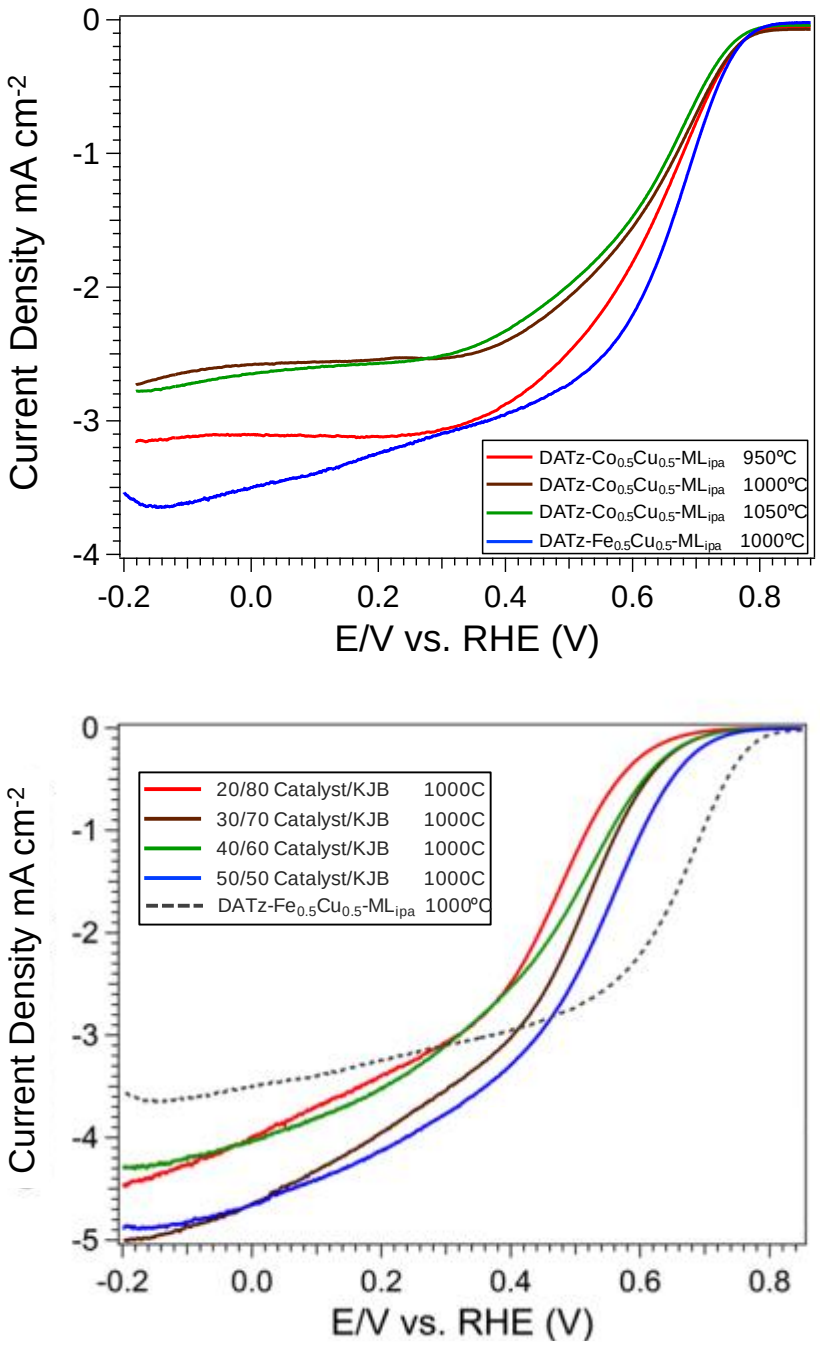

Figure 28 - (a) RDE onset potential plots for unsupported lignin-based non-PGM organometallic catalysts after pyrolysis and (b) RDE onset potentials for post-pyrolysis lignin-based catalyst/KJB mixtures. Electrolyte used was 0.1M H_2SO_4 with a $Hg/HgSO_4$ reference electrode, Au wire counter electrode and glassy carbon working electrode.

A study of the electron transport mechanism was also performed on these mixed catalyst systems to determine if the unsupported lignin catalyst was efficiently reducing oxygen via the four-electron pathway, as is preferred in PEM fuel cell applications. Incomplete oxygen reduction leads to peroxide formation and subsequent performance degradation. Using a rotating ring disc electrode (RRDE) that employs a uniform ring of platinum around the central electrode of an RDE, the ring is held at the oxidation potential of H_2O_2, while current response is measured.[94]

$$n = \frac{4|I_d|}{|I_d| + \frac{|I_r|}{N}} \qquad [3.2]$$

The result of this experiment is plotted in **FIGURE 29**, which shows a graphical representation of *n* as the potential of the central disc electrode is varied. What this graphic indicates is that the reduction of oxygen by way of this catalyst system is largely incomplete. Throughout most of the potential window, the number of electrons transferred appears to remain between 3 and 3.5. This likely means that both the 4 electron and 2 electron (as shown in equations 3.3 and 3.4) ORR pathways are occurring simultaneously, resulting in the production of both water and hydrogen peroxide. This is almost certainly due to the lignin catalyst itself and not the addition of un-pyrolyzed carbon to the mixture, as it has been shown in the literature that carbon plays a negligible role in the cathodic formation of peroxide species in acidic media.[95]

$$O_2 + 4H^+ + 4e^- \rightarrow H_2O \quad [3.3]$$

$$O_2 + 2H^+ + 2e^- \rightarrow H_2O_2 \quad [3.4]$$

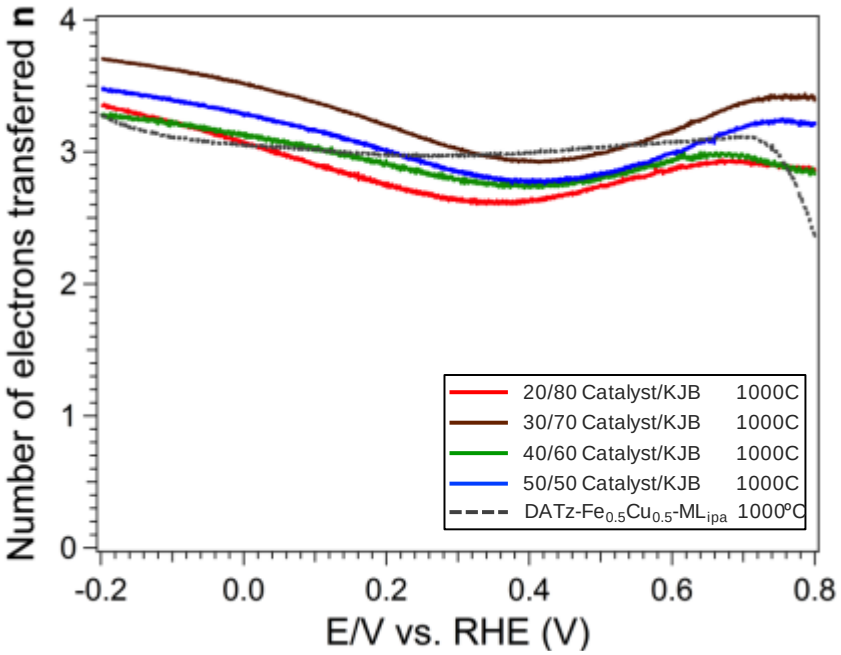

Figure 29 - Number of electrons transferred in ORR using an RRDE with a Pt ring under acidic conditions (0.1M H_2SO_4) as calculated by equation [3.2].

3.5 O-alkyl-modified lignin for use as catalyst binder

Alternatively, instead of using diazonium chemistry to functionalize lignin in acidic conditions using the benzyl rings, it is quite possible to use several of the oxygen containing functional moieties to attach a variety of groups to tune the

properties of the unmodified lignin toward a specific aim. The leftward shaded pathway illustrated in FIGURE 30 shows one such possible family of mechanisms. Theoretically, one of the simplest means of functionalizing unmodified organosolv lignin is through the alkaline deprotonation of the phenolic hydroxyl group to form the reactive phenolate anion. Organosolv lignin is ideally suited to this type of chemical modification due to its relatively high concentration of phenolic hydroxyl units. Numerous non-nucleophilic bases were used in this process to include hindered amines like diisopropylethyl amine (DIEA) and 2,2,6,6-tetramethylpiperidine as well as several polymer-supported bases and inorganic bases. The shaded box in FIGURE 30 shows a the basic 2-step scheme for the O-alkylation in the synthesis of a catalyst binder polymeric material. First, lignin hydroxyl units are deprotonated and an electrophilic linking-unit (i.e. 1,5-dibromopentane or tetraethylene glycol ditosylate) is substituted, which serves the dual purpose of modifying the physical properties (i.e. solubility, hydrophobicity, etc.) of the material as well as providing a suitable site for an additional substitution reaction. The second step in the general reaction scheme is the substitution of a tertiary amine, which, once quarternized, gives the synthesized material the ability to facilitate charge transfer.

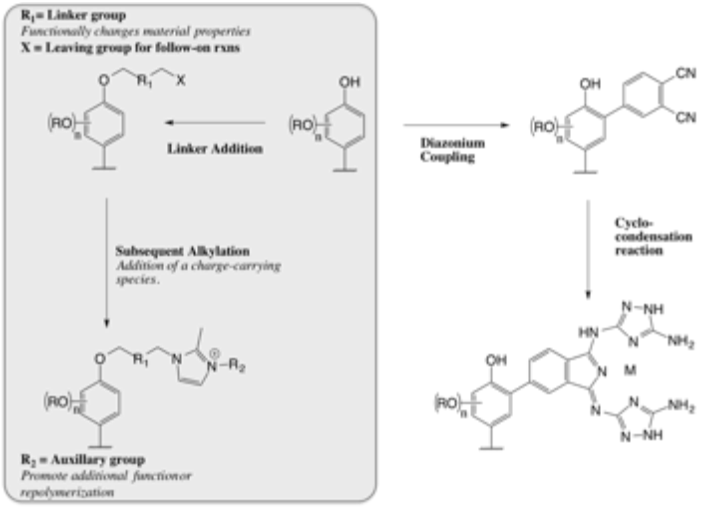

Figure 30 - Use of lignin as a polymeric building block material for conductive polymer material

Several of these first-generation lignin binders were tested in a standard 3-electrode half-cell testing stand. After centrifuging the mixture and decanting the solvent, the solid product was recovered, washed and dried overnight at 90°C under vaccum. The dried solid was dissolved in methanol at 5% w/w and stirred at room termperature for 24h. Solution was discarded if any precipitate was formed after overnight stirring. Initially, 20% w/w solutions were made but concentrations were lowered to mitigate solubility issues with the resultant lignin materials and to facilitate long-term stability of the solution. This also allowed for greater accuracy in binder quantification and solution transfer during the ink-making process. Similar to the apparatus used to test catalysts, resultant “inks” were deposited on a glassy carbon rotating ring disk electrode (Pine Instruments model AFE2M050GC) and allowed to

dry. After drying, deposited inks were wetted with water prior to immersion in the alkaline solution. Many of these inks showed poor adhesion to the glassy carbon surface of the electrode and fell into the reaction vessel making it difficult or impossible to test.

A gold wire counter electrode (separated by a ground glass frit) and a Pine Instruments Hg/HgO (0.1M KOH) reference electrode were utilized in a 0.1M aqueous solution KOH. The working electrode was rotated at 1600 rpm at a sweep rate of 10 mV/s.

The general reaction sequences for the series of binders tested is shown below in **FIGURE 31**. Modified lignin Binders 1-4 were synthesized using an dihalide alkyl linker to bridge the lignin compound and the charge-carrying amine group. Modified lignin Binder 5 utilized the same reaction conditions, however, as show, a tetraethylene glycol linker was used in place of the alkyl linker used in materials 1-4.

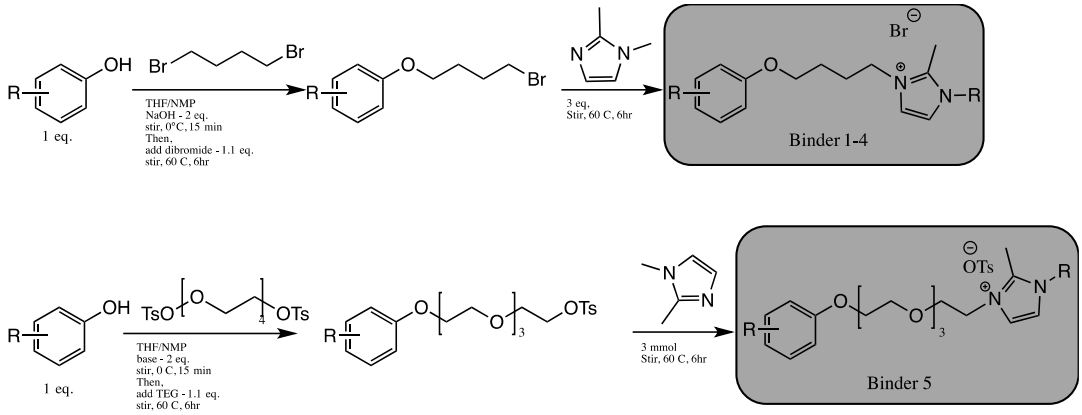

Figure 31 - Reaction schemes for the synthesis of Binder 1 (alkyl-lined) and Binder 2 (TEG-linked).

For the reasons discussed above in the case of catalyst testing, an RDE was used to measure onset potential of the alkaline ORR reaction. As shown in **FIGURE 32**, onset potentials for modified lignin binders, although lower than with Nafion at the same concentration, were reasonably stable in solution and did not hinder the ORR electron transfer properties as the *n*-value according to Equation 4.1 was relatively stable across the potential range. The experiment illustrated in **FIGURE 32** varied by binder composition while the catalyst system remained the same. Binders 1/2 and binders 3/4 (shown in **FIGURE 31**) differed from one another based on solvent media used during synthesis. The synthesis for Binders 1 and 2 were performed in THF and binder 2 underwent an additional alkylation step with methyl iodide to cap any unreacted phenolates or aliphatic alkoxides that were not alkylated in the first step. Binders 3 and 4 were both synthesized in NMP undergoing the same steps as binders 1 and 2, respectively. Binder 5, as shown in the figure, used a tetraethylene glycol linker (polar) instead of a significantly lighter molecular weight alkyl halide. It was assumed that, because *p*-toluenesulfonic acid is, under most conditions, a better electrophile than the bromide, a higher conversion would be achieved resulting in better performance. It was surprising, however, that the TEG linked lignin binder did not perform as well as alkyl-chain linker. This sample was prepared numerous times and experienced very poor adhesion to the electrode surface causing some of the deposited catalyst layer to detach upon submersion into the electrolyte solution.

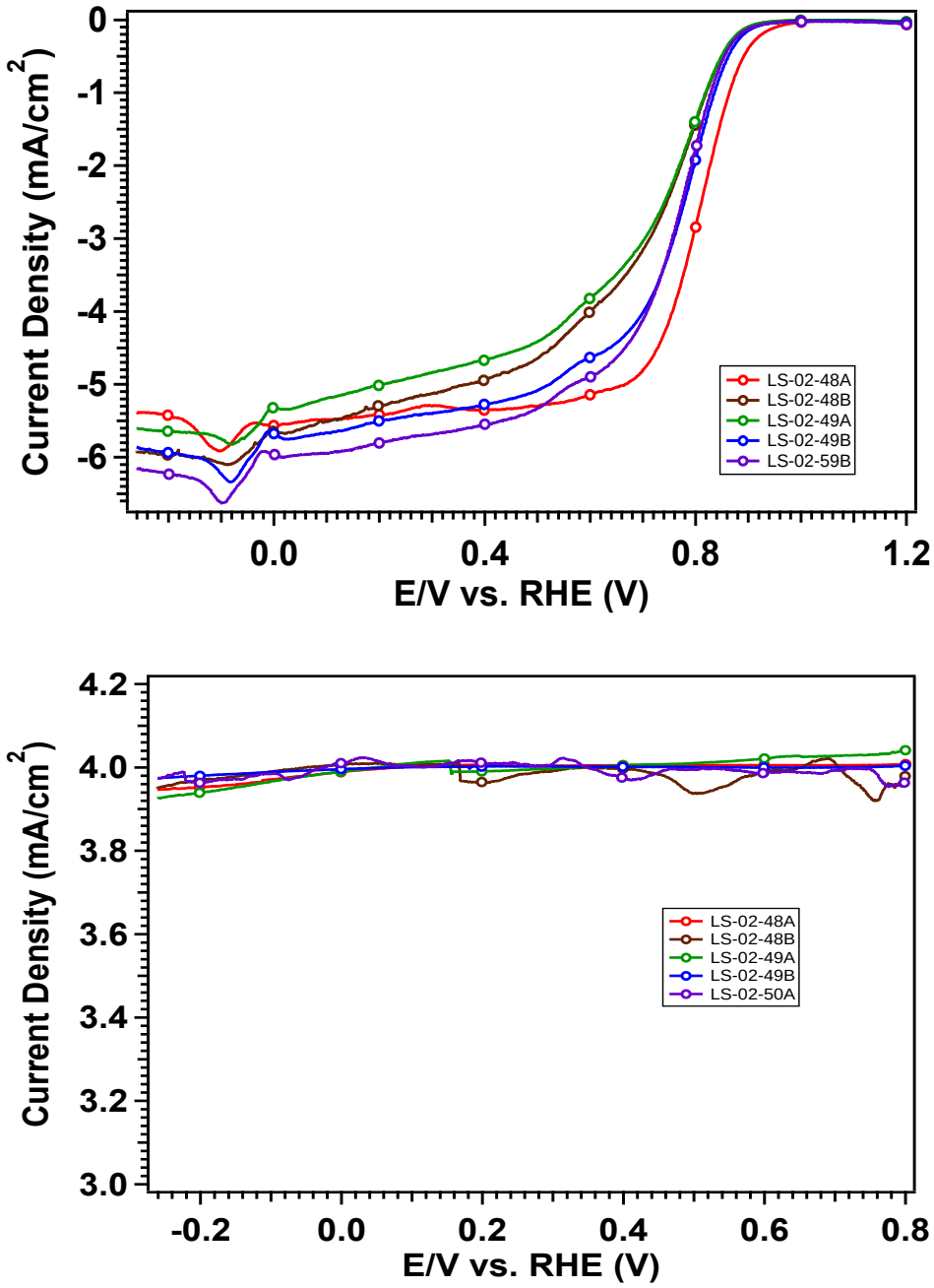

Figure 32 - (a) RRDE linear scan voltammetry for lignin-based binders in solution using a non-PGM organometallic catalyst system (b) Electron transfer study using a RRDE with Pt ring. Electrolye: 0.1M KOH, reference electrode: Hg/HgO, CE: Au wire, WE: glassy carbon disk.

Comparated to the modified lignin ORR electrocatalysts, the performance of modified lignin binders show good onset potential with binder 1 measuring approximately 0.95V v RHE and binders 2-5 all measuring approximately 0.91V v RHE. All binders showed reasonably well-defined diffusion limiting current plateaus however, binder 1 displayed the most stable behavior in this region with all samples approaching a current density of 6 mA cm^{-2}. RRDE ring currents were also measured to determine the number of electrons transferred in the reaction. All binders displayed stable 4 electron transfer across the full potential window indicating high specificity for the desired ORR pathway.

GDLs were also fabricated using 5% weight loading Pt/C on carbon paper in order to use the SEM to explore the morphology and dispersion of the lignin binder over carbon. SEM micrographs and associated electron dispersion X-ray spectroscopy (EDS) are shown in **FIGURE 33**, below. As shown in the cross sectional micrograph, there is a distinct linear domain where the catalyst layer adjoins with the carbon paper. The corresponding EDS in part B of the figure clearly shows that nearly all of the catalyst mixture sits on top of the carbon paper. Part C and D indicate that the binder is evenly dispersed throughout the catalyst layer although integration of the EDS spectrum indicates that the nitrogen content is only half that of oxygen. This is evidence to support possible low chemical conversion in the modification of lignin that could lead to lower than desired conductivity.

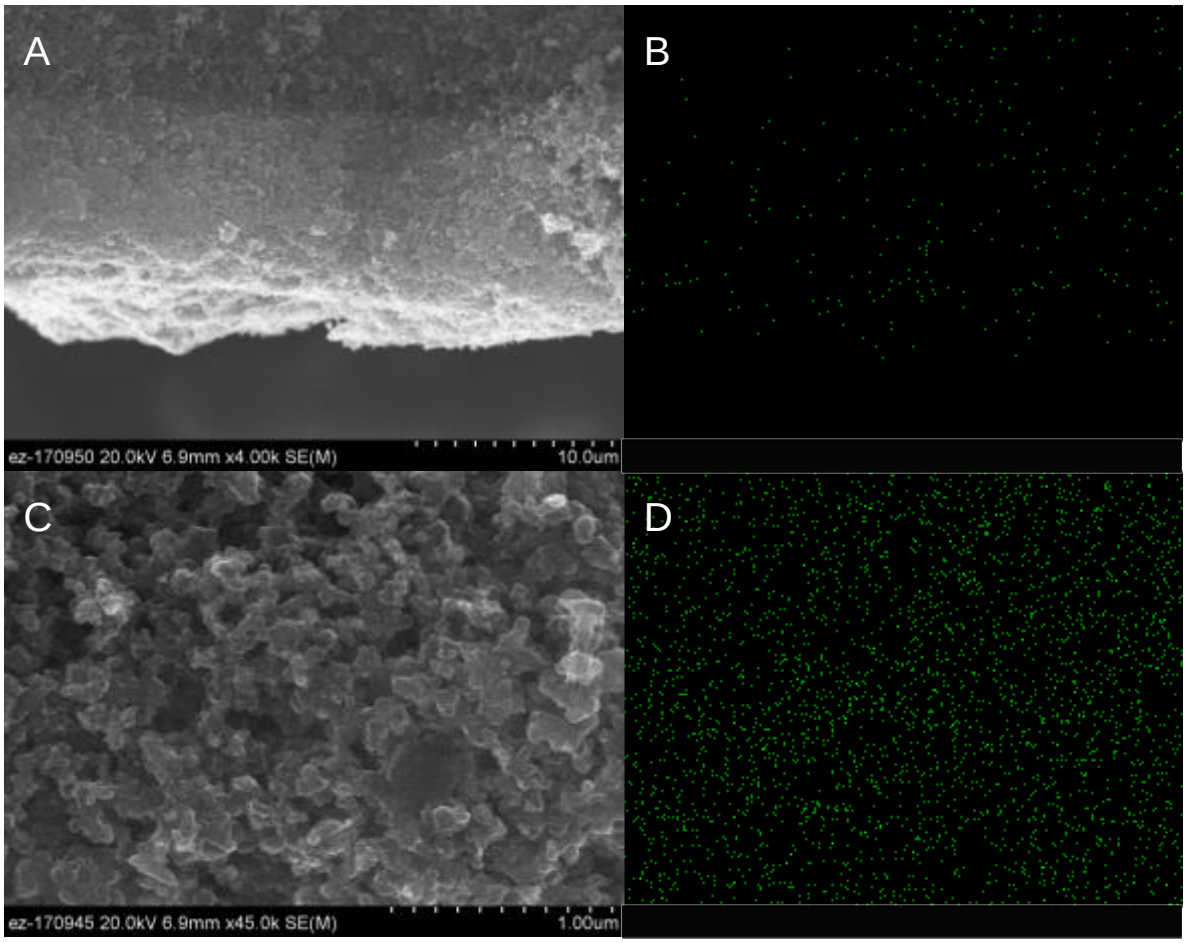

Figure 33 – SEM micrographs and corresponding EDS plots for nitrogen abundance of lignin binder with 5% by weight Pt/C GDL. A – cross-sectional view showing the depth of the catalyst layer; B – corresponding EDS spectrum indicating the dispersion of nitrogen throughout the layer; C – surface micrograph showing the catalyst layer; D – EDS spectrum showing the nitrogen dispersion on the surface of the catalyst layer.

3.9 Conclusions

Unsupported lignin catalysts and ionic binder materials were synthesized and tested under alkaline conditions on RDE and RRDE test apparatuses. By modifying organosolv lignin using a diazonium coupling scheme, we were able to attach a diaminotriazole ligand to the lignin that is capable of chelating a number of different metal groups. Using non-PGM metals, this material was tested under alkaline ORR conditions to determine onset potential and peroxide formation. In both cases, the unsupported lignin showed poor onset and a 3-electron transfer, resulting in peroxide formation.

Lignin binders were tested with cobalt and iron catalysts in alkaline ORR conditions and exhibited onset potentials from approximately 0.9 to 0.95V v. RHE and measured a 4-electron transfer across the potential window. Most of the binders tested, however, showed poor affinity toward the modified carbon catalysts as well as showing poor dispersion on the electrode surface. SEM micrographs and corresponding EDS of the GDLs (gas diffusion layers) made with lignin binders and 5% Pt/C on carbon paper showed that while the binder was well dispersed on the carbon support, the visible nitrogen (ionic moiety) to oxygen ratio was only approximately 0.5:1, indicating poor conversion of hydroxyl units to impart ionic character to the binder.

Although lignin catalyst and binder testing was halted, follow-on lignin modification work successfully showed a number of different ways to add

functional/ionic character to lignin fragments – some of which were utilized in subsequent work.

CHAPTER 4 –

LIGIN-MODIFIED CROSSLINKED ANION EXCHANGE MEMBRANES

4.1 Abstract

Anion exchange membrane fuel cells (AEMFCs) have emerged as a promising area of research in the field of energy conversion devices due to their potential low relative cost and high performance. One of the major impediments to the current implementation of this technology is the efficient synthesis of high-performance membranes that are both highly ionically conductive and chemically stable. This research focuses on the synthesis of lignin-modified polymers and their application as potential anionic exchange membranes (AEMs). The central hypothesis rests upon the idea that lignin, a renewable feedstock material, can serve as a suitable analog to various petroleum-derived materials traditionally used in the chemical modification of polymers (i.e. poly-ethers, poly-acrylics). In this work, organosolv lignin was modified to function as a cross-linking additive to increase both ion exchange capacity (IEC) as well as the stability of prospective AEMs. To measure the effectiveness of the employed synthetic methods, crosslinking percentage (%CL) and theoretical IEC were varied across several different polymer chain chemistries. Electrochemical impedance, water uptake and swelling, and hydroxide anion concentration were measured to evaluate the resultant performance characteristics of the modified polymer. Lignin-modified crosslinked AEMs having olefin and poly-phenylene oxide (PPO) backbones displayed conductivity values as high as 64 and 127 mS cm^{-1}, respectively, in 1M NaOH. The PPO-based membrane, however, showed significantly better dimensional stability and retention of IEC after 7 days in 1M NaOH.

4.2 Introduction

The synthesis of novel anion exchange membranes has been an important and rapidly emerging field of research over the last decade. As an analog to the more heavily studied PEMFC, AEMFCs offer an interesting possibility in the production of power as well as other novel electrochemical separations. Interest, both industrial and academic, is owed in large part to the physical and chemical benefits of many chemical/electrochemical processes becoming more efficient (lower over-potentials) at high pH, which, in turn, necessitates less catalyst or simply allows for the usage of non-platinum group metals (non-PGM).[96,97]

The untethered or unsupported elongation of lignin for usage as either a solid or liquid electrolyte proves to be a difficult problem to solve for a number or reasons. Solubility difficulties complicate synthetic methods as the chemical modification of the lignin dramatically changes the overall character of the material. This can lead to overall low yields for desired products and the inefficient substitution of reactive moieties for usage in follow-on reactions. Additionally, lignin tends to suffer from poor chemical stability in alkaline environments, especially when hydroxyl units remain unsubstituted as they might in low-yield reactions – the highly nucleophilic phenolate anion is then free to react with nearby β-protons to begin elimination-based degradation.

Similar to prior approaches to modifying lignin, this work began with the premise that the unmodified organosolv lignin was essentially an amorphous macro-molecule with multiple, quantifiable functional moieties that would be used to

stoichiometrically calculate reactants. A simple way to think about this is by considering lignin as a di-, tris-, tetrakis-, etc substituted molecule except that lignin is not a pure compound. For example, considering a compound like 1,3,5-*tris*(bromomethyl)benzene) is three [3] times substituted with benzylic bromides, the pertinent molar quantity is that of the bromides and not necessarily the molar concentration of the parent species, itself. Lignin must be thought of in this way – in that, per gram of lignin, the concentration of –R group of interest must be known.

To that end, lignin was initially thought of as a functional polymer building-block that, given the right modification, could participate in a more traditional polymerization scheme. Considering that the library of publications on olefin polymerization is both broad and deep, the decision was made to employ olefin monomers, mainly pre-synthesized aryl and alkyl halides, to modify lignin so that it might be traditionally polymerized (as opposed to chemically elongated) for usage in the fabrication of anionic exchange membranes. To complement these olefinated lignin macromolecules, a number of other compounds were also synthesized to participate in the olefin polymerization schemes to help control the physical properties like hydrophilicity, structural flexibility, charge density, matrix morphology, etc of the resultant material.

There are numerous polymerization routes available to employ during the synthesis of a polymeric material. Some of the earliest methods employ the simple acid/base catalyzed polymerization of olefin monomers. Modern synthetic methods have been focused on achieving highly controlled reaction rates resulting in low polydispersity and high turnover. One of the most prevalent polymerization methods

used in the industrial production of a wide array of polymers is living chain growth or chain addition polymerization.

There are a growing number of polymerization methods that utilize the chain growth mechanism. One such method is the reversible-deactivation radical polymerization (RDRP) sometimes and previously referred to as living free-radical polymerization (LRP). In this method, an initiator molecule is employed in the synthesis of a radical species to start the propagation of the growing chain. Chain growth is dependent upon the equilibrium between a dormant and active species of the chain. Likewise, chain size can be carefully controlled by controlling the concentration ratio between initiator and monomer species. In this work, two different LRP methods were utilized in the synthesis of polymer chains – atom transfer reversible polymerization (ATRP) and nitroxide mediated reversible polymerization (NMRP).

Due to the presence of halogens in many of the olefin monomers employed in the modification of these polymerization precursors, atom transfer reversible polymerization (ATRP) was initially employed as the primary means of polymerization. Broadly, ATRP involves the reaction of an organic initiator containing a transferable halide with a metal-halide/ligand complex. The metal-halide must be capable of multiple stable oxidation states. Initiation occurs when the metal-halide abstracts the transferable halide from the organohalide, thus creating the activated initiator species and the dormant/deactivator (higher oxidation) state of the catalyst (M^n-X/L --> M^{n+1}-X_2/L).[98] The general reaction scheme for this mechanism is shown below in **FIGURE 34A**. As shown in the figure, the initiated

radical then begins the radical propagation of the growing chain. The rate of chain growth, size of the chain and polydispersity of the polymer are directly associated with the reactivity of the catalyst as well as the relative concentration of the non-activated organohalide and the dormant/deactivator metal-halide species.[99] Additionally, the reversible nature of this polymerization method as well as the possibility for the use of bi-functional initiator species make ATRP an ideal candidate for grafted and block polymers.[100] **FIGURE34B** illustrates the general ATRP scheme as it associates to olefin-modified lignin molecules in the polymerization of a styrene-lignin polymer.

As seen in the reaction scheme, an initiator with an activated halogen is required to begin the growing chain. This allows for a large degree of tenability when designing materials with multiple functional moieties that can be used to control morphology. A copper (I) catalyst was used because of the metal center's relatively high affinity to accepting the bromide/halogen atom from the initiator to induce the initial radical. Shown in **FIGURE 34B**, the initiator that was first used, which is also generally the compound sourced in the classical examples of ATRP, was ethyl α-bromoisobutyrate [EBIB] due to the highly-activated bromide alpha to the carbonyl. Here the nitrogenous ligand can serve to both stabilize the oxidation states of the metal as well as to help enable the alkoxide intermediate of the carbonyl to facilitate the bromide leaving. The resultant de-bromination/halogenation of the initiator activates the molecule and begins the living, propagating polymer chain, as the radical is continuously regenerated by the successive addition of free-radical

building blocks like styrene, 4-vinylbenzyl chloride and other olefin groups. The "living chain" is terminated with the thermodynamic equilibrium between the free-radical monomer and the displaced halide is achieved and the propagating chain is capped by the leaving halide from the metal catalyst. Generally, this type of polymerization is performed in a highly concentrated environment, often times opting to perform the reaction "neat" or, without the presence of solvent. Smart choice of metal catalyst can alleviate the need for solvent if a liquid monomer is used in conjunction with the modified lignin to form the polymer chain.

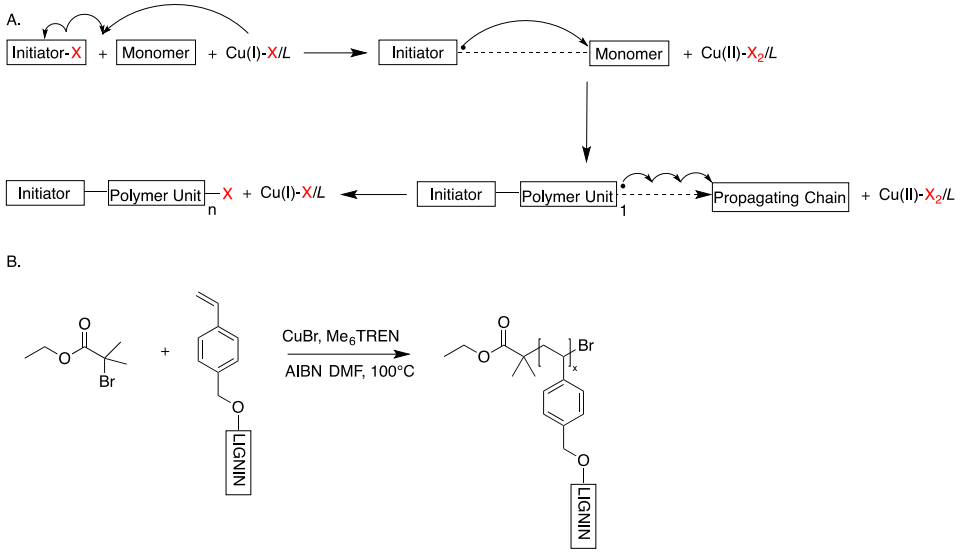

Figure 34 - a) ATRP chemical mechanism illustrating the initiation of the propagating chain predicated on the halide abstraction event; b) illustrates the general reaction scheme of the polymerization of modified/olefinated lignin subunits via the ATRP.

Similar to ATRP, NMRP is also an RDRP synthetic method for which chain growth and termination events are both a function of the equilibrium between active propagating and dormant species. Illustrated in **FIGURE 35**, NMRP utilizes a stable nitroxyl-radical species to mediate the propagation of the growing polymer chain.[101] The most common of these stable radical species is TEMPO ((2,2,6,6-tetramethylpiperidin-1-yl)oxyl), a derivative of 2,2,6,6-tetramethylpiperidine, however, there are many commercially available molecules that are suitable nitroxide radical species that may also add increased functionality to the chain terminal. Additionally, as shown in the literature, a number of synthetic procedures exist to modify commercially available nitroxide species with a number of functional groups to expand the capabilities of these materials.[102,103,104] Nitroxide mediators can be purchased in either the stable radical form or in the form of protected alkoxyamines that decompose to form the radical species under increased temperatures. The ability to make modifications to the mediator as well as the thermodynamically reversible mechanism make this method of polymerization an extremely powerful tool in the synthesis of both linear block-style as well as grafted polymeric materials. An example of this functionality is illustrated in **FIGURE 36**. In most cases, an organic initiator is used that thermally decomposes to generate a radical (or, two radicals) in order to initiate the propagating radical chain. This was the methodology used in this research. Benzoyl peroxide (BPO) was used as the radical initiator and TEMPO was used as the reversible terminating radical or mediator, as shown below.

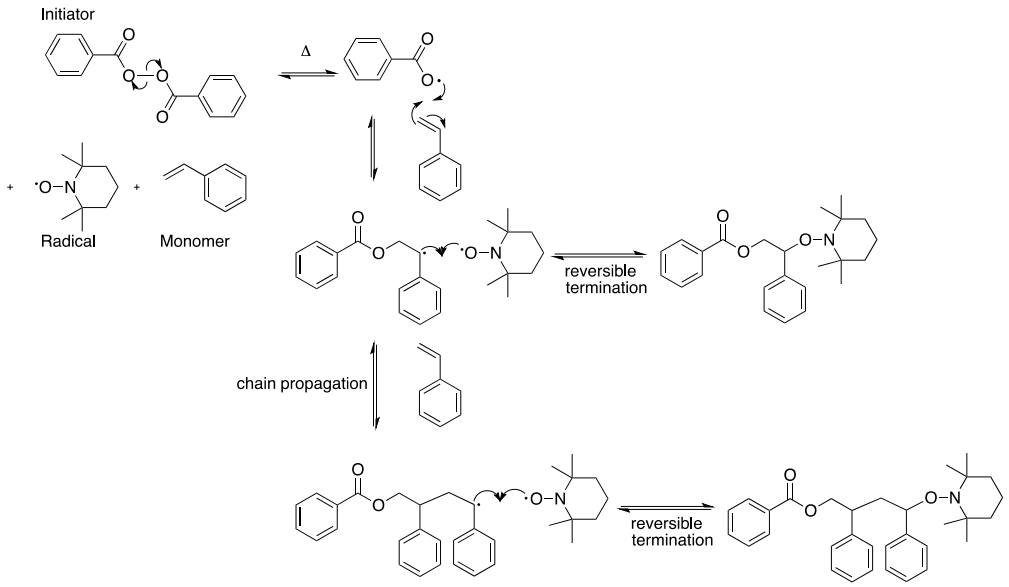

Figure 35 - Nitroxide mediated polymerization reaction mechanism illustrating the thermodynamic decomposition of benzoyl

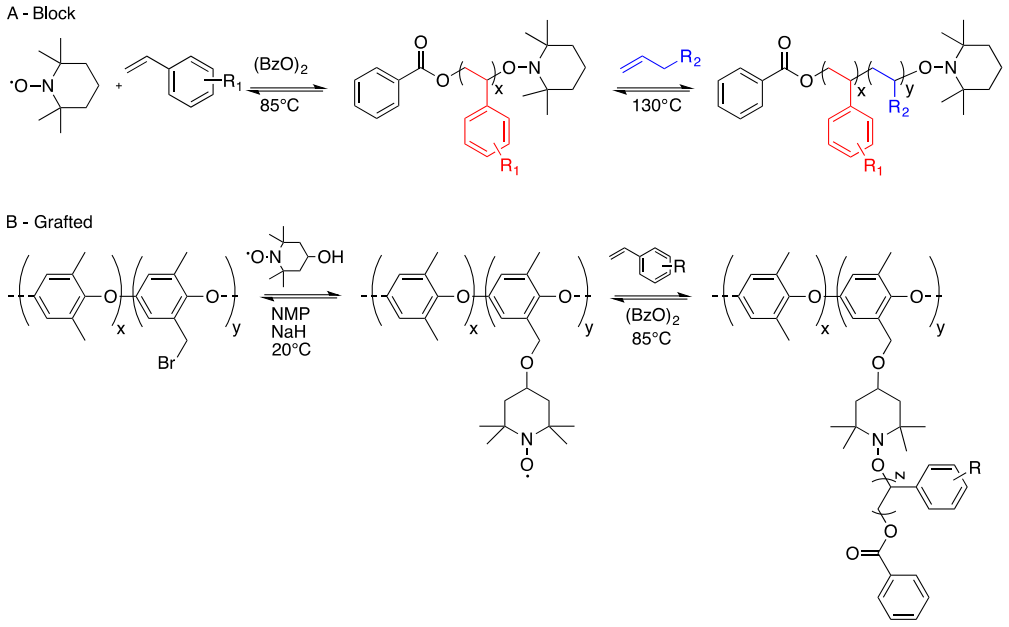

Figure 36 - A) Schematic illustration of NMRP in the synthesis of a block copolymer; B) Schematic illustration of NMRP in the synthesis of a grafted polymer (styrene on PPO).

Olefin-modified lignin molecules were synthesized using the same general reaction conditions as prior lignin modification schemes. The lignin-phenolate-sodium salt was induced by dissolving the solid in aqueous base (NaOH) in equimolar quantities as hydroxide concentration in the material, at room temperature for one to two [1-2] hours. Water was then removed under vacuum and the remaining solid was washed with water to remove any remaining base. After drying, the sodium salt form of the lignin can be dissolved in almost any appropriate solvent. THF was often used due to ease of vacuum evaporation. Remaining solid should be washed with chloroform or dichloroethane and dried. Similar olefinated molecules were synthesized to be utilized as pendant charge-carrying groups by attaching various amines to create the iminium ion as well as di-olefinated species that could be used to crosslink or dope the backbone.

4.3 Experimental Methods

4.3.1 Synthetic procedures

para-vinylbenzylchloride-modified lignin [VBCML]. [VBCML] was synthesized by reacting dry, organosolv lignin with *p*-VBC in a suitable solvent in the presence of a quaternary ammonium salt. Crushed, dry oranosolv lignin was added (1 g, 3.15 mmol –OH, 1 eq.) to a solution of 1M NaOH (5 mL) and stirred at room temperature until dissolved. After complete dissolution, commercially available *p*-VBC (90%) was added (1 mL, 6.38 mmol, 2 eq.) to the mixture and stirred. A small amount of

tetrabutylammonium bromide was added (100 mg, 0.31 mmol, 0.1 eq.) to the mixture and stirred at 40°C for 12 hours. Following the reaction, the mixture was diluted with H_2O (50 mL) and quenched with HCl. The suspension was then centrifuged and the solvent decanted and discarded. The remaining solid was washed with water (2 x 50 mL) and ether (1 x 50 mL) and dried overnight under vacuum at 40°C. ν_{max}/cm^{-1} – 3058 (sp^2-hybridized CH), 1591 (C=C bend), 1511 (aromatic C-H bend), 1454 (symmetric CH_2 bending), 1008 (aryl CO) – abs/KBr.

Tetraethylene glycol-bis-azide ([TEG-bis-N_3]) [TEG-bis-N_3] was synthesized by stirring tetraethylene glycol-bis-ditosylate and sodium azide (or, other suitable azide, like, tetrabutylammonium azide, etc) in DMF. Commercially available tetraethylene glycol ditosylate (98%) was added (1.02 g, 2 mmol, 1 eq.) to 5 mL of DMF and stirred at room temperature until fully dissolved (about 10 minutes). Sodium azide was then carefully added (162 mg, 2.5 mmol, 1.25 eq) to the mixture and stirred at room temperature for 12 hours and then 60°C for 12 hours. Reaction was monitored via TLC. Following the reaction, the mixture was centrifuged and the precipitate was separated and discarded by decanting. The solvent mixture was then concentrated under vacuum. The resulting material was diluted in ethyl acetate (30 mL) and washed with water (3 x 50 mL). The organic layer was separated and the solvent removed under vacuum. The remaining material was dried under vacuum at 60°C overnight. This procedure was adapted from Kimura, et. al., 2016.[105] GC/(EI)MS *m/z*:

42.05 (100%), 43.05 (60.3), 44.05 (59.2), 45.05 (56.5), 107.0 (51.78), 109.0 (50.5), 56.05 (31.6), 72.05 (27.1), 216 (M-N_2 0.69).

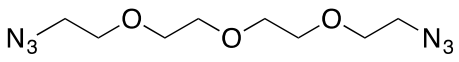

tetraethylene glycol-bis-azide
Exact Mass: 244.13

2-methyl-1-(4-vinylbenzyl)-1H-imidazole [MVBIm] monomer. [MVBIm] was synthesized by reacting p-vinylbenzyl chloride (pVBC) with 2-methylimidazole in a suitable solvent of moderate polarity with a non-nucleophilic, moderately strong base. Dry potassium *tert*-butoxide (99%) was added (745mg, 6.5 mmol, 1.02 eq.) to 10 mL of THF. HMIm (98%) was then added (529 mg, 6.39 mmol, 1 eq.) to the mixture and stirred at room temp for 15 minutes or until gas evolution ceased. Following room temperature stirring, pVBC (90%) was added (1 mL, 6.39 mmol, 1 eq.) to the mixture and stirred overnight at 40°C. Following the reaction, the mixture was cooled and the solvent was removed under vacuum. The resultant oil was dissolved in dichloromethane (20 mL) and washed with water (3 x 50 mL). The organic phase was recovered and solvent removed under vacuum. The resulting oil was dried overnight under vacuum at 40°C. GC/(EI)MS *m/z*: 117.05 (100%, M – $CH_3C_3H_2N_2$), 198.15 (68.35, M^+), 115.1 (64.26), 91.1 (36.5), 199.15 (11.32).

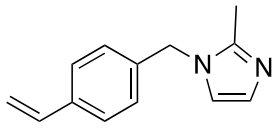

2-methyl-1-(4-vinylbenzyl)-1*H*-imidazole
Exact Mass: 198.12

p-vinylbenzyl-N,N,N-trimethylaminium ([pVB-TMA][Cl]) monomer. [pVB-TMA][Cl] was synthesized by stirring a mixture of p-vinylbenzyl chloride (p-VBC) and 1 molar trimethylamine (THF) in dry THF at 40°C for 12 hours. Commercially available pVBC (90%) was added (785 μL, 5.0 mmol, 1.0 eq.) to 5 mL of dry THF and stirred at room temperature. Dry TMA (1M in THF) was added (5.5 mL, 5.5 mmol, 1.1 eq) to the mixture at room temperature. The temperature was increased to 40°C and the mixture was stirred for 12 hours. The mixture was then cooled and centrifuged. The solvent was decanted and a yellow-ish/white solid precipitate was recovered. The solid was washed with DCM (2 x 20 mL) and ether (1 x 20 mL). The resulting white powder solid was dried overnight at 40°C under vacuum to yield a white, hygroscopic powder. Kept in desiccator to reduce moisture content. Yield: 994mg (94%). HR(ESI)MS m/z: 176.17 (100%, M^+), 117.089 (53.6), 100.096 (47.1), 117.169 (4.55) – 1:1 acetonitrile/H_2O.

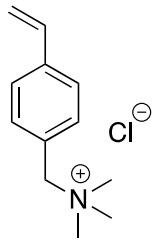

p-vinylbenzyl-*N,N,N*-trimethylaminium chloride

Exact Mass: 211.11

p-vinylbenzyl-2,3-dimethyl-1H-imidazol-3-ium chloride ([pVB-DMIm][Cl]) monomer. [p-DVB-DMIm][Cl] was synthesized by stirring a mixture of p-vinylbenzyl chloride (p-

VBC) and 1,2-dimethylimidazole in THF at 40°C for 12 hours. Commercially available p-VBC (90%) (800 μL, 5.1 mmol, 1.02 eq) and commercially available DMIm (96%) (500 mg, 5.0 mmol, 1 eq) were added to dry THF (10 mL) and stirred for 6 hours at 50°C. After stirring and cooling, a yellow-ish/white solid precipitate formed. Mixture was centrifuged and the solvent was removed by decanting. Remaining solid was washed with DCM (2 x 30 mL) and sonicated for 20 minutes at room termperature and then centrifuged and the solvent decanted. The solid was also washed with diethyl ether (1 x 30 mL). Solid was dried overnight at 40°C under vacuum to yield a white, hygroscopic powder. Solid was stored over $MgSO_4$. Yield: 1.024g dry solid. HR(ESI)MS m/z: 213.163 (100%, M^+), 100.095 (37), 117.091 (30.5), 214.166 (10.5) – 1:1 acetonitrile/H_2O.

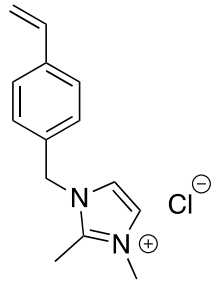

p-vinylbenzyl-2,3-dimethyl-1*H*-imidazol-3-ium chloride
Exact Mass: 248.11

1-(azidomethyl)-4-vinylbenzene ([AMVB]). [AMVB] was synthesized by reacting *p*-VBC with a source of azide in a suitable solvent and low heat. Commercially available p-VBC was added (1 mL, 6.39 mmol, 1 eq.) to 20 mL of dry DMF and stirred at room temperature. Solid NaN_3 (495 mg, 7.5 mmol, 1.17 eq.) was added to

the mixture and stirred at room temperature for 24h. Following reaction completion, the mixture was diluted with 50 mL of ethyl acetate. The mixture was then centrifuged and the precipitate was separated and discarded by decanting. The organic mixture was recovered and transferred to a 250 mL separatory funnel and subsequently washed with 3x150 mL volumes of saturated brine. Following recovery of the organic phase, a 250 mL round bottom flask was used to concentrate the remaining mixture under vacuum using the rotary evaporator. The resulting oil was dried overnight in the vacuum oven at 60°C. GC/(EI)MS *m/z*: 105.1 (100%), 91.1 (58.8), 118.1 (41.31), 117 (4.97) – $CHCl_2$.

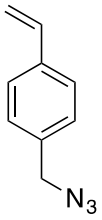

1-(azidomethyl)-4-vinylbenzene
Exact Mass: 159.08

1-(azidomethyl)-4-(bromomethyl)benzene ([AMBMB]). [AMBMB] was synthesized by reacting α,α'-dibromo-p-xylene with 1 molar equivalent of a suitable source of the azide moiety in polar solvent at moderate heat. Commercially available α,α'-dibromo-p-xylene (97%) was added (1360 mg, 10 mmol-Br, 2 eq.-Br) to sodium azide (NaN_3) (330 mg, 5 mmol, 2 eq.) and dissolved in 10 mL of DMF. The mixture was stirred room temperature for 48 hours. Reaction was monitored by TLC (9:1 DCM/MeOH). Following reaction completion, the mixture was diluted with 50 mL of

ethyl acetate to precipitate any remaining NaBr in solution. The mixture was centrifuged and the solvent was decanted and recovered for further purification. The crude product mixture was transferred to a 250 mL separatory funnel and subsequently washed with 3x 150 mL volumes of saturated brine. Following recovery of the organic phase, a 250 mL round bottom flask was used to concentrate the remaining mixture under vacuum using the rotary evaporator. The resulting oil was dried overnight in the vacuum oven at 60°C. GC/(EI)MS *m/z*: 146.1 (100%, M – CH_2Br), 91.1 (52.55), 104.1 (36.44), 183 (8.03), 117.1 (7.79), 225 (3.04) – $CHCl_2$.

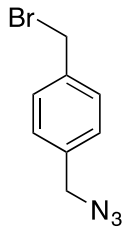

1-(azidomethyl)-4-(bromomethyl)benzene
Exact Mass: 224.99

Propargylated Lignin ([ProLig]). [ProLig] was synthesized by reflexing organosolv lignin and propargyl bromide in acetonitrile over solid NaOH. Dry, solid NaOH was added (252 mg, 6.3mmol, 2 eq.) to 20 mL of dry acetonitrile in a round bottom flask. Dry, organosolv lignin was added (1 g, 3.15 mmol-Br, 1 eq.) to the mixture along with propargyl bromide (80%) (1mL, 8.98mmol, 2.85 eq.) and refluxed for 24 hours. The mixture was then transferred to 40 mL shell vials to be centrifuged. The solvent was decanted and discarded and the remaining solid was combined and washed with water (3 x 50 mL) and sonicated in toluene (2 x 50 mL) for 20 minutes. Solid

was then dried under vacuum at 60°C. ν_{max}/cm^{-1} – 3288 (≡C-H) stretch, 2931 (sp^3-hybridized CH), 2122 (C≡C), 1712 (C-O) – abs/KBr.

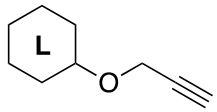

propargylated lignin
**hexagon used to generically denote lignin structures*

1,2-dimethyl-3-(prop-2-yn-1-yl)-1H-imidazol-3-ium bromide ([Pro-DMIm)][Br]. Commercially available HMIm (98%) was added (294 mg, 3 mmol, 1 eq.) to 10 mL of dry toluene in a round bottom flask and stirred at room temperature for 30 minutes after which propargyl bromide (80% w/w in toluene) was added (368 μL, 3.3 mmol, 1.1 eq.) to the mixture. The mixture was then refluxed for 12 hours. The mixture, which had become heterogeneous, was then cooled and centrifuged. The solvent was decanted and discarded leaving a yellowish-white solid. The solid was washed with dry THF (2 x 30 mL) and dry toluene (2 x 30 mL) and dried under vacuum at 60°C overnight. The product was a white powder. Yield: 75%. This method was adapted the synthesis performed by from Li, Wang, Wu and Wang, 2012.[106] HR(ESI)MS m/z: 214.12 (M^+), 103.095, 149.05 – 1:1 acetonitrile/H_2O.

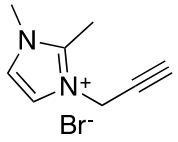

1,2-dimethyl-3-(prop-2-yn-1-yl)-1*H*-imidazol-3-ium bromide
Molecular Weight: 215.09

Polyphenylene oxide-azide ([PPO-N_3]). [PPO-N_3] was synthesized by reacting PPO-Br with trimethylsilane-azide (TMS-N_3) at room temperature. TMS-N_3 (95%) was added (523 μL, 3.75 mmol, 3 eq.) to 14.4 mL of dry NMP and stirred at room temperature. PPO-Br (10% w/w in NMP) was added (4.8 mL, 1.248 mmol –Br, 1 eq.) to the mixture to make a 2%w/w solution of polymer. The mixture was stirred at room temperature for 72hrs. The polymer mixture was then cooled to room temperature and precipitated (added dropwise) into cold methanol. The solid was washed (3x50mL) with methanol and sonicated for 20min at room temperature in methanol. The resulting off-white solid was dried under vacuum at room temperature. ν_{max}/cm^{-1} – 2919 (sp^3-hybridized CH), 2098 (N_3), 1602 (C=C), 1465 (aromatic C-H bend), 1189 (aryl CO) – abs/KBr.

Lignin-modified poly-phenylene oxide-DMIm ([LMPPO-DMIm]). [LMPPO-N_3] was synthesized by mixing [Pro-Lig] and [PPO-N_3] in NMP at 2-6% w/w modified polymer in the presence of suitable copper catalyst. For this reaction, dry PPO-N_3 was added (165 mg, 0.416 mmol –N_3, 1 eq.) to 3mL of dry NMP and stirred at room temperature until dissolved. In a separate vile, dry [Pro-Lig] was added (13 mg, 0.042 mmol, 0.1

eq.) to 1mL of dry NMP and stirred at room temperature until dissolved. CuI was then added (5 mg, 0.045 mmol, 0.1 eq.) to the lignin mixture along with solid, dry [Pro-DMIm] (80 mg, 0.374 mmol, 0.9 eq.) and stirred at room temperature until dissolved. The two mixtures were then combined and DMIm (96%) was added (40 mg, 0.4 mmol, 0.96 eq.) and stirred at 80°C for 6 hours. ν_{max}/cm^{-1} – 2921 (sp^3-hybridized CH),1598 (C=C), 1465 (aromatic C-H bend), 1193 (aryl CO) – HATR/ZnSe.

Model Compounds

1-(3-bromopropyl)-2-methoxybenzene ([BPMeOBn]). For this reaction, NaH (60%) was added (44 mg, 1.1 mmol, 1.1 eq.) to dry THF (4 mL) and stirred at room temperature until uniformly mixed. Next, commercially available guaiacol (98%) was added (113 μL, 1 mmol, 1 eq.) to the mixture and stirred at room temperature for 15 minutes until bubbling had stopped. Then, 1,3-dibromopropane (99%) was added (113 μL, 1.1 mmol, 1.1 eq.) to the mixture and stirred at 60°C for 6 hours. Reaction was monitored by TLC. Reaction mixture was then cooled and centrifuged. The solvent was recovered by decanting and solids were discarded. Remaining solvent was then removed under vacuum in two steps – first to remove THF and second to remove excess 1,3-dibromopropane. The remaining oil was dried overnight under vacuum at 80°C. GC/(EI)MS m/z: 109 (100%), 135 (94), 137 (90), 124 (84), 215 – M^+ (1.34).

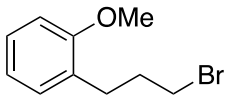

1-(3-bromopropyl)-2-methoxybenzene
Molecular Weight: 229.12

1-methoxy-2-(prop-2-yn-1-yloxy)benzene ([MPYnBn]). [*MPYnBn*] was synthesized by reacting propargyl bromide and guaiacol in DMSO in the presence of NaH (to form the dimsyl anion). Commercially available NaH (60%) was added (44 mg, 1.1 mmol, 1.1 eq.) was added to 2 mL of dry DMSO and stirred until fully dissolved. The temperature was raised to 80°C and the mixture was stirred for 4 hours. Then, commercially available guaiacol (98%) was added (113 μL, 1 mmol, 1 eq.) to the mixture along with propargyl bromide (80%/toluene) (111 μL, 1 mmol, 1 eq.). The mixture was stirred at 80°C for 12 hours. The mixture was then cooled and washed with dry ether (3 x 30 mL). The ether phase was collected and the solvent was removed under vacuum to yield a pale, yellow liquid. GC/(EI)MS m/z: 123.079 (100%, M – CH_2C_2H), 95.207 (48.2), 77.674, (48.2), 162.208 (47.4, M^+) – $(C_2H_5)_2O$.

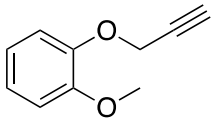

1-methoxy-2-(prop-2-yn-1-yloxy)benzene
Exact Mass: 162.07

3-(2-methoxyphenoxy)-2,2-dimethylpropyl-4-methylbenzenesulfonate [MPDMPOTs]. [MPDMPOTs] was synthesized by adding guaiacol (99%) (248 mg, 2 mmol, 2 eq.) to a 2mM solution of of NaDMSO and stirred at 0°C until dissolved. Commercially sourced 1,3-bis(tosyloxy)-2,2,-dimethylpropane (97%) was then added (415 mg, 1 mmol, 1 eq.) to the solution and stirred at 80°C for 12 hours. The reaction was monitored by TLC. Following completion, the solution was centrifuged and the solvent was decanted and recovered to remove solids. Solvent was then removed under vacuum. The resulting solids were dissolved in DCM (20 mL). DCM was then washed with water (50 mL x 3). The aqueous phase was discarded. Solvent was again removed under vacuum to yield a light-yellow liquid which was dried overnight at 80°C under vacuum. GC/MS(EI) *m/z*: GC/MS(EI) *m/z*: 124 (100%), 364 (M^+), 194 (M – guaiacol-OTs).

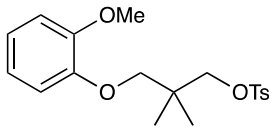

3-(2-methoxyphenoxy)-2,2-dimethylpropyl 4-methylbenzenesulfonate
Molecular Weight: 364.46

2,2'-((2,2-dimethylpropane-1,3-diyl)bis(oxy))bis(methoxybenzene) [DMoBzDMP] was synthesized by adding guaiacol (99%) (124 mg, 1 mmol, 1 eq.) to a 2mM solution of of NaDMSO and stirred at 0°C until dissolved. Commercially sourced 1,3-bis(tosyloxy)-2,2,-dimethylpropane (97%) was then added (830 mg, 2 mmol, 2 eq.)

to the solution and stirred at 80°C for 12 hours. The reaction was monitored by TLC. Following completion, the solution was centrifuged and the solvent was decanted and recovered to remove solids. The mixture was then washed with diethyl ether (50 mL x 3). The non-polar phase was recovered. Solvent was removed under vacuum to yield a light-yellow liquid. Remaining material was dried overnight at 80°C under vacuum. GC/MS(EI) *m/z*: 124 (100%), 316 (M^+), 194 (M-OTs).

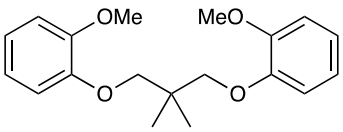

2,2'-((2,2-dimethylpropane-1,3-diyl)bis(oxy))bis(methoxybenzene)
Molecular Weight: 316.40

4.3.2 Spectroscopy and physical measurements

FT-IR was performed on a Bruker Vertex Series 80 spectrometer. Dry solids were analyzed in a Pike Technologies solid pellet absorbance cell. Samples were pressed into KBr pellets at 2% w/w at 1500 lbs in^{-1} for 30 seconds. Thin film samples were measured using the Pike Technologies horizontal attenuated total reflectance (ATR) attachment using a flat ZnSe sample window. Sample compartment was purged with dry N_2 for 5 minutes prior to sampling to remove atmospheric moisture. Samples were measured between 500 and 4000 cm^{-1} using 100 scans at a resolution of 4 cm^{-1}. All spectra were baseline corrected using 2nd order Savitzky-Golay smoothing and corrected for atmospheric artifacts.

GPC was performed to approximate the average numerical molecular weight (M_N) calculated by equation [3.2], weighted average molecular weight (M_W) calculated by equation [3.3] and polydispersity (D). All samples were run on a Tosoh EcoSEC utilitizing refractory index and UV-Vis at λ = 254 nm. All samples were dissolved in THF at 1.5-2 mg per mL of solvent. Elution time-based molecular weights were calculated based on a column calibration curve performed on polystyrene.

GCMS was performed on a Shimadzu GCMS-QP2010 SE with autosampler. All samples were tested in dry acetone at 0.1 mM concentration unless solubility issues arose, in which case methanol was used. GC peaks were integrated using the provided software.

High resolution ESI-MS was measured using a API QSTAR™ Pulsar Hybrid LC/MS/MS time of flight instrument. Samples were measured in 1:1 water/acetonitrile mixtures at 1 mM concentrations. Samples were run in positive mode with a 0.1% mixture of formic acid in methanol used as a co-solvent/ionizing mixture.

Electrochemical impedance spectroscopy (EIS) was performed using a standard 4-electrode impedence cell under atmospheric conditions. Frequency was measured between 1 Hz and 200 kHz at 6 points per decade and an amplitude of 10 mV.

Membrane hydroxide concentrations measurements were performed via acid-base titration. Membranes in the hydroxide form were soaked for 24 hours at

room temperature in a 0.1M solution (25 mL) of NaCl to form the chloride anionic membrane. Following the soak step, the membrane was removed and washed with deionized water (washing solution was saved and added to the soak solution. The total soak and wash solution was then titrated with 5 mM HCl to determine total exchangeable hydroxide concentration.

Membrane water uptake measurements were performed by measuring the mass difference between saturated and completely dehydrated samples of membrane. Membranes were soaked in pure water for 24 hours at room temperature. Membranes were then removed from water, quickly blotted dry and weighed. They were then dehydrated at 90°C under vacuum overnight and re-weighed. The mass difference was recorded as the mass of water absorbed.

Membrane thickness was measured using a benchtop digital comparator with a granite base. Membranes were measured in three places and the average thickness recorded for both saturated and dehydrated materials.

4.4 Discussion

In this research, three main synthetic routes were employed in the synthesis of lignin modified crosslinked AEMs. Two free-radical polymerization methods, NMRP and ATRP, were used to synthesize lignin-modified olefin-based (LMOB) membranes. The third method employed a commercially available PPO-Br polymer that was then modified similarly to the olefin-based membranes.

The most successful of these synthetic routes utilized the commercially available polymer utilizing brominated PPO. PPO has become an attractive material for applications in AEM synthesis. This is in large part due to the relative chemical robustness of the backbone in alkaline environments, relative to other common polymers used in this endeavor. In this work, PPO-Br was commercially sourced as a 4% w/w solution in NMP. The degree of substitution was 40%. Stock PPO-Br was modified according to the step-wise schematic shown in FIGURE 37. In this synthetic method, PPO-Br was globally azidified to modify the polymer to a suitable form to facilitate follow on click reactions. [ProLig] was used as a crosslinking agent while

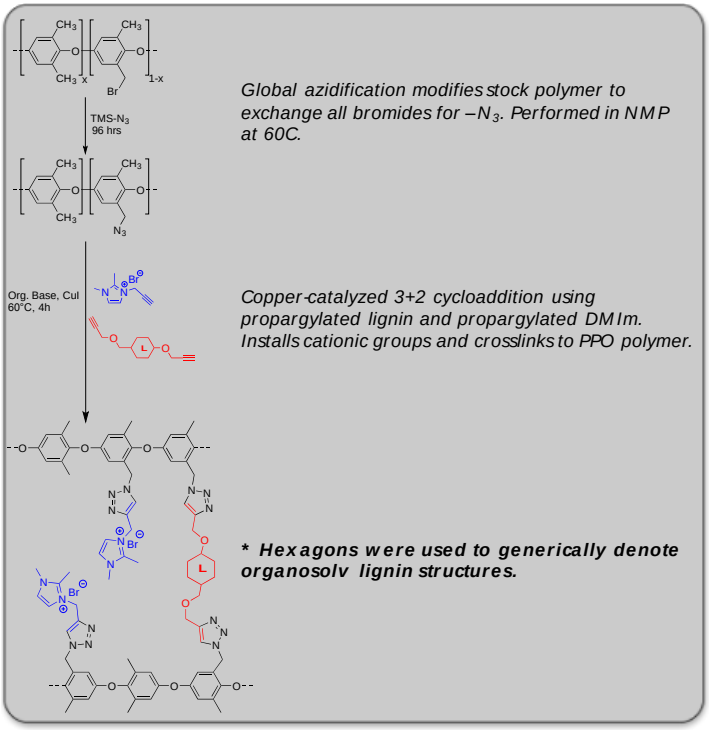

Figure 37 - Schematic of PPO-Br modification via copper-catalyzed click reaction employing propargylated lignin as a crosslinking agent and propargylated DMIm as a cationic group.

propargylated DMIm was added to impart cationic character to the polymer to synthesize [LMPPO-DMIm]. The level of crosslinking was controlled by controlling the concentration of propargyl units in the reaction mixture. LMPPO-DMIm crosslinking percentages were modified from 0% in control materials to a maximum of 30%. This translated to 13 mg and 40 mg of propargylated lignin for 10% and 30% crosslinking, respectively. In a 4% w/w casting solution of modified PPO, the total amount of polymer used was 165mg. A maximum of 6% w/w polymer loading was used in NMP, however, the higher loading mixtures were prone to solidification prior to casting, making them exceptionally difficult to manipulate. For this reason, only two 6% loading PPO membranes were successfully cast.

Lignin modified AEMs having PPO backbones were initially synthesized by direct substitution methods similarly to previous methods described to modify lignin. These materials, however, all suffered poor mechanical stability and swelling-induced decomposition. For this reason, the alkyne-azide cycloaddition chemistry was employed in an attempt to synthesize a crosslinked polymer with high cationic concentration and enhanced mechanical stability relative to direct substituted membranes.

In the literature, the [3+2] azide-alkyne cycloaddition can be performed both thermally as well as with a copper (I) catalyst. Under thermal conditions, the products of the cycloaddition yield a mixture of both 1,4- and 1,5-disubstituted regioisomers of the 1,2,3-triazole.[107] When the reaction is catalyzed using a copper (I) catalyst, however, the only the 1,4-disubstituted triazole product is observed.[108] In the synthesis of lignin-modified PPO AEMs using click chemistry, only the copper-

catalyzed reaction was performed. Based on a previous study using polymers synthesized via ATRP, FTIR spectra indicated that the copper-catalyzed click reaction allowed for lower reaction temperatures and yielded better conversion relative to thermal reaction procedures. FTIR spectra were also taken for lignin-modified, crosslinked PPO AEMs. Shown in **FIGURE 38**, the top spectra shows the complete disappearance of the peak associated with the alkyne C-H stretch at 3282 cm^{-1} that is clearly visible in the spectra of propargylated lignin shown in red in the bottom spectrum. The peak at 2100 cm^{-1} which is indicative of the $–N_3$ moiety, which is clearly visible in the middle spectrum for PPO-N_3 is also significantly diminished in the top spectrum for the cast polymer film indicating that the copper-catalyzed click reaction yielded high conversion prior to curing.

A parallel study was performed to investigate the effect of varying crosslinking percentage on click reaction conversion was performed. Polymer mixtures were identically arranged except for the quantity of [Pro-Lig] added. [Pro-Lig] was varied to synthesize crosslinked AEMs of 10, 20 and 30% at 4% w/w of polymer in NMP. This corresponded to additions of 13, 27 and 40 mg of [Pro-Lig] while the mass of dry polymer was 165 mg. The spectra for these parallel reactions are displayed in **FIGURE 39**. At 10% crosslinking, the peak for N_3 stretching at 2100 cm^{-1} is still clearly visible. Once the crosslinking percentage reaches 20%, this feature has disappeared indicating the azide moiety has completely reacted.

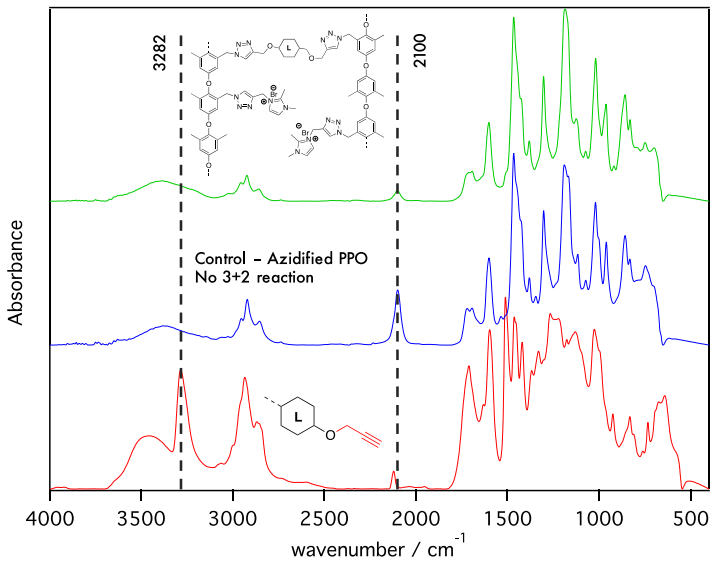

Figure 38 - FTIR spectra showing the copper-catalyzed [3+2] azide-alkyne cycloaddition of propargylated lignin (bottom spectrum), propargylated 1,2-DMIm and globally azidified PPO (middle spectrum) resulting in a lignin-modified, crosslinked PPO AEM (top spectrum). A hexagon, shown in the bottom spectrum, is used to generically denote lignin structures.

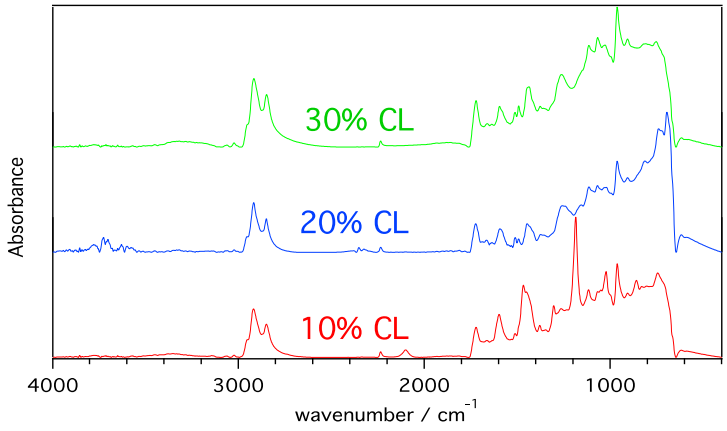

Figure 39 – ATR-IR spectra of parallel reactions with varied crosslinking percentage. Polymer mixtures were prepared in parallel at 4% w/w in NMP and cast onto a 5x10 glass casting area. Polymer films were dried under vacuum prior to measurement via ATR-IR.

Cured membranes were characterized by several different performance measures to assess the suitability of each material as a possible AEM. Polymers were cast in quantities of approximately 150-400 mg of dry polymer in 4 mL of solvent, either DMF or NMP, in a casting area of 5 x 10 cm and cured at 70°C for 12 hours. This yielded a suitable area from which to cut 8 uniform strips of membrane to characterize in parallel. Membranes were soaked in DI water for 24 hours, 1M HCl for 24 hrs and finally, in a 1M NaOH solution for an additional 24 hours to exchange all accessible counter ions to hydroxide anions prior to testing. This is done to test the conductivity of hydroxide anions (instead of the other anions that are native to the polymer after modifications) in both 1M alkaline solution, where free hydroxide anions can participate as well as in pure water.

Conductivity was measured using a standard 4-electrode cell to measure potentiometric electrochemical impedance (PEIS). By varying the frequency by which a potential is applied, it is possible to ascertain the ohmic resistance by calculating the x-intercept using a Nyquist Plot. Conductivity (σ) was calculated from this value using equation [4.1] where *d* is the distance between the two working electrodes, R_m is the measured resistance in ohms, L_s is the thickness and W_s is the width of the measured sample.

$$\sigma = \frac{d}{R_m L_s W_s} \qquad [4.1]$$

Membranes were also prepared to measure water uptake which is calculated as the difference in the wet vs dry weight divided by the total weight of polymer in the membrane, as seen in equation [4.2]. Ion exchange capacity, IEC, was also calculated using [4.3], which is essentially the quantitative capacity of a material to allow a particular ion to pass through the polymer matrix. Stated another way, IEC is the physical capacity of a material to hold exchangeable ions. To calculate IEC, the total moles of OH^{-1} must be measured. To accomplish this, membranes that were previously soaked in 1M NaOH were washed with DI water and transferred to a solution of 0.1M NaCl for a period of 24 hours. Following the equilibration period, membranes were removed from the solution, washed with DI water (the wash was recovered to be measured) and the equilibrating solution was titrated with 0.001-0.005M HCl to determine total OH^{-} content. The difference between this calculated number and the stoichiometric calculation of the number of charged species in the sample gives information about the polymer morphology. For example, a large difference between these numbers would indicate that the microstructure of the polymer has resulted in a high number of “dead end” channels that might hold bulk water but that do not allow for the facile flow of ions. Another important calculation was the water content, λ, which is defined as the number of water molecules per available anion in the polymer matrix [4.4]. This number can also give an indication regarding the IEC of the material in that as a polymer becomes more ionically conductive, it will also absorb more water due to the strong hydration effects of ionic functional groups.[109]

$$water\ uptake = \varphi = \frac{m_h - m_d}{m_d} \times 100 \quad [4.2]$$

$$IEC = \frac{mmol\ OH^-}{g\ polymer} \quad [4.3]$$

$$\lambda = \left(\frac{m_h - m_d}{m_d}\right)\left(\frac{1000}{IEC\ x\ M_{H_2O}}\right) \quad [4.4]$$

The tabulated data for these [LMPPO] membranes are displayed below in **TABLE 6**. LM_xPPO_y-$DMIm_z$ was used as the naming basis for these membranes where the subscript 'x' denotes the crosslinking percentage (i.e. x = 0.2 means the membrane was crosslinked to a degree of 20%). The subscript 'y' denotes the weight percent of polymer used in the mixture. The subscript 'z' denotes the molar equivalents of propargylated DMIm used. In cases where a secondary alkylating agent was used to alkylate the 1,2,3-triazole generated from the click reaction, that material is annotated at the end of the sample name. Structures are displayed in the table. In all membranes shown in the table, the calculated ionic concentration of the membrane, which is defined as the mmol OH^- per gram of polymer, is significantly higher than the measured IEC, which was determined by titrating the mobile hydroxide content in the membrane. It is possible that a number of phenomena could be occurring to account for this difference. Firstly, the ionic groups could be eliminating in the presence of free-hydroxide ionic in solution, as previously discussed, by Hoffman elimination, etc. Secondly, chemical conversion, especially

Table 6 - PPO-based membrane synthesis material quantities and tested performance metrics. Numbers in parentheses refer to molar equivalent values relative to the concentration of azidified polymer.

	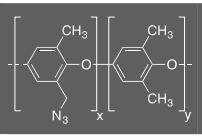	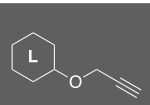	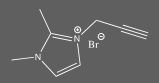	Secondary Alkylating agent	Calculuated IEC (mmol OH/g polymer)	Measured IEC (mmol OH/g polymer)	Water Content	λ (# of water molecules/ ionic group)	Conductivity mS cm^{-1} (1M NaOH)
$LM_{0.2}PPO_{0.04}DMIm_{0.8}$-Prop	165mg = 0.417mmol (1)	26mg = 0.084mmol (0.2)	45mg = 0.334mmol (0.8)	0.417 mmol (1) 	2.02	0.66	40.0	3.4	26.4
$LM_{0.2}PPO_{0.06}DMIm_{0.8}$-Prop	247mg = 0.625mmol (1)	40mg = 0.125mmol (0.2)	67.5mg = 0.5mmol (0.8)	0.417 mmol (1) 	2.02	0.43	44.5	5.8	6.0
$LM_{0.1}PPO_{0.04}DMIm_{0.9}$-Prop	165mg = 0.417mmol (1)	13mg = 0.042mmol (0.1)	51mg = 0.375mmol (0.9)	0.417mmol (1) 	4.8	0.44	24.3	3.0	
$LM_{0.3}PPO_{0.04}DMIm_{0.7}$-Prop	165mg = 0.417mmol (1)	40mg = 0.039mmol (0.3)	40mg = 0.292mmol (0.7)	0.417mmol (1) 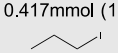	4.3	0.17	39.4	12.4	0.1
$LM_{0.1}PPO_{0.04}DMIm_{0.9}$-BPDMI-Br	165mg = 0.417mmol (1)	13mg = 0.042mmol (0.1)	50mg = 0.375mmol (0.9)	124mg (1) 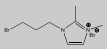	7.33	0.20	54.5	14.8	5.0
$LM_{0.1}PPO_{0.06}DMIm_{0.9}$	247mg = 0.625mmol (1)	20mg = 0.0625mmol (0.1)	76mg = 0.563mmol (0.9)	----	n.a	n.a	n.a	n.a	n.a
$LM_{0.2}PPO_{0.04}DMIm_{0.8}$-BDMHA-Br	165mg = 0.417mmol (1)	40mg = 0.039mmol (0.3)	40mg = 0.292mmol (0.7)	0.29mmol (0.7) 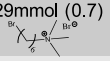	5.27	0.52	117	12.3	127
$PPO_{0.04}DMIm_{1.0}$	165mg = 0.417mmol (1)	---	56mg = 0.417mmol (1)	----	2.52	0.58	32.1	3.1	36
$PPO_{0.04}DMIm_{1.0}$-Prop	165mg = 0.417mmol (1)	---	56mg = 0.417mmol (1)	0.417mmol (1) 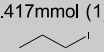	5.05	0.29	26.2	5.0	8.8

with regards to the alkylation of the 1,2,3-triazole, could be relatively low, resulting in poorly coordinated ionic groups that move into solution upon solvation. Thirdly, it is possible that the microstructure of the membrane is such that a high degree of non-continuous channels exist that inhibit the flow of hydroxide ions and that trap bulk water in non-ionic pores.[110]

As an alternative to using the commercially-sourced PPO-Br as a polymer precursor for synthesizing AEMs, in-house polymerization of LMOB membranes offered attractive synthetic route due to low costs and high tunability of the resultant materials. NMRP was the primary mode of polymerization in the synthesis of lignin-modified olefin polymer precursors in this synthetic route. Commercially-sourced *p*VBC, styrene and 8-bromo-1-octene were used as the polymer building blocks and stirred at 125°C under nitrogen in the presence of BPO and TEMPO. According to literature, the optimal molar ratio of TEMPO to BPO is 1.3:1 rather than the expected 2:1 ratio that would account for the splitting of the peroxo-species.[111,112] It is reasonable to assume that this is due to the many possible side reactions that are possible with the reactive peroxide. For this reason, NMRP reactions were performed in the absence of solvent to avoid unwanted solvent oxidation products contaminating the polymer.

The general reaction sequence for the synthesis of LMOB AEMs using the NMRP method of polymerization is show with annotations in **FIGURE 40.** The polymerization step, as shown, is performed neat and at a temperature between 90-130°C. Benzoyl peroxide decomposes in styrene at around 70°C however, in order

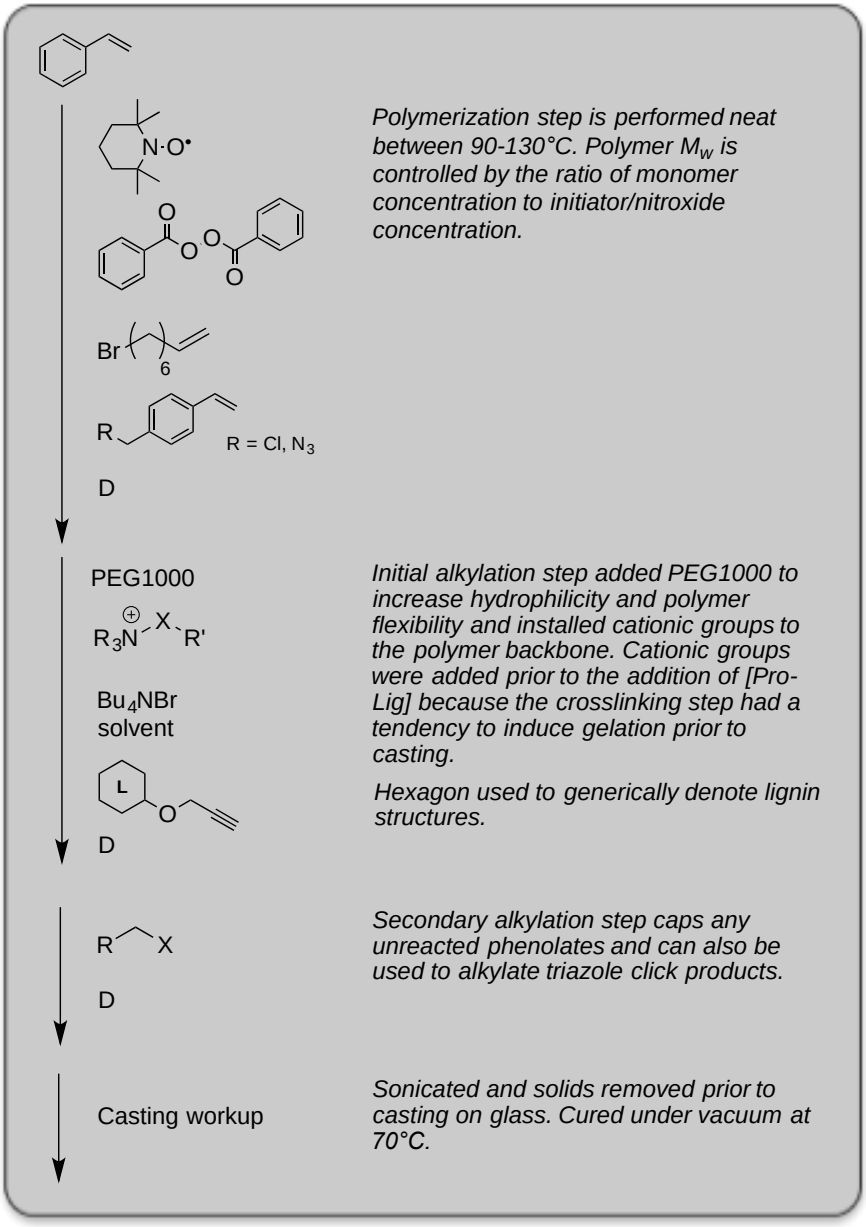

Figure 40 - Step-wise reaction sequence illustrating the synthesis of a lignin-modified polymer membrane via NMRP.

to ensure that the alkoxyamine species is reversibly formed, temperatures above 110°C are necessary. In-house synthesized olefin polymers were a mixture of styrene, *p*VBC and 8-bromo-1-octene. As with PPO-Br, halogenated olefins were modified via substitution reaction to exchange the halogen species to azides to allow for follow-on click reactions with [Pro-Lig]. Final workup of the mixture prior to casting involved sonication at room temperature for 60 minutes and centrifuging to remove any solids. Mixtures were cast onto glass and cured under vacuum at 70°C in the same method used to prepare LMPPO AEMs. GPC was performed on the NMRP-synthesized polymer precursors for LMOB AEMs to measure average molecular weight, (M_N) calculated by equation [4.5], weighted average molecular weight (M_W) calculated by equation [4.6] and polydispersity (D), calculated by equation [4.7].

$$M_N = \frac{\sum N_i M_i}{\sum N_i} \quad [4.5]$$

$$M_W = \frac{\sum N_i M_i^2}{\sum N_i M_i} \quad [4.6]$$

$$D = \frac{M_W}{M_N} \quad [4.7]$$

The data for these materials is displayed in **TABLE 7**. Samples names are indicative of the molar equivalents of each monomer used where 'S' is styrene, 'VBC' is *p*VBC and 'O' is 8-bromo-1-octene.

Table 7 - GPC data for NMRP-synthesized polymer precursors for LMOB AEMs.

				Target Weight	Average Molecular Weight (M_N)	Polydispersity (D)
$S_0VBC_{0.75}O_{0.25}$	n.a	6.39 mmol (18.75)	2.13 mmol (6.25) (-octene)	~4000	~6500	1.47
$S_{0.66}VBC_{0.22}O_{0.12}$	5.62 mmol (17)	1.87 mmol (5.66)	0.94 mmol (2.84) (-octene)	~4000	~5100	1.55
$S_0VBC_{0.75}O_{0.25}$ (performed in air)	n.a	6.39 mmol (18.75)	2.13 mmol (6.25) (-octene)	~4000	~4900	3.9
$S_{0.66}VBC_{0.23}O_{0.11}$	6.7 mmol (16.75)	2.20 mmol (5.5)	1.1 mmol (2.75) (-decene)	~4500	~7500	2.3
$S_{0.75}VBC_{0.25}O_0$	18.75 mmol (24.4)	6.25 mmol (8.13)	n.a	~7800	~7450	1.3
$S_{0.90}VBC_0O_{0.1}$	26.46 mmol (80)	n.a	2.5 mmol (7.58) (-decene)	~13500	~5200	2

Post-polymerization modifications were performed in NMP at concentrations varying from 0.25 – 0.8 moles/L. Halides were exchanged with azides via substitution with tetrabutylammonium azide at molar equivalents corresponding with the desired crosslinking percentage to be achieved with [Pro-Lig]. This lies in contrast to the method employed with LMPPO AEMs where benzyl bromides were globally substituted for azides. Polymers were then doped with commercially sourced PEG1000 to both increase water uptake properties and aid in the mechanical stability of the resulting membrane. Polyethers generally produce a more flexible polymer than poly-olefins and because polyether chains are significantly more polar than polystyrene, they tend to create hydrophilic domains as well as acting as a plasticizer for rigid polymer systems.[113] Stable membranes were tested for conductivity, IEC and water uptake using the same methods

previously outlined for LMPPO AEMs. Data for these membranes is tabulated in TABLE 8, below. General material names follow the convention of $NML_xPEG_yDMIm_z$, where 'N' refers to the molar quantity of halide on the polymer backbone, 'x' describes the molar equivalents of lignin, 'y' denotes the molar equivalents of PEG and 'z' denotes the molar equivalents of DMIm. When a secondary alkylating agent, like 1-bromopropane (Prop), it was annotated in the last space.

Generally, polymer AEMs display a positive relationship between IEC and conductivity as well as generally the same trend with water uptake and λ vs conductivity. As shown below in FIGURE 41, only conductivity v. λ exhibits a positive, linear trend, shown in part A. Both conductivity v. calculated IEC and conductivity v. water uptake display poor trending even when displayed relative to crosslinking percentage. In part D of the figure, ionic conductivity in 1M NaOH v. water uptake exhibits a reasonably defined linear relationship however there is still a high number

Table 8 - NMRP polymerized LMOB AEM testing data. Mass reported for polymer backbone is dry mass. Quantity in mmols refers to mmols of available halide for follow-on reactions.

	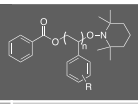	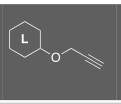	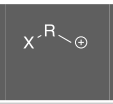	Secondary Alkylating agent	As-synthesized ionic content	IEC mmol OH/g polymer	Water Content	λ (# of water molecules/ ionic group)	Conductivity mS cm^{-1} (1M NaOH)
0.55LM$_{0.2}$PEG$_{0.1}$DMIm$_{0.6}$	270mg = 0.55mmol –Cl/Br (1)	35mg = 0.11mmol (0.2)	33mg = 0.33mmol (0.6)	---	1.22	0.64	54.5	4.7	95
1.54LM$_{0.2}$PEG$_{0.05}$DMIm$_{0.7}$	250mg = 1.54mmol (1)	91mg = 0.285mmol (0.2)	140mg = 1.4mmol (0.7)	---	5.6	1.0	81.9	4.5	52
0.65LM$_{0.2}$PEG$_{0.05}$DMIm$_{0.7}$-B	250mg = 0.65mmol (1)	41mg = 0.13mmol (0.2)	59mg = 0.59mmol (0.7)	---	2.03	0.64	62.7	5.4	48
1.54LM$_{0.2}$PEG$_{0.05}$DMIm$_{0.7}$-A-Prop	250mg = 1.54mmol (1)	91mg = 0.285mmol (0.2)	140mg = 1.4mmol (0.7)	0.286 mmol (0.2)	5.46	0.98	80	4.5	25
0.96LM$_{0.2}$PEG$_{0.05}$DMIm$_{0.7}$-Prop	290mg = 0.956mmol (1)	60mg = 0.191mmol (0.2)	100mg = 1.0mmol (0.7)	0.191mmol (0.2)	3.0	0.58	43.6	4.2	64

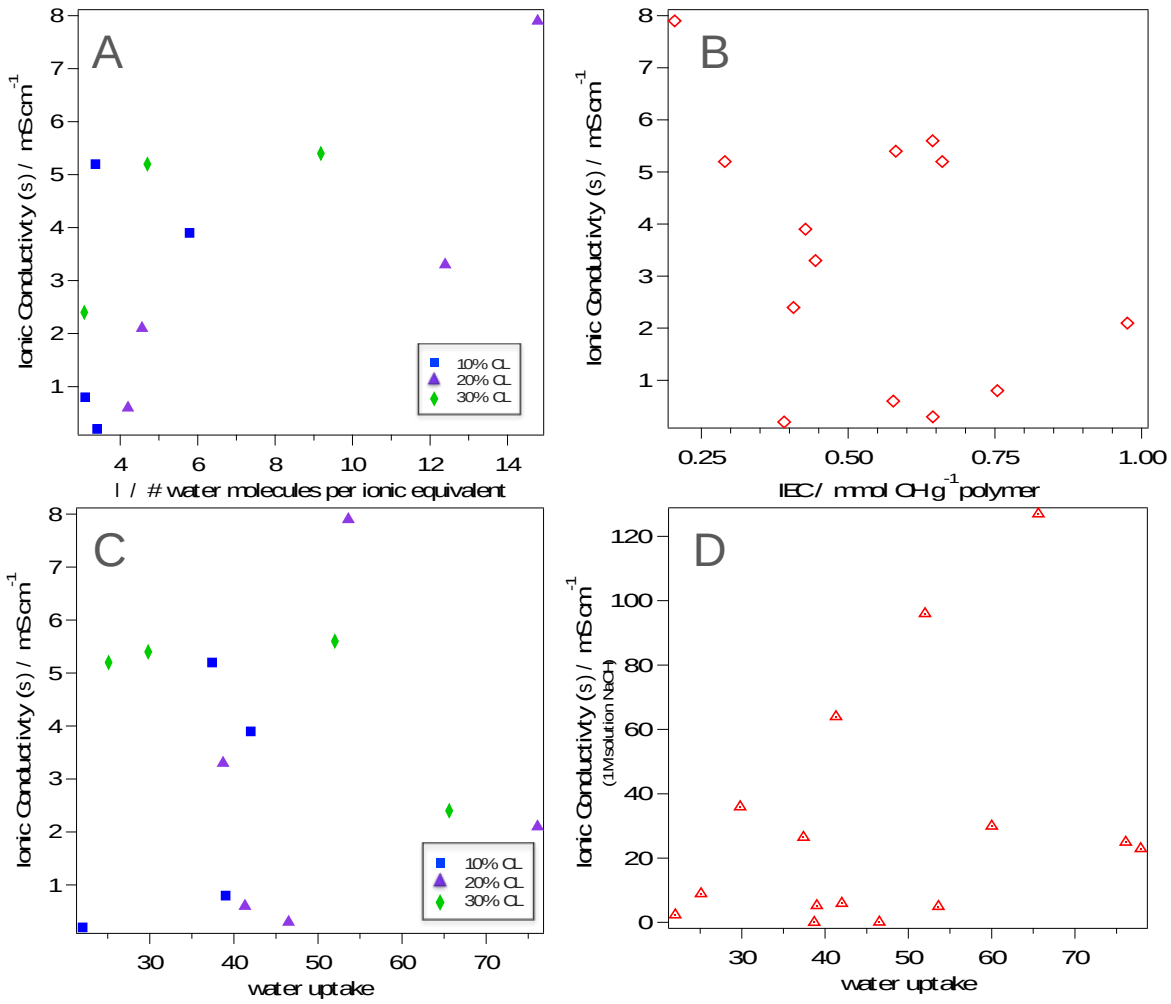

Figure 41 - Lignin-modified crosslinked AEM performance testing A) conductivity v. lambda relative to crosslinking percentage; B) conductivity v. IEC; C) conductivity v. water uptake relative to crosslinking percentage; and D) conductivity v water uptake.

of outlier data points that point to potential problems with the membranes. All of the membranes tested, as shown in part B of the figure, measured very low IEC values. The stoichiometric additions made during the synthesis of these membranes dictate theoretical IEC values of between 1.2-7, depending on the mixture while the measured values were often close to an order of magnitude lower. This could be explained either by poor chemical conversion resulting in a low concentration of cationic sites or potentially a high degree of tortuosity in the polymer matrix resulting in poor ionic exchange.

Water uptake was also evaluated relative to IEC, as shown in **FIGURE 42**, below. The relationship is graphed relative to the crosslinking percentage of the polymer, as indicated by color. This relationship should show a direct, positive relationship as water uptake is strongly influenced by the concentration of ionic groups present in the polymer. The graphic shows that, when categorized by crosslinking percentage, the membranes tested follow this trend reasonably well, though, there are certainly several outliers. It is interesting to note that the 30% crosslinked membranes display the steepest trend line slope, while the 10% and 20% crosslinked membranes have roughly the same slope. It is possible that the higher crosslinking percentage allows for greater water uptake due to the added structural stability afforded by increased polymer crosslinking. It's worth noting, also, that the 30% crosslinked membranes measured the lowest average conductivity.

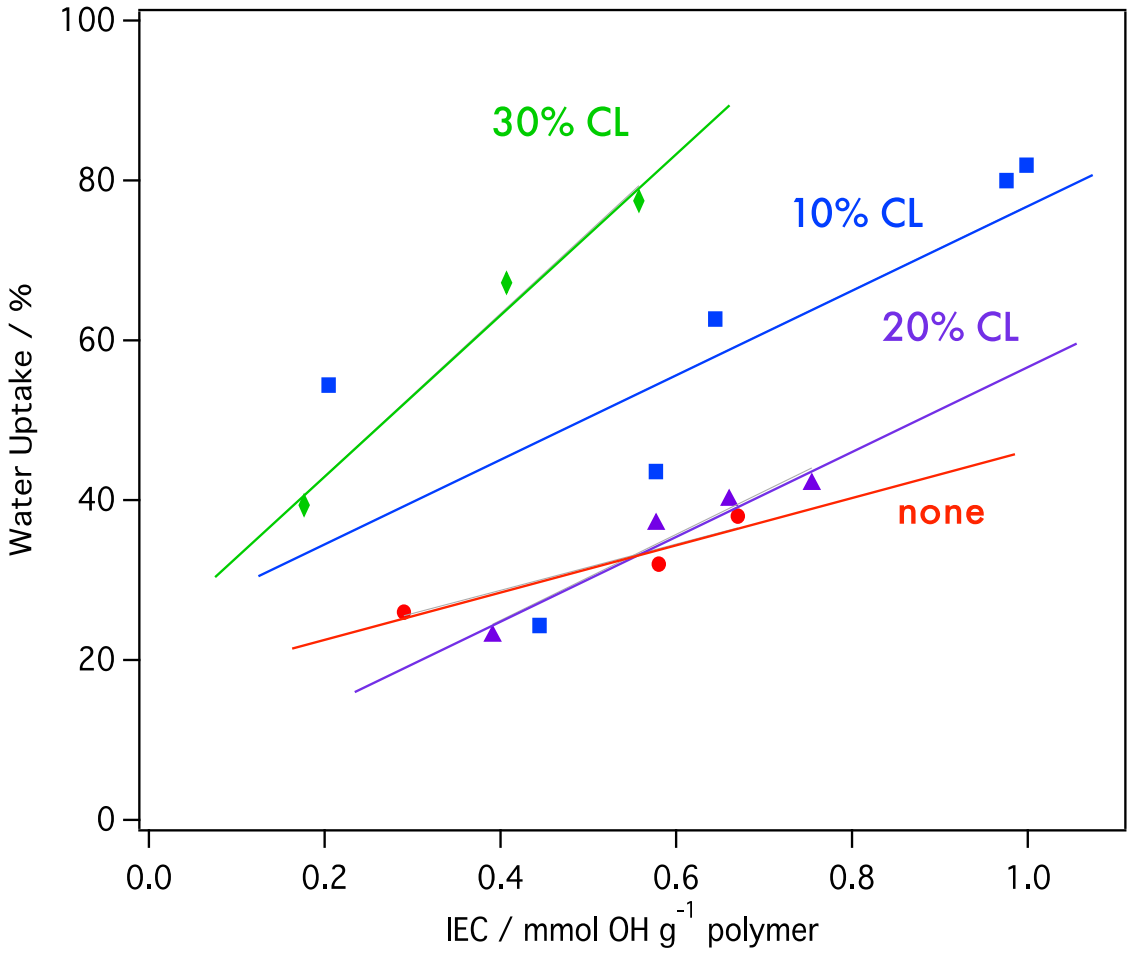

Figure 42 - Water uptake v. IEC graphed by crosslinking percentage.

HATR-IR spectra, however, taken of several AEMs (FIGURE 43) indicated qualitatively high conversion. This was noted by the significant decrease in the peak 2100 cm-^{1} (from spectra B to A) associated with the N_3 group on the modified PPO-N_3. It is likely, then, that the poorly trending data was not caused by poor chemical conversion but could easily be caused by the reaction of OH^- groups with CO_2 in the ambient air to form carbonate. It has been shown in previous studies that 5 minutes exposure to the ambient environment can cause as high as 20% conversion of exchangeable –OH groups to CO_3. This would both lower the measured IEC as well as conductivity calculated via impedance measurements.

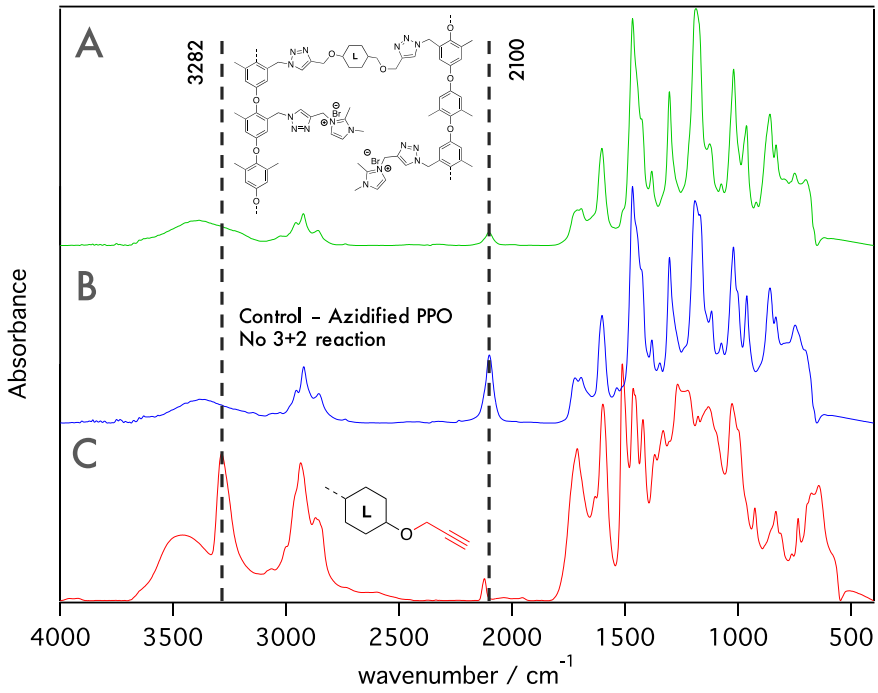

Figure 43 - FTIR spectra of A – as-synthesized LMPPO-DMIm AEM (HATR); B – a solvent cast thin film of globally exchanged PPO-N_3 (HATR) ; C – dry propargylated lignin (abs/KBr).

Additional to the use of NMRP as a means of olefin polymerization, ATRP was also initially investigated as a potential synthetic route. Olefinated lignin or [VBCML], as described in the synthetic methods, was used in polymerization reactions as a macromolecule alone with olefin monomers to synthesize anionic exchange polymeric material in a living radical mechanism. As shown in **FIGURE 44**, olefin modified lignin was mixed with an excess of olefin monomer and polymerized via ATRP using a copper bromide catalyst. In an alkylation step, following polymerization, a heterocyclic amine was employed as a means of adding cationic character to the polymer base. This step was always followed with an additional alkylation step to cap unreacted phenolates as well as any excess amine to make removal easier during the workup step. The final casting solutions were then casted onto a 5x10 glass casting area and oven-cured under vacuum at 70°C for up to 12 hours.

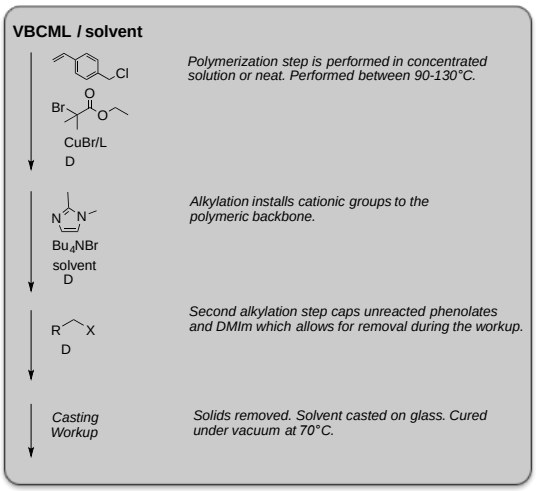

Figure 44 – General reaction sequence for the step-wise polymerization and synthesis of lignin-modified olefin-based (LMOB) crosslinked AEMs.

These membranes displayed extremely poor structural stability and often cracked during the initial pure water soaking immediately following removal from the casting oven. Cracked samples were recovered, dried and saved to analyze via FTIR. **FIGURE 45** displays three spectra to note the qualitative differences between the materials. The spectra for VBCML, shown in part b) of the figure, displays a strong, distinctive peak in the region associated with the sp^2 hybridized C-H stretch at 3058 cm^{-1}. This was the expected result due to the addition of a high concentration of vinyl groups to the lignin structure. The additional appearance of the peak at 1591 cm^{-1} in part b) is indicative of aromatic C=C stretching and further supports the olefination of the organosolv lignin. The spectrum in part c) of the figure is representative of the polymer membrane synthesized via ATRP using VBCML, excess p-VBC and ethyl 2-bromopropionate (as shown in **FIGURE 44**). Since the material was a thin, polymeric film, horizontal ATR-IR was used to measure the IR spectrum of the material. The most significant differences between the spectra of the polymer precursor shown in part b) and the polymer film shown in part c) are the complete disappearance of the peak at 3058 cm^{-1} associated with the alkenyl C=C stretch of the vinyl group and the appearance of the peak associated with the C=O stretching of the ester group of the initiator molecule at 1670 cm^{-1}.

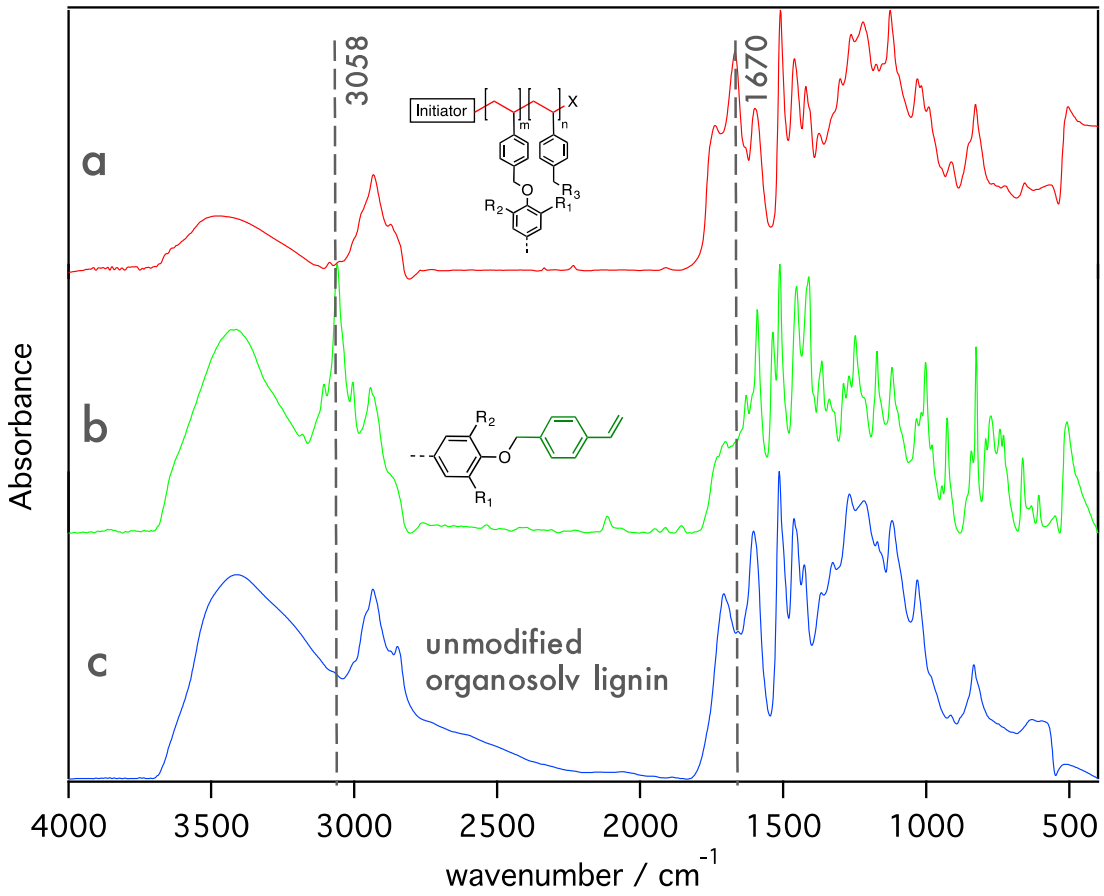

Figure 45 - FTIR spectrum of a) ATRP polymerized olefin-modified lignin AEM (HATR); b) purified olefin-modified lignin (abs/KBr); and c) unmodified organosolv lignin (abs/KBr).

One of the most attractive and potentially powerful attributes of ATRP as a synthetic method is the possibility of using a one-pot synthesis method that incorporates both living radical polymerization as well as copper-based click chemistry to create a functional polymeric material. By careful modification of the initiator, it is possible to use a synthesized, bi-functional molecule to serve as both a radical initiator as well as the click [3+2] cycloaddition initiation site. As seen in the schematic below (**FIGURE 46**), the use of 2,4,6-Tris(bromomethyl)mesitylene allows for the azidification of one or more of the benzylic bromides so that it might take part in the click reaction with a suitable alkyne. In the case of lignin-modified AEM polymer membranes, previously propargylated lignin was used in the ATRP/click synthesis of this polymer membrane utilizing a single copper catalyst/ligand combination. These polymers were doped with polyethylene glycol to increase hydrophilicity as well as mechanical stability. Polymers were solvent cast on glass using NMP at approximately 400 mg polymer in 3 mL of NMP into a 5x10cm casting area. Cast polymers were cured at 70°C under 5 inHg vacuum overnight. Following removal from the oven, casting plates were cooled on the benchtop before being submerged into a water bath at 23°C (room temperature). Upon hydration, all of these membranes suffered catastrophic cracking that did not allow for membrane performance characterization. Cracked membranes were dried and ground into a

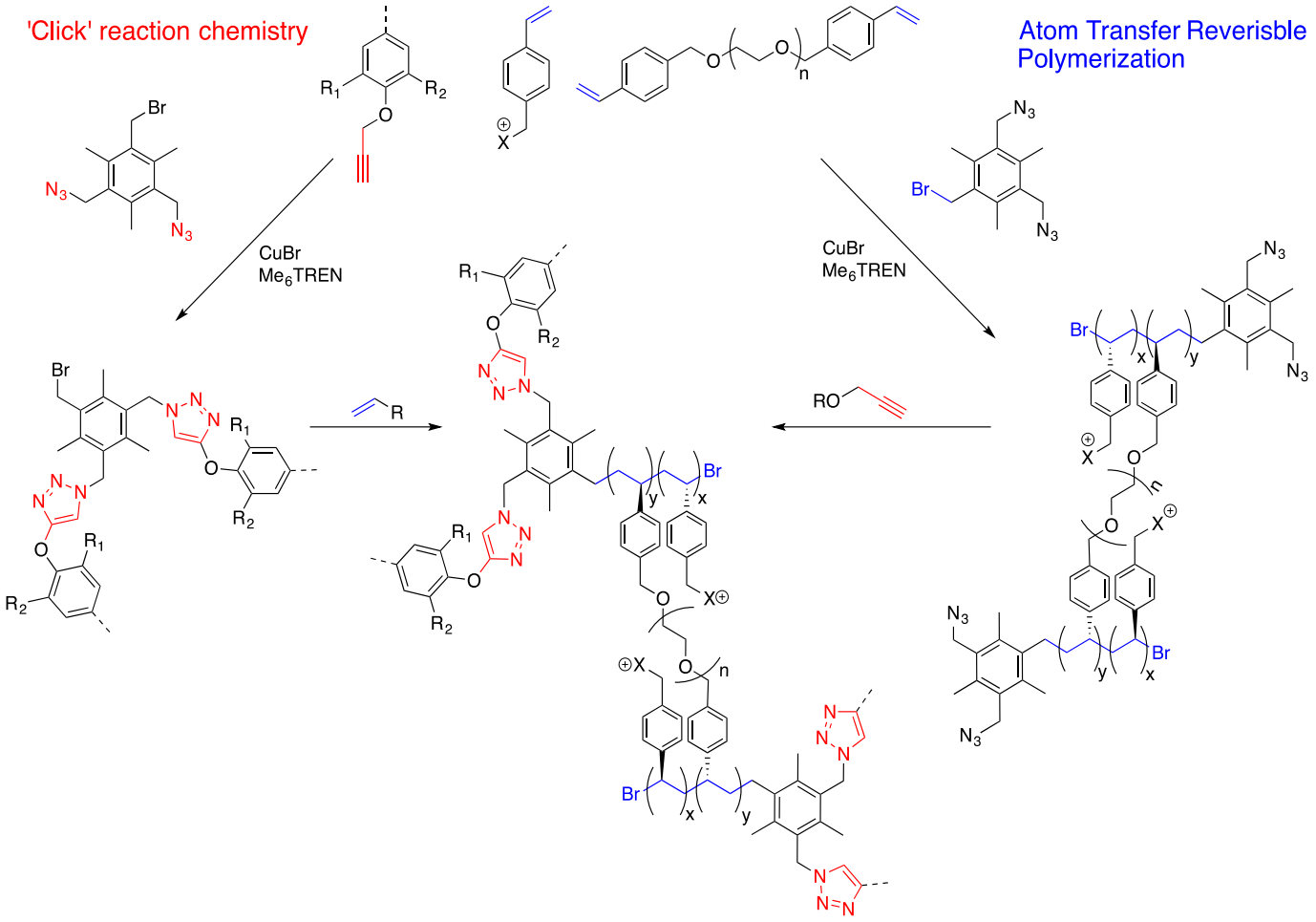

Figure 46 - Simultaneous ATRP-Click polymerization reaction utilizing a bi-functional azidilated benzylbromide initiator for both 'arms' of the reaction.

powder and pressed into a KBr pellet for absorbance FTIR analysis. **FIGURE 47** displays polymers that were synthesized with di-functional ATRP/click initiators. The spectrum in part A of the figure was synthesized with mono-azidilated α,α'-dibromo-*p*-xylene, such that the ratio of bromide to azide was one. Part B of the figure was synthesized using 2,4,6-Tris(bromomethyl)mesitylene such that there were 2 eq. of benzylic azide groups relative to bromide. In both cases, the dotted lines were thermally driven reactions while the solid lines were catalyzed using Cu(I)Br. It should come as no surprise that the spectra for the copper-driven reactions seemed to indicate higher [3+2] cycloaddition conversion by virtue of the decreased size of the alkyne C≡C stretch peak at approximately 2120 cm^{-1}. The copper-driven polymerization/click reaction was performed at 60°C while

Several of this series of membranes were modified post-polymerization. Alkylation of the 1,2,3-triazoles was attempted in NMP, prior to casting. Using 1-bromopropane, added in 1.2 eq. to propargyl lignin units, the mixture was stirred at 80°C overnight prior to casting. It was noted that the solution had turned from dark brown to a lighter tan color with a fine particulate that was centrifuged and dried, resulting in a sticky, brown residue that was not dissolvable in any solvent in our lab.

It is highly likely that the use of 2,4,6-tris(bromomethyl)mesitylene (or similar) bi-functional initiator with a multi-functionalized molecule like Pr-O-Lignin essentially acted as a cross-linking agent. This could easily account for the brittle mechanical properties of these membranes as higher cross linking percentages tend to put strain on the polymer matrix, especially under swelling conditions.

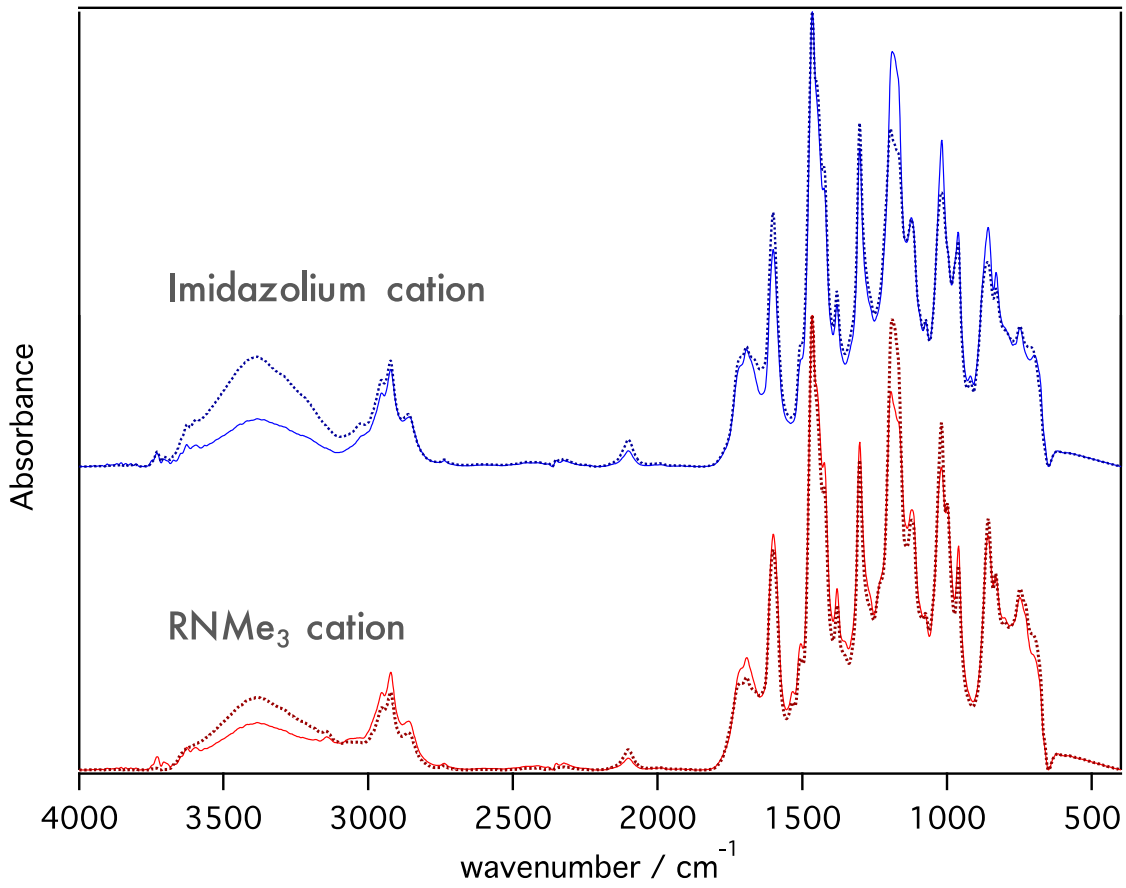

Figure 47 - FTIR spectrum of ATRP/click polymer film employing proparylated lignin and a bifunctional initiator (as shown in Figure 46). Spectra are differentiated by cationic group employed, as noted in the graphic. Solid spectra followed a synthetic scheme that included a CuI catalyst to facilitate the click reaction. The dotted spectra we synthesized via a thermally-driven click reaction.

ATR-IR (attenuated total reflectance infrared spectroscopy) was used to qualitatively characterize membranes after conductivity testing was performed. Since these polymers generally have a refractive index of 1.5-1.7, as measured by GPC, the use of a zinc selenide crystal was reasonable. The refractive index of the crystal must be greater than that of the sample otherwise the evanescence effect will not be great enough and light will be lost to the sample. Conversely, using a crystal that is too dense will simply result in loss of signal. The spectra in **FIGURE 48** shows both high (A) and low (B) loading membranes following performance testing (soaking in 1M NaOH). Most important to note about these two spectra are the peaks associated with the $-N_3$ and terminal alkyne functional groups at 2233 and 2100 cm^{-1}, respectively (note: ATR is a lower-energy, indirect absorbance method which causes functional group peaks to shift to slightly lower wavenumbers than direct transmission methods of FTIR). These spectra lend strong evidence to the assertion that the higher loading of polymer results in lower turnover of the [3+2] click cycloaddition, which would result in lower than expected IEC, water content and conductivity measurements. Additionally, click reactions necessitated being performed at lower temperatures (60°C) when high polymer loadings were used due to rapid gelation at higher temperatures.

It is interesting to note that the highest tested membrane, $LM_{0.2}PPO_{0.4}$-$DMIm_{0.8}$BDMHA-Br, was synthesized with 0.2 molar equivalents of propargylated lignin. By definition, a membrane with higher lignin content will have a lower concentration of ionic moieties than those with lower lignin content (all other

concentrations being equal). This sample was synthesized in sequence, as opposed to a 1-pot synthesis. The hypothesis was that the addition of lignin caused polymer gelation that inhibited high chemical conversion, thus lowering conductivity. In this case, the ionic species was added first since there should be little risk of gelation (no possibility of cross-linking) and following that, subsequently alkylated with an additional ionic species and allowed to run overnight prior to adding the lignin and casting in the normal durations and temperatures. This membrane also measured the highest water content, which is reasonable considering that a higher ionic concentration should cause greater water absorption.[114]

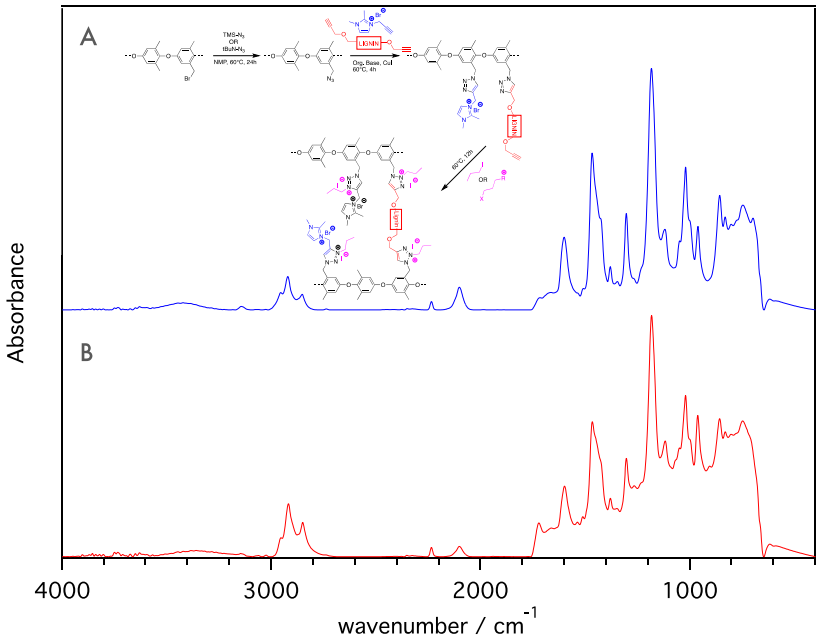

Figure 48 **- ATR-IR spectrum of a) high polymer loading (6% w/w) PPO-N_3 based membrane and b) low polymer loading (4% w/w) PPO-N_3 based membrane following casting. The spectrum indicates that the higher loading of polymer results in a lower reaction conversion of the [3+2] cycloaddition click reaction.**

4.5 Unsupported Lignin Elongation

Prior to using lignin as a crosslinking agent for more traditional polymers like PPO-Br, styrene and other olefins, great efforts were made to “elongate” lignin fragments in order to both increase the average molecular weight of the chain as well as to install cationic groups. In this context, elongation refers to the chemical modification and linking-together of smaller lignin molecules to create a larger network of crosslinked material. This work included a large amount of synthesis-driven trial and error. The goal was the synthesis of modified lignin materials capable of being solvent cast like traditional polymer films to potentially be used as ion or gaseous exchange membranes and thin films. Ultimately, this endeavor was abandoned. Cured thin films were never mechanically robust enough to survive the post-curing workup procedures and suffered from dissolution issues in strong base. Some of this work, as it informed the research that moved into lignin-modified crosslinked polymer membranes, is presented here.

This work began in parallel with the work that yielded several lignin-based ionomers and continued to move in the direction of linking together smaller lignin molecules to create a charged, crosslinked network that was structurally and chemically robust. Like with the ionomers, alkyl and ethylene glycol chains were used to link lignin molecules together as well as to alter the physical properties of the material. In this case, however, the purpose was large-scale crosslinking. A generic reaction diagram is shown in **Figure 49**. In this case, the first step is used to link together lignin fragments while the second step is used to install cationic

groups for ion exchange. The cationic groups in the second step have the possibility of being pendent groups or cationic groups capable of crosslinking additional hydroxyl groups.

To investigate this approach, models were used to explore the reactivity of phenolic units with alkyl and polyether chains. As in other cases, guaiacol was the primary choice of model due to simplicity and similarity to the parent structure. To ensure complete consumption of the model, the electrophilic chain was often added in molar excess. Electron ionization mass spectrometry (EI-MS) in conjunction with gas chromatography (GC) was predominantly utilized to characterize these model reactions due to the ease of sample preparation and the direct nature of the results.

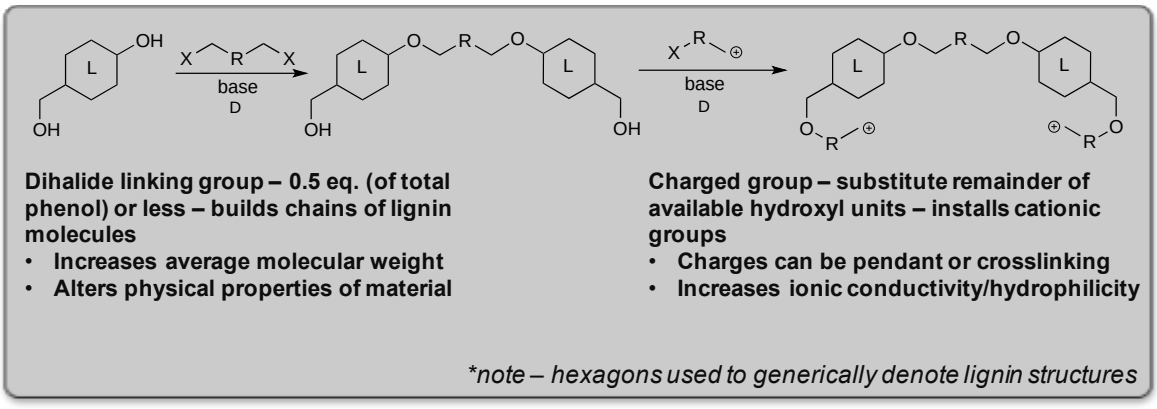

Figure 49 - Generic reaction diagram for the elongation of unsupported lignin.

The GC/MS results for the model reaction of guaiacol with 1,4-bromobutane, as seen in **FIGURE 50C,** indicate that the reaction produced the desired product. The dihalide alkane was added in 3 times greater molar quantity than the nucleophilic guaiacol. Integration shows the yield was about 85% with about 15% of the remaining starting concentration of guaiacol eluting around 4 minutes. The alkylated guaiacol is clearly identifiable via the small split M^+ peaks at m/z 258 and 260 characteristic of the isotopic distribution of the bromide. There is also very weak peak associated with the α- fragmentation loss of CH2-Br; however, the parent peak is very clearly visible at m/z 109. This peak is likely a result of the loss of the bromo-alkyl chain as well as the fragmentation of the methyl group from the C-2 methoxy-group. There is no bromide associated with this species and the peak appears as a singlet.

Guaiacol was also used in model reactions with methylated alkyl chains. The use of alkyl chains that do not possess β-hydrogens decreases the possibility for elimination reaction degradation pathways in alkaline environments, as shown **FIGURE 51**. In the figure to the left, alpha and beta hydrogens are labeled. Alkyl chains containing beta hydrogens, in the presence of a base, can undergo elimination. This graphic shows two possible pathways for this type of degradation. In a modified lignin chain containing an un-methylated alkyl linker and a cationic group, elimination can cause the removal of the lignin fragment, as shown by the top (red) pathway or it can result in the cationic group leaving the chain in a Hoffman-type elimination, as shown in the bottom (blue) pathway.[115]

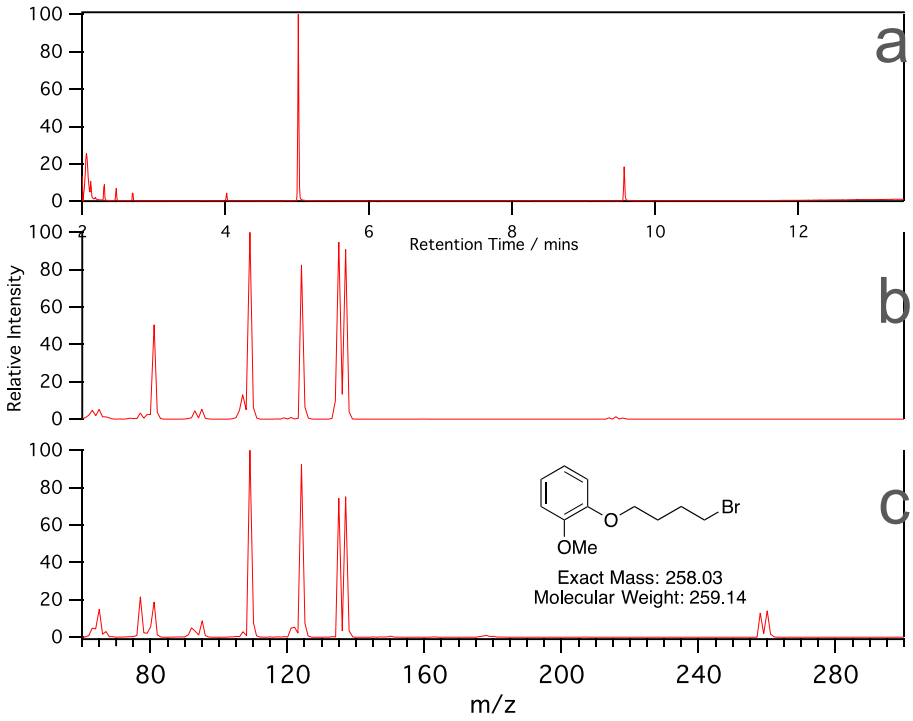

Figure 50 – (a) GC chromatograph of the model reaction for the bromobutylation of guaiacol under alkaline conditions; (b) MS spectrum of dibromobutane; (c) MS spectrum of the desired product, 1-(4-bromobutoxy)-2-methoxybenzene.

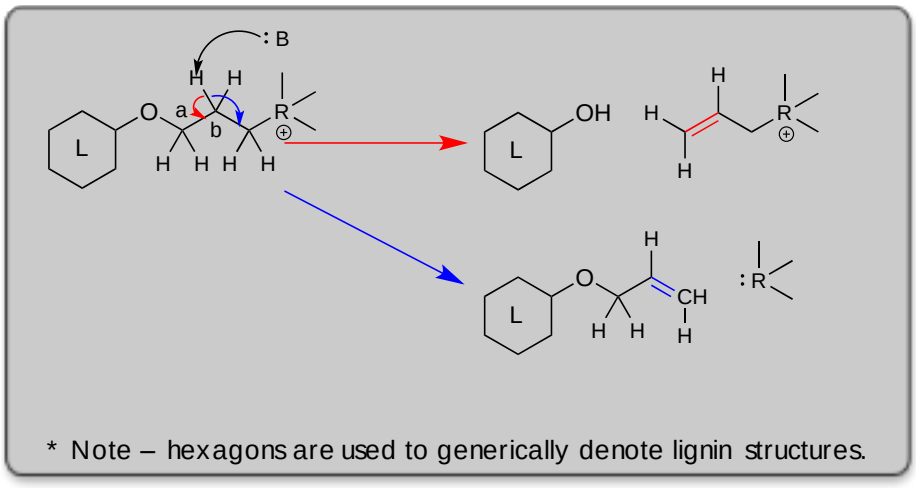

Figure 51 - Dipiction of two B-hydride elimination degradation pathways for alkylated lignin.

Numerous reaction conditions and reagents were attempted in the synthesis of a linker utilizing 2,2-dimethylpropyl linker. Literature indicated that reaction temperatures above 130°C, often using DMF or other polar, aprotic solvent with a strong base for a period of at least 24 hours. However, upon following these synthetic methods, especially those using DMF as a solvent, at the completion of the reaction, a distinct amine smell as well as a darkened solid precipitate. A literature search indicated that other groups had encountered similar occurrences with an unknown decomposition product when using DMF in the presence of strong bases.[116,117] For this reason, these synthetic methods were abandoned in favor of utilizing sodium hydride and DMSO to produce the dimsyl-sodium form of the solvent to use as a non-nucleophilic base. Model reactions were performed during which guaiacol was alkylated with 1,3-*bis*(tosyloxy)-2,2-dimethylpropane [*bis*OTS-DMP] in a 1:1 ratio and also in a 2:1 ratio of guaiacol to linker. The results of both of these models are shown below in **FIGURE 52** and **FIGURE 53**, respectively. Both chromatographs indicate that the desired product was reached, however, for the dimerized guaiacol product, the yield is undesirably low. Integration of the peaks indicated the yield of the desired product was just over 30%. The alkylation of guaiacol using the 1:1 ratio of methylated linker yielded 90% desired product, as shown in part D of the figure. Part C indicated that some starting guaiacol remained and part B was solvent.

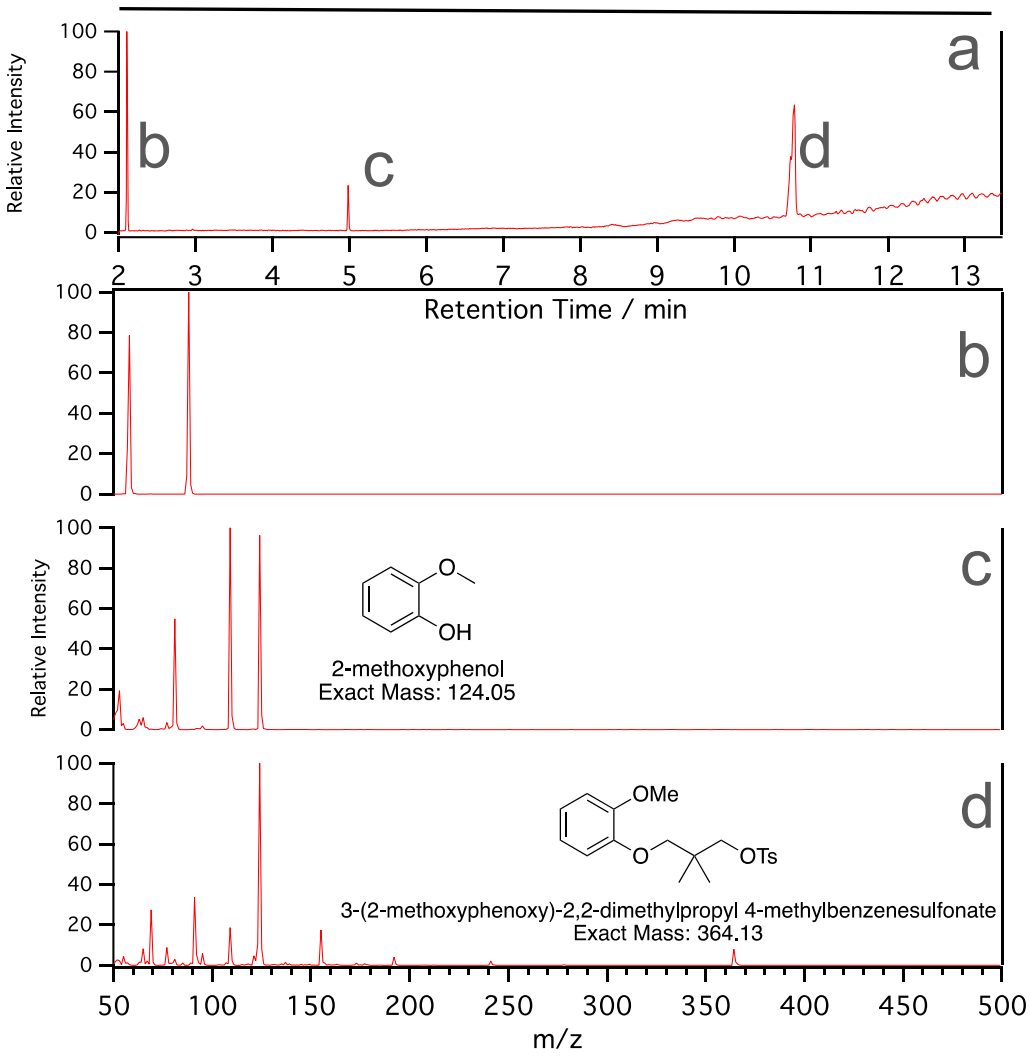

Figure 52 - (a) GC chromatogram for alkylated guaiacol product indicating 90% converstion; (b) MS spectrum of peak b (solvent); (c) MS spectrum of peak c (starting material); (d) MS spectrum of desired product

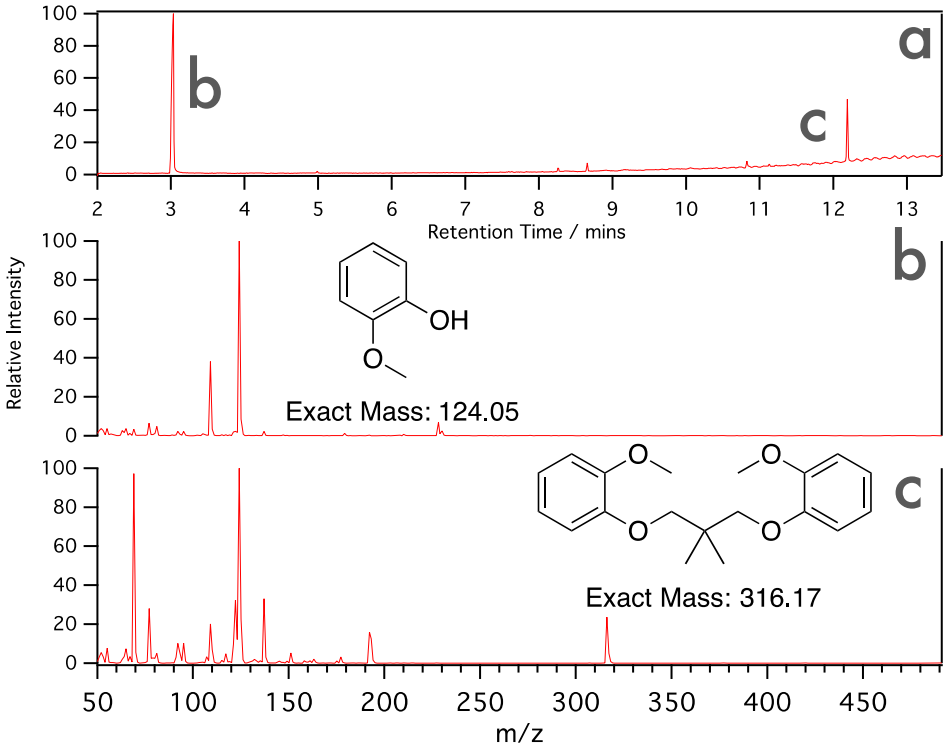

Figure 53 - GC/MS spectrum of the model compound reaction showing the cross-linking of guaiacol with 1,3-*bis*(tosyloxy)-2,2-dimethylpropane (a) GC chromatograph; (b) MS spectrum of starting material indicative of GC peak from RT 5; (c) MS spectrum of desired product from GC peak of RT 12.2 mins.

To increase both the effect of the linking group's influence on altering the physical properties of the lignin as well as increasing their reactivity with the lignin, polyether chains were also used to link lignin fragments. Polyether chains are more flexible than alkyl chains as well as being more hydrophilic – both properties needed to make lignin a potentially suitable material for solvent casting. Polyether chains were either purchased as bis-dimesylates, bis-ditosylates, or synthesized from unmodified tetraethylene glycol (TEG) with the chloride salts of those leaving groups. All of the reported figures for TEG-based linkers were synthesized using commercially sourced TEG-ditosylate. **FIGURE 54** includes four inset positive mode MS(ESI) spectra taken in 1:1 acetonitrile and water illustrating the relative cleanliness of the product spectra. The synthesis for these molecules is also surprisingly simple and the products may be diluted with ethyl acetate and extracted with water. The spectra show almost no m/z peaks for starting material as tosyl-groups are generally on the order of reactivity of iodides – they are excellent leaving groups for S_N2 reactions. Further separation of TEG units and imidazole starting materials requires column chromatography, however, the mass spectrum seems to indicate that measure of specific purification was not necessary for our purposes.

Alkyl-linker groups capable of carrying multiple charges were also possible by increasing the temperature of the reaction mixture to increase reaction rate. This ultimately results in longer chains and more charges per chain. **FIGURE 55** displays the positive mode MS(ESI) spectrum of mono- and di-cationic alkylated imidazolium chains. Only a very small percentage of starting 2-MeIm remains (m/z: 83) while the desired mono- and di-cationic group signatures present strong isotopic

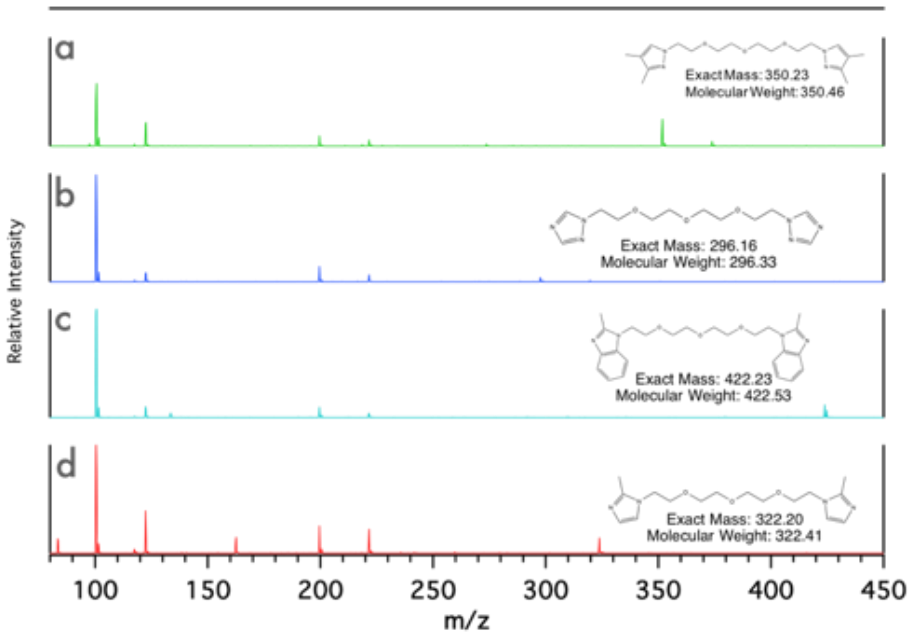

Figure 54 - GC/MS spectra of TEG-based linker groups used in lignin elongation schemes

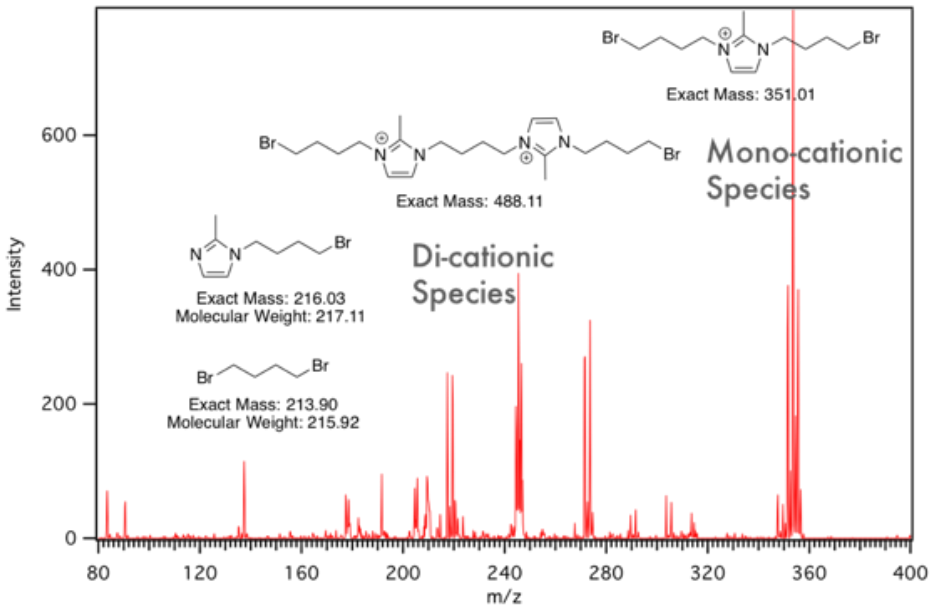

Figure 55 - ESI-MS spectrum for the alkylation of 2-methylimidazole under alkaline conditions showing both cationic and di-cationic species in significant abundance with very low relative abundance of the starting dibromide.

peaks. Both mono- and di-cationic molecules display in quintuplet peaks around m/z 353 and 244, respectively, due to the presence of two bromides on each molecule.

FTIR was use in the characterization of modifications performed on dry organosolv lignin. **FIGURE 56** shows the stack FTIR spectra for organosolv lignin modified with 1,3-dibromopropane vs unmodified organosolv lignin. The spectra clearly shows the predominant signature of alkylated lignin – the increased signal of the -sp^3 hybridized (unsubstituted) C-H stretch at 2930 cm^{-1} relative to the broad –OH stretch associated with the high concentration of phenols and aliphatic hydroxyl units that are deprotonated during the S_N2 alkylation. The opposite is seen to be true for the unmodified lignin where the unsubstituted alkane C-H stretch signal is lower than that of the –OH stretch.

FIGURE 57 shows the stacked FTIR spectra for TEG-modified lignin vs unmodified organosolv lignin. The TEG-modified lignin shows significant similarities to the spectrum for lignin modified with 1,3-bromopropane in that the predominant features are the increase of the -sp^3 hybridized C-H stretch at 2930 cm^{-1} the increase of the signal at 1244 cm-1 which is indicative the vibrations of aryl C-O bonds. In both cases, these modified lignin precursors could be used in subsequent modification schemes to install cationic charge groups prior to casting.

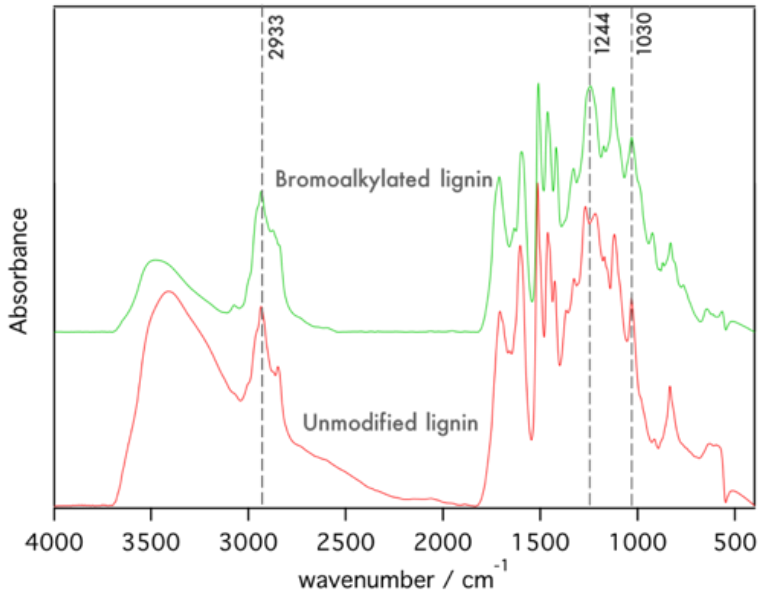

Figure 56 - FTIR spectrum stack of unmodified lignin and bromo-alkylated lignin

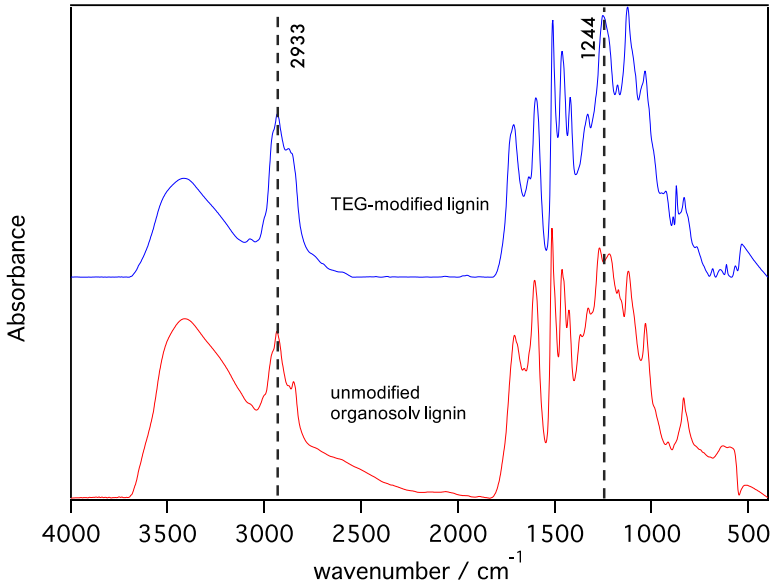

Figure 57 - FTIR stack of unmodified lignin and TEG-modified lignin

4.6 Conclusions

Lignin was used as a structural component in the final post-polymerization modification synthesis of anion exchange membranes (AEMs). Unlike prior studies in which lignin was used as unsupported functional material, this project aimed to utilize lignin in a role more analogous to that which it fills in nature. Several different methods of radical polymerization were employed in the synthesis of polymer chains with nitroxide mediated polymerization ultimately being the most successful, resulting in long polymer chains and in producing structurally sound membranes. Lignin was modified by substitution to install propargyl groups to be used in click reactions with post-polymerization modified azidified polymer. Lignin was also used as a crosslinking agent in the post-polymerization modification LMPPO AEMs by employing a similar click chemistry strategy. Though they produced mixed results, LMPPO AEMs produced the highest recorded conductivity of 127 mS cm^{-1}. Overall, however, styrene-based membranes synthesized using an NMRP polymerization method resulted in better average conductivity measurements but all suffered from poor mechanical stability causing many to break prior to or during conductivity and IEC testing. Interestingly, the highest conductivity measurement was achieved by a membrane with the highest loading of propargylated lignin. This could be coincidental but, in parallel studies, greater lignin concentration seemed to allow the polymer to remain soluble with a higher charge concentration.

Moving forward, despite the higher cost of stable nitroxide radical species, it is possible to use this synthetic method to co-polymerize PPO polymers with olefin-based polymers as branched chains. In this case, it would be advantageous for the olefin polymerizations to make significantly lower M_N polymers such that the best attributes of the PPO (mechanical/chemical stability) are melded with the best attributes of the olefin membranes (hydrophobic domains/high conductivity).

WORKS CITED

[1] Gouérec, P.; Poletto, L.; Denizot, J.; Sanchez-Cortezon, E.; Miners, J. H. The evolution of the performance of alkaline fuel cells with circulating electrolyte. *J. Power Sources* **2004**, *129* (2), 193–204.

[2] Cifrain, M.; Kordesch, K.; Vielstich, W.; Lamm, A.; Gasteiger, H. Hydrogen/oxygen (Air) fuel cells with alkaline electrolytes. *Fuel* **2003**, *1*, 267–280.

[3] Brushett, F. R.; Zhou, W.-P.; Jayashree, R. S.; Kenis, P. J. A. Alkaline Microfluidic Hydrogen-Oxygen Fuel Cell as a Cathode Characterization Platform. *J. Electrochem. Soc.* **2009**, *156* (5), B565–B571.

[4] Ghamouss, F.; Mallouki, M.; Bertolotti, B.; Chikh, L.; Vancaeyzeele, C.; Alfonsi, S.; Fichet, O. Long lifetime in concentrated LiOH aqueous solution of air electrode protected with interpenetrating polymer network membrane. *J. Power Sources* **2012**, *197*, 267–275.

[5] Kordesch, K.; Gsellmann, J.; Cifrain, M.; Voss, S.; Hacker, V.; Aronson, R. R.; Fabjan, C.; Hejze, T.; Daniel-Ivad, J. Intermittent use of a low-cost alkaline fuel cell-hybrid system for electric vehicles. *J. Power Sources* **1999**, *80* (1), 190–197.

[6] Brushett, F. R.; Thorum, M. S.; Lioutas, N. S.; Naughton, M. S.; Tornow, C.; Jhong, H. R. M.; Gewirth, A. A.; Kenis, P. J. A. A carbon-supported copper complex of 3,5-diamino-1,2,4-triazole as a cathode catalyst for alkaline fuel cell applications. *J. Am. Chem. Soc.* **2010**, *132* (35), 12185–12187.

[7] Bidault, F.; Brett, D. J. L.; Middleton, P. H.; Brandon, N. P. Review of gas diffusion cathodes for alkaline fuel cells. *J. Power Sources* **2009**, *187* (1), 39–48.

[8] Kirubakaran, A.; Jain, S.; Nema, R. K. A review on fuel cell technologies and power electronic interface. *Renewable and Sustainable Energy Reviews* **2009**, *13* (9), pp 2430–2440.

[9] Merle, G.; Wessling, M.; Nijmeijer, K. Anion exchange membranes for alkaline fuel cells: A review. *J. Memb. Sci.* **2011**, *377* (1–2), 1–35.

[10] Gulzow, E.; Giilzow, E. Alkaline fuel cells: A critical view. *J. Power Sources* **1996**, *61* (1–2), 99–104.

[11] Hickner, M. A.; Herring, A. M.; Coughlin, E. B. Anion exchange membranes: Current status and moving forward. *J. Polym. Sci. Part B Polym. Phys.* **2013**, *51* (24), 1727–1735.

[12] Danks, T. N.; Slade, R. C. T.; Varcoe, J. R.; Cruickshank, J.; Scott, K.; Taama, W.; Adzic, R. R.; Aramtor, M. C.; Tripkovic, A. V.; Taraszewska, J.; et al. Comparison of PVDF- and FEP-based radiation-grafted alkaline anion-exchange membranes for use in low temperature portable DMFCs. *J. Mater. Chem.* **2002**, *12* (12), 3371–3373.

[13] Varcoe, J. R.; Slade, R. C. T.; Lam How Yee, E. An alkaline polymer electrochemical interface: a breakthrough in application of alkaline anion-exchange membranes in fuel cells. *Chem. Commun. (Camb).* **2006**, *5* (13), 1428–1429.

[14] Goldemberg, J. Ethanol for a sustainable energy future. *Science* **2007**, *315* (5813), 808–810.

[15] McKendry, P. Energy production from biomass (part 1): Overview of biomass. *Bioresour. Technol.* **2002**, *83* (1), 37–46.

[16] Muradov, N. Z.; Veziroğlu, T. N. “Green” path from fossil-based to hydrogen economy: An overview of carbon-neutral technologies. *Int. J. Hydrogen Energy* **2008**, *33* (23), 6804–6839.

[17] Dias, A. A.; Freitas, G. S.; Marques, G. S. M.; Sampaio, A.; Fraga, I. S.; Rodrigues, M. A. M.; Evtuguin, D. V.; Bezerra, R. M. F. Enzymatic saccharification of biologically pre-treated wheat straw with white-rot fungi. *Bioresour. Technol.* **2010**, *101* (15), 6045–6050.

[18] Duval, A.; Lawoko, M. A review on lignin-based polymeric, micro- and nano-structured materials. *React. Funct. Polym.* **2014**, *85*, 78–96.

[19] Chan, R. W. C.; Krieger, B. B. Kinetics of Dielectric-Loss Microwave Degradation of Polymers: Lignin. *J. Appl. Polym. Sci.* **1981**, *26* (5), 1533–1553.

[20] Shafizadeh, F.; Chin Peter P, S. Thermal Deterioration of Wood. In *Wood Technology: Chemical Aspects*; Missoula, MT, 1977; Vol. 43, pp 57–81.

[21] D Demirbaş, A. Relationships between lignin contents and heating values of biomass. *Energy Convers. Manag.* **2001**, *42* (2), 183–188.

[22] Badamali, S. K.; Luque, R.; Clark, J. H.; Breeden, S. W. Microwave assisted oxidation of a lignin model phenolic monomer using Co(salen)/SBA-15. *Catal. Commun.* **2009**, *10* (6), 1010–1013.

[23] Stöcker, M. Biofuels and biomass-to-liquid fuels in the biorefinery: Catalytic conversion of lignocellulosic biomass using porous materials. *Angew. Chemie - Int. Ed.* **2008**, *47* (48), 9200–9211.

[24] Adam, J.; Blazsó, M.; Mészáros, E.; Stöcker, M.; Nilsen, M. H.; Bouzga, A.; Hustad, J. E.; Grønli, M.; Øye, G. Pyrolysis of biomass in the presence of Al-MCM-41 type catalysts. *Fuel* **2005**, *84* (12–13), 1494–1502.

[25] Martinez, D.; Larrondo, L. F.; Putnam, N.; Gelpke, M. D. S.; Huang, K.; Chapman, J.; Helfenbein, K. G.; Ramaiya, P.; Detter, J. C.; Larimer, F. Genome sequence of the lignocellulose degrading fungus Phanerochaete chrysosporium strain RP78. *Nat. Biotechnol.* **2004**, *22* (6), 695–700.

[26] Pearl, I. A. *The chemistry of lignin*; M. Dekker: Indiana, 1967.

[27] Chakar, F. S.; Ragauskas, A. J. Review of current and future softwood kraft lignin process chemistry. *Ind. Crops Prod.* **2004**, *20* (2), 131–141.

[28] Ai, J.; Tschirner, U. Fiber length and pulping characteristics of switchgrass, alfalfa stems, hybrid poplar and willow biomasses. *Bioresour. Technol.* **2010**, *101* (1), 215–221.

[29] Andersson, S.; Serimaa, R.; Paakkari, T.; SaranpÄÄ, P.; Pesonen, E. Crystallinity of wood and the size of cellulose crystallites in Norway spruce (Picea abies). *J. Wood Sci. 49* (6), 531–537.

[30] Monties, B. Plant cell walls as fibrous lignocellulosic composites: relations with lignin structure and function. *Anim. Feed Sci. Technol.* **1991**, *32* (1–3), 159–175.

[31] Zakzeski, J.; Jongerius, A. L.; Weckhuysen, B. M. Transition metal catalyzed oxidation of Alcell lignin, soda lignin, and lignin model compounds in ionic liquids. *Green Chem.* **2010**, *12* (7), 1225.

[32] Bozell, J. J.; Hames, B. R.; Dimmel, D. R. Cobalt-Schiff Base Complex-Catalyzed Oxidation of Parasubstituted Phenolics - Preparation of Benzoquinones. *J. Org. Chem.* **1995**, *60* (8), 2398–2404.

[33] Kapturkiewicz, A.; Behr, B. Voltammetric studies of Co(salen) and Ni(salen) in nonaqueous solvents at Pt electrode. *Inorganica Chim. Acta* **1983**, *69*, 247–251.

[34] Pavlishchuk, V. V; Addison, A. W. Conversion constants for redox potentials measured versus different reference electrodes in acetonitrile solutions at 25°C. *Inorganica Chim. Acta* **2000**, *298* (1), 97–102.

[35] Bond, A. M.; Oldham, K. B.; Snook, G. A. Use of the ferrocene oxidation process to provide both reference electrode potential calibration and a simple measurement (via semiintegration) of the uncompensated resistance in cyclic voltammetric studies in high-resistence organic solvents. *Anal. Chem.* **2000**, *72* (15), 3492–3496.

[36] Laviron, E. General expression of the linear potential sweep voltammogram in the case of diffusionless electrochemical systems. *J. Electroanal. Chem. Interfacial Electrochem.* **1979**, *101* (1), 19–28.

[37] Xie, Y.; Anson, F. C. Analysis of the cyclic voltammetric responses exhibited by electrodes modified with monolayers of catalysts in the absence and presence of substrates. *J. Electroanal. Chem.* **1995**, *384* (145).

[38] Dalton, E. F.; Surridge, N. A.; Jernigan, J. C.; Wilbourn, K. O.; Facci, J. S.; Murray, R. W. Charge transport in electroactive polymers consisting of fixed molecular redox sites. *Chem. Phys.* **1990**, *141* (1), 143–157.

[39] Gowda, J. I.; Nandibewoor, S. T. Carbon paste sensor for the determination of an anticancer drug paclitaxel in pharmaceuticals and biological fluids. *Anal. Bioanal. Electrochem* **2015**, *7* (5), 539–554.

[40] Zare, H. R.; Chatraei, F.; Nasirizadeh, N. Differential pulse voltammetric determination of hydroxylamine at an indenedione derivative electrodeposited on a multi-wall carbon nanotube modified glassy carbon electrode. *J. Braz. Chem. Soc* **2010**, *21* (10), 1977–1985.

[41] Kanyong, P.; Rawlinson, S.; Davis, J. Fabrication and electrochemical characterization of polydopamine redox polymer modified screen-printed carbon electrode for the detection of guanine. *Sensors Actuators, B Chem.* **2016**, *233*, 528–534.

[42] Bond, A. M.; Oldham, K. B.; Snook, G. A. Use of the ferrocene oxidation process to provide both reference electrode potential calibration and a simple measurement (via semiintegration) of the uncompensated resistance in cyclic voltammetric studies in high-resistence organic solvents. *Anal. Chem.* **2000**, *72* (15), 3492–3496.

[43] Kervinen, K.; Korpi, H.; Leskelä, M.; Repo, T. Oxidation of veratryl alcohol by molecular oxygen in aqueous solution catalyzed by cobalt salen-type complexes: The effect of reaction conditions. *J. Mol. Catal. A Chem.* **2003**, *203* (1–2), 9–19.

[44] Khandar, A. A.; Shaabani, B.; Belaj, F.; Bakhtiari, A. Synthesis, characterization and spectroscopic and electrochemical studies of new axially coordinated cobalt(III) salen (salen=N,N′-bis(salicylidene)-1,2-ethylenediamine) complexes. The crystal structure of [CoIII(salen)(aniline)2]ClO4. *Polyhedron* **2006**, *25* (9), 1893–1900.

[45] D Díaz-González, M.; Vidal, T.; Tzanov, T. Phenolic compounds as enhancers in enzymatic and electrochemical oxidation of veratryl alcohol and lignins. *Appl. Microbiol. Biotechnol.* **2011**, *89* (6), 1693–1700.

[46] Simandi, L. I. *Advances in Catalytic Activation of Dioxygen by Metal Complexes*; Simándi, L. I., Ed.; Catalysis by Metal Complexes; Springer US: Boston, MA, 2002; Vol. 26.

[47] Rajendran, L.; Sangaranarayanan, M. V. Diffusion at Ultramicro Disk Electrodes: Chronoamperometric Current for Steady-State Ec‘ Reaction Using Scattering Analogue Techniques. *J. Phys. Chem. B* **1999**, *103*, 1518–1524.

[48] Rieppo, L.; Saarakkala, S.; Närhi, T.; Helminen, H. J.; Jurvelin, J. S.; Rieppo, J. Application of second derivative spectroscopy for increasing molecular specificity of fourier transform infrared spectroscopic imaging of articular cartilage. *Osteoarthr. Cartil.* **2012**, *20* (5), 451–459.

[49] Hitchman, M. A. Electronic Structure of Low-Spin Cobalt(II) Schiff Base Complexes. *Inorg. Chem.* **1977**, *16* (8), 1985–1993.

[50] Ghosh, P.; Taube, H.; Hasegawa, T.; Kuroda, R. Vanadium(II) Salts in Pyridine and Acetonitrile Solvents. *Inorg. Chem.* **1995**, *34* (23), 5761–5775.

[51] Hall, M. B. Bonding of Dioxygen to Transition Metals. *Oxygen Complexes and Oxygen Activation by Transition Metals*; Springer US: New York, 1988; pp 3–17.

[52] Jones, R. D.; Summerville, D. A.; Basolo, F. Synthetic oxygen carriers related to biological systems. *Chem. Rev.* **1979**, *79* (2), 139–179.

[53] Huber, A.; Müller, L.; Elias, H.; Klement, R.; Valko, M. Cobalt(II) complexes with substituted salen-type ligands and their dioxygen affinity in N,N-dimethylformamide at various temperatures. *Eur. J. Inorg. Chem.* **2005**, *2005* (8), 1459–1467.

[54] Myers, W. K.; Duesler, E. N.; Tierney, D. L. Integrated paramagnetic resonance of high-spin Co(II) in axial symmetry: Chemical separation of dipolar and contact electron-nuclear couplings. *Inorg. Chem.* **2008**, *47* (15), 6701–6710.

[55] Zarembowitch, J.; Kahn, O. Magnetic properties of some spin-crossover, high-spin, and low-spin cobalt(II) complexes with Schiff bases derived from 3-formylsalicylic acid. *Inorg. Chem.* **1984**, *23* (5), 589–593.

[56] Nishida, Y.; Kida, S. Ground States of the Square Planar Low-Spin Cobalt(II) Complexes. *Bull. Chem. Soc. Jpn.* **1978**, *51* (1), 143–149.

[57] Nishida, Y.; Kida, S. Splitting of d-orbitals in square planar complexes of copper(II), nickel(II) and cobalt(II). *Coord. Chem. Rev.* **1979**, *27* (3), 275–298.

[58] Meek, D. W.; Drago, R. S.; Piper, T. S. Spectrochemical Studies of Dimethyl Sulfoxide, Tetramethylene Sulfoxide, and Pyridine N-Oxide as Ligands with Nickel(II), Chromium(I11), and Cobalt (11). *Inorg. Chem.* **1962**, *1* (2), 285–289.

[59] Drago, R. S.; Meek, D. W.; Joesten, M. D.; LaRoche, L. Spectrochemical Studies of a Series of Amides as Ligands with Nickel(II) and Chromium(III). *Inorg. Chem.* **1963**, *2* (1), 124–127.

[60] Cockle, S. A. Electron-paramagnetic-resonance studies on cobalt(II) carbonic anhydrase. Low-spin cyanide complexes. *Biochem. J.* **1974**, *137* (3), 587–596.

[61] Boettcher, A.; Elias, H.; Jaeger, E. G.; Langfelderova, H.; Mazur, M.; Mueller, L.; Paulus, H.; Pelikan, P.; Rudolph, M.; Valko, M. Comparative study on the coordination chemistry of {cobalt(II),} {nickel(II),} and {copper(II)} with derivatives of salen and tetrahydrosalen: metal-catalyzed oxidative dehydrogenation of the carbon-nitrogen bond in coordinated tetrahydrosalen. *Inorg. Chem.* **1993**, *32* (19), 4131–4138.

[62] Cockle, S. A.; Williams, R. J.; Hill, H. A. The formation of some superoxo-cobalt(III) complexes; An investigation by EPR. *Inorg. Nucl. Chem.* **1970**, *6* (3), 131–134.

[63] Emara, A.; Ali, A. M.; El-Asmy, A. F.; Ragab, E. S. Investigation of the oxygen affinity of manganese(II), cobalt(II) and nickel(II) complexes with some tetradentate Schiff bases. *J. Saudi Chem. Soc.* **2014**, *18* (6), 762–773.

[64] Floriani, C.; Calderazzo, F. Oxygen Adducts of Schiff's Base Complexes of Cobalt Prepared in Solution. *J. Chem. Soc.* **1969**, 946–953.

[65] Cedeno, D.; Bozell, J. J. Catalytic oxidation of *para*-substituted phenols with cobalt-Schiff base complexes/O_2 selective conversion of syringyl and guaiacyl lignin models to benzoquinones. *Tetrahedron Lett.* **2012**, *53*, 2380–2383.

[66] Cozzi, P. G. Metal-Salen Schiff base complexes in catalysis: practical aspects. *Chem. Soc. Rev.* **2004**, *33* (7), 410–421.

[67] Norgren, M.; Edlund, H. Lignin: Recent advances and emerging applications. *Curr. Opin. Colloid Interface Sci.* **2014**, *19* (5), 409–416.

[68] Sheng, C.; Azevedo, J. L. T. Estimating the higher heating value of biomass fuels from basic analysis data. *Biomass and Bioenergy* **2005**, *28* (5), 499–507.

[69] Nelson, R. G.; Schrock, M. D. Energetic and economic feasibility associated with the production, processing, and conversion of beef tallow to a substitute diesel fuel. *Biomass and Bioenergy* **2006**, *30* (6), 584–591.

[70] Tejado, A.; Peña, C.; Labidi, J.; Echeverria, J. M.; Mondragon, I. Physico-chemical characterization of lignins from different sources for use in phenol-formaldehyde resin synthesis. *Bioresour. Technol.* **2007**, *98* (8), 1655–1663.

[71] Han, Y.; Yuan, L.; Li, G.; Huang, L.; Qin, T.; Chu, F.; Tang, C. Renewable polymers from lignin via copper-free thermal click chemistry. *Polym. (United Kingdom)* **2016**, *83*, 92–100.

[72] Zhu, Liang, Jing Pan, Ying Wang, Juanjuan Han, Lin Zhuang, and Michael A. Hickner. “Multication Side Chain Anion Exchange Membranes.” *Macromolecules* 49, no. 3 (February 9, 2016): 815–24.

[73] Li, S. L.; Lan, Y. Q.; Ma, J. F.; Yang, J.; Wei, G. H.; Zhang, L. P.; Su, Z. M. Structures and luminescent properties of seven coordination polymers of zinc(II) and cadmium(II) with 3,3’,4,4’-benzophenone tetracarboxylate anion and bis(imidazole). *Cryst. Growth Des.* **2008**, *8* (2), 675–684.

[74] El Mansouri, N. E.; Salvadó, J. Analytical methods for determining functional groups in various technical lignins. *Ind. Crops Prod.* **2007**, *26* (2), 116–124.

[75] G Gosselink, R. J. A.; Abächerli, A.; Semke, H.; Malherbe, R.; Käuper, P.; Nadif, A.; Van Dam, J. E. G. Analytical protocols for characterisation of sulphur-free lignin. *Ind. Crops Prod.* **2004**, *19* (3), 271–281.

[76] Wroblewski, a E.; Lensink, C.; Markuszewski, R.; Verkade, J. G. Phosphorus-31 NMR spectroscopic analysis of coal pyrolysis condensates and extracts for heteroatom functionalities possessing labile hydrogen. *Energy & Fuels* **1988**, *2* (6), 765–774.

[77] Argyropoulos, D. S. Quantitative Phosphorus-31 NMR Analysis of Lignins, a New Tool for the Lignin Chemist. *J. Wood Chem. Technol.* **1994**, *14* (1), 45–63.

[78] Jiang, Z.-H.; Argyropoulos, D. S.; Granata, A. Correlation analysis of31P NMR chemical shifts with substituent effects of phenols. *Magn. Reson. Chem.* **1995**, *33* (5), 375–382.

[79] Ben, H.; Ragauskas, A. J. NMR characterization of pyrolysis oils from kraft lignin. *Energy and Fuels* **2011**, *25* (5), 2322–2332.

[80] Lai, Y.-Z. Determination of Phenolic Hydroxyl Groups. In *Methods in Lignin Chemistry*; Springer: Berlin, 1992; pp 423–434.

[81] Lugemwa, F.; Shaikh, K.; Hochstedt, E. Facile and Efficient Acetylation of Primary Alcohols and Phenols with Acetic Anhydride Catalyzed by Dried Sodium Bicarbonate. *Catalysts* **2013**, *3* (4), 954–965.

[82] Chakar, F. S.; Ragauskas, A. J. Review of current and future softwood kraft lignin process chemistry. *Ind. Crops Prod.* **2004**, *20* (2), 131–141.

[83] Mansouri, N. E. El; Salvadó, J. Structural characterization of technical lignins for the production of adhesives: Application to lignosulfonate, kraft, soda-anthraquinone, organosolv and ethanol process lignins. *Ind. Crops Prod.* **2006**, *24* (1), 8–16.

[84] Sammons, R. J.; Harper, D. P.; Labbé, N.; Bozell, J. J.; Elder, T.; Rials, T. G. Characterization of organosolv lignins using thermal and FT-IR spectroscopic analysis. *BioResources* **2013**, *8* (2), 2752–2767.

[85] Evans, P. A. Differentiating “hard” from “soft” woods using Fourier transform infrared and Fourier transform spectroscopy. *Spectrochim. Acta Part A Mol. Spectrosc.* **1991**, *47* (9–10), 1441–1447.

[86] Hu, G.; Cateto, C.; Pu, Y.; Samuel, R.; Ragauskas, A. J. Structural characterization of switchgrass lignin after ethanol organosolv pretreatment. In *Energy and Fuels*; 2012; Vol. 26, pp 740–745.

[87] Faix, O. Classification of Lignins from Different Botanical Origins by FT-IR Spectroscopy. *Holzforschung* **1991**, *45* (s1), 21–28.

[88] Schultz, T. P.; Glasser, W. G. Quantitative structural analysis of lignin by diffuse reflectance fourier transform infrared spectrometry. *Holzforschung* **1986**, *40* (suppl.), 37–44.

[89] Rodrigues, J.; Faix, O.; Pereira, H. Determination of lignin content of Eucalyptus globulus wood using FTIR spectroscopy. *Holzforschung* **1998**, *52* (1), 46–50.

[90] Demarconnay, L.; Coutanceau, C.; Léger, J. Electroreduction of dioxygen (ORR) in alkaline medium on Ag/C and Pt/C nanostructured catalysts—effect of the presence of methanol. *Electrochim. Acta* **2004**, *49* (25), 4513–4521.

[91] Ge, X.; Sumboja, A.; Wuu, D.; An, T.; Li, B.; Goh, F. W. T.; Hor, T. S. A.; Zong, Y.; Liu, Z. Oxygen reduction in alkaline media: From mechanisms to recent advances of catalysts. *ACS Catal.* **2015**, *5* (8), 4643–4667.

[92] Schmidt, T. J.; Stamenkovic, V.; Arenz, M.; Markovic, N. M.; Ross, P. N. Oxygen electrocatalysis in alkaline electrolyte: Pt(hkl), Au(hkl) and the effect of Pd-modification. *Electrochim. Acta* **2002**, *47* (22), 3765–3776.

[93] Prasanna Misra, R.; Das, S.; Mitra, S. K. Electric double layer force between charged surfaces: Effect of solvent polarization. *J. Chem. Phys.* **2013**, *138* (11), 114703.

[94] Sánchez-Sánchez, C.; Bard, A. Hydrogen peroxide production in the oxygen reduction reaction at different electrocatalysts as quantified by scanning electrochemical microscopy. *Anal. Chem.* **2009**, *81* (19), 8094–8100.

[95] Schmidt, T. J.; Paulus, U. A.; Gasteiger, H. A.; Behm, R. J. The oxygen reduction reaction on a Pt/carbon fuel cell catalyst in the presence of chloride anions. *J. Electroanal. Chem.* **2001**, *508* (1–2), 41–47.

[96] Hibbs, M. R. Alkaline stability of poly(phenylene)-based anion exchange membranes with various cations. *J. Polym. Sci. Part B Polym. Phys.* **2013**, *51* (24), 1736–1742.

[97] Ren, X.; Price, S. C.; Jackson, A. C.; Pomerantz, N.; Beyer, F. L. Highly Conductive Anion Exchange Membrane for High Power Density Fuel-Cell Performance. *ACS Appl. Mater. Interfaces* **2014**, *6* (16), 13330–13333.

[98] Matyjaszewski, K. Atom Transfer Radical Polymerization (ATRP): Current status and future perspectives. *Macromolecules* **2012**, *45* (10), 4015–4039.

[99] Tang, W.; Matyjaszewski, K. Effects of initiator structure on activation rate constants in ATRP. *Macromolecules* **2007**, *40* (6), 1858–1863.

[100] Akeroyd, N.; Klumperman, B. The combination of living radical polymerization and click chemistry for the synthesis of advanced macromolecular architectures. *Eur. Polym. J.* **2011**, *47* (6), 1207–1231.

[101] Hawker, C. J. Molecular Weight Control by a “Living” Free-Radical Polymerization Process. *J. Am. Chem. Soc.* **1994**, *116* (24), 11185–11186.

[102] Matsuno, R.; Yamamoto, K.; Otsuka, H.; Takahara, A. Polystyrene- and poly(3-vinylpyridine)-grafted magnetite nanoparticles prepared through surface-initiated nitroxide-mediated radical polymerization. *Macromolecules* **2004**, *37* (6), 2203–2209.

[103] Morris, J. C.; McMurtrie, J. C.; Bottle, S. E.; Fairfull-Smith, K. E. Generation of profluorescent isoindoline nitroxides using click chemistry. *J. Org. Chem.* **2011**, *76* (12), 4964–4972.

[104] Zhao, X.-D.; Fan, X.-H.; Chen, X.-F.; Chai, C.-P.; Zhou, Q.-F. Surface modification of multiwalled carbon nanotubes via nitroxide-mediated radical polymerization. *J. Polym. Sci. Part A Polym. Chem.* **2006**, *44* (15), 4656–4667.

[105] Kimura, Y.; Miyabara, Y.; Terashima, T.; Sawamoto, M. Polyacrylamide pseudo crown ethers via hydrogen bond-assisted cyclopolymerization. *J. Polym. Sci. Part A Polym. Chem.* **2016**, *54* (20), 3294–3302.

[106] Li, L.; Wang, J.; Wu, T.; Wang, R. Click ionic liquids: A family of promising tunable solvents and application in Suzuki-Miyaura cross-coupling. *Chem. - A Eur. J.* **2012**, *18* (25), 7842–7851.

[107] Rostovtsev, V. V.; Green, L. G.; Fokin, V. V.; Sharpless, K. B. A stepwise Huisgen cycloaddition process: Copper(I)-catalyzed regioselective “ligation” of azides and terminal alkynes. *Angew. Chemie* **2002**, *114* (14), 2708–2711.

[108]Himo, F.; Lovell, T.; Hilgraf, R.; Rostovtsev, V. V.; Noodleman, L.; Sharpless, K. B.; Fokin, V. V. Copper(I)-catalyzed synthesis of azoles. DFT study predicts unprecedented reactivity and intermediates. *J. Am. Chem. Soc.* **2005**, *127* (1), 210–216.

[109] Li, Y.; Xu, T.; Gong, M. Fundamental studies of a new series of anion exchange membranes: Membranes prepared from bromomethylated poly(2,6-dimethyl-1,4-phenylene oxide) (BPPO) and pyridine. *J. Memb. Sci.* **2006**, *279* (1–2), 200–208.

[110] Mahajan, C. V.; Ganesan, V. Atomistic simulations of structure of solvated sulfonated poly(ether ether ketone) Membranes and their comparisons to Nafion: I. Nanophase segregation and hydrophilic domains. *J. Phys. Chem. B* **2010**, *114* (25), 8357–8366.

[111] Chan, S. C.; Kuo, S. W.; Lu, C. H.; Lee, H. F.; Chang, F. C. Syntheses and characterizations of the multiple morphologies formed by the self-assembly of the

semicrystalline P4VP-b-PCL diblock copolymers. *Polymer (Guildf).* **2007**, *48* (17), 5059–5068.

[112] Georges, M. K.; Veregin, R. P. N.; Kazmaier, P. M.; Hamer, G. K. Narrow molecular weight resins by a free-radical polymerization process. *Macromolecules* **1993**, *26* (11), 2987–2988.

[113] Cheng, C. L.; Wan, C. C.; Wang, Y. Y. Preparation of porous, chemically cross-linked, PVdF-based gel polymer electrolytes for rechargeable lithium batteries. *J. Power Sources* **2004**, *134* (2), 202–210.

[114] Komkova, E. N.; Stamatialis, D. F.; Strathmann, H.; Wessling, M. Anion-exchange membranes containing diamines: Preparation and stability in alkaline solution. *J. Memb. Sci.* **2004**, *244* (1–2), 25–34.

[115] Vega, J. A.; Chartier, C.; Mustain, W. E. Effect of hydroxide and carbonate alkaline media on anion exchange membranes. *J. Power Sources* **2010**, *195*, 7176–7180.

[116] Armarego, W. L. F.; Perrin, D. D. *Purification of Laboratory Chemicals, Fourth Edition.*; Butterworth-Heinemann: Oxford, 1997; Vol. 2.

[117] Ropponen, J.; Lahtinen, M.; Busi, S.; Nissinen, M.; Kolehmainen, E.; Rissanen, K. Novel one-pot synthesis of quaternary ammonium halides: new route to ionic liquids. *New J. Chem.* **2004**, *28* (12), 1–5.

VITA

Luke T. Servedio was born in Poughkeepsie, NY and grew up in Boca Raton, Fl. In 1998, he was accepted to attend the United States Military Academy (USMA) in West Point, NY. There, he studied under the guidance of Dr. Andrew I. Biaglow and Dr. Robert G. Bozic (LTC-ret.) and, in 2002, graduated with a BS in Chemistry as a commissioned officer in the United States Army. Luke served as an Infantry Officer for 7 years, to include two year-long deployments to Iraq for OIF. In 2010, he joined the research group of Dr. Thomas A. Zawodzinski at the University of Tennessee to perform research in biomass conversion and membrane synthesis.